Influence of Blood Oxygen Level Dependent Signals Frequencies on Brain Connectivity

By

Suril Gohel

A Dissertation Submitted in Partial Fulfillment of the Requirements for the Degree of Doctor of Philosophy in Biomedical Informatics

Department of Health Informatics

School of Health Related Professions

Rutgers, the State University of New Jersey

Fall 2015

APPROVAL PAGE

Dr. Syed Haque, Dissertation Committee Chair and Advisor

Date:

Dr. Bharat Biswal, Dissertation Committee Co-Chair and Advisor

Date:

Dr. Shankar Srinivasan, Dissertation Committee Member

Date:

Dr. Fredrick Coffman, Dissertation Committee Member

Date:

TABLE OF CONTENTS

ABSTRACT

Resting state functional MRI (fMRI) studies have demonstrated temporal correlation across physically distant voxels (or brain regions) in functionally related regions. Studies have shown that these temporal correlations are dominated by low frequency fluctuations in the range of approximately 0.01 – 0.1 Hz. While these studies have been widely replicated, due to hardware limitation the sampling rate of an fMRI machine has been limited to about 1 data point every 2 seconds resulting in a Nyquist sampling rate of 0.25 Hz, have focused on fMRI signal <025 Hz. Yet various electrophysiological measurements like EEG, LFP, and MEG acquire data at much faster rate at up to 200 times points every second and study neuronal fluctuations in range from 1 ~ 100 Hz. In addition, to be limited by the lower sampling rate of fMRI, resting state fMRI studies, are primarily focused on sub segment (0.01-0.1 Hz) of the whole frequency bands (0-0.25 HZ), due to higher power of BOLD signal in this frequency ranges. The goal of the current dissertation is to utilize recent advancements in fMRI signal acquisition techniques, which can acquire 1 data point in 0.5 seconds, to study functional integration between brain regions during resting state fMRI in higher frequency BOLD fluctuations. In order to achieve this goal, we obtained resting state fMRI data acquired from healthy subjects at higher sampling frequency of 1.5 Hz as well as resting state fMRI data acquired from schizophrenic patients at sampling frequency of 0.5 Hz from open-access data repositories. Using this open access fMRI data, we performed three distinct studies to investigate frequency specific differences in resting state functional connectivity. In the first study, we quantified RSFC across five different frequency bands. We implemented two of the most widely used methods: independent component analysis and seed based correlation to estimate RSFC across frequency bands. Commonly known

RSNs such as the default mode, the fronto-parietal, the dorsal attention and the visual networks were consistently observed across multiple frequency bands. Significant inter-hemispheric connectivity was observed between a seed and its contralateral brain region across all frequency bands, though overall spatial extent of seed based correlation maps decreased in higher frequency BOLD fluctuations (slow-2 and slow-1 frequency bands). These results suggest that functional integration between brain regions at rest occurs over multiple frequency bands and RSFC is a multi-band phenomenon. These results also suggest further investigation of BOLD signal in multiple frequency bands and related changes in whole brain network topologies. In lieu of the results from the first study, in the second study we investigated changes in whole brain network topologies associated with changes in frequency bands based RSFC. We performed graph theory analysis on whole brain RSFC in five distinct frequency bands to study the whole brain network architecture. We observed significant differences in local connectivity properties across frequency bands and corresponding changes in network hubs, modularity and small-world network index. The brain network topologies at all the frequency bands showed small-world topologies though, RSFC network at slow-4 and slow-5 networks showed significantly higher small-world indices compared to that of slow-1 and slow-2 networks. Lastly, due to differential power distribution of BOLD signal across resting state networks observed in the first project, we studied changes in BOLD signal power in clinical populations. In this regard, we studied disruptions of BOLD signal power in various frequency bands in schizophrenia. We observed significant increase in frontal cortex power in psychosis patients compared to healthy controls across slow-2, slow-3 and slow-4 and opposite effect was observed in posterior brain regions, where controls

showed increased BOLD signal power compared to psychosis patients. By performing these three coherent studies, we investigated frequency specific changes in RSFC and their disruption in psychosis patients, implying neurocognitive importance of resting state BOLD signal in higher frequency bands (>0.1 Hz).

ACKNOWLEDGEMENTS

This dissertation would be incomplete without acknowledging all of those who have contributed and/or helped me throughout this process. First, I must acknowledge my committees chair Dr. Syed Haque. Dr. Haque has provided me with constant guidance; inspirations and valuable insights that have made me enable to do this research. Secondly, I must acknowledge the members of my advisory committee, Dr. Shankar Srinivasan and Dr. Fredrick Coffman, for their challenging questions and in-depth recommendations, which have made this research whole. Moreover, I must acknowledge, Dr. Bharat Biswal, at New Jersey Institute of Technology, for providing me with invaluable guidance on all the projects, for his patience, continuous inspiration, for giving me freedom to pursue my research goals and most importantly to lead me on this path of neuroimaging and neuroscience research throughout my career. Without the guidance of Dr. Bharat Biswal, I would have never pursued a career in neuroscience /neuroimaging research and would have never enrolled in the PhD program at school of health related professions. Moreover, I really would like to thank my colleagues; Dr. Paul Taylor and Dr. Xin Di, for their continuous guidance and counter-intuitive questions that has helped me explain the results in the current dissertation. I would also like to thank Rui Yuan and Keerthana Karunakaran, for sharing my workload throughout my dissertation period and providing me important feedback on my writing skills.

Lastly, I would like to thank people, who have made me who I am today, my parents Rajesh Gohel, Vina Gohel, and my brother Nishank Gohel, for letting me pursue my career and for their patience, encouragement and confidence in me. They have been a continuous inspiration to work harder, smarter every day. I also want to thank my dearest

friends, chaku, sunny, priya, parth desai, sagar, khushi, jp, harsh, parth patel ,jaymin, zil, jalpa, krunal, amit patel,nishit mamtora, and all others, I might have missed for being a continuous support and if not for you I would have graduated a year earlier.

DEDICATION

I want to dedicate, this dissertation to my parents Rajesh Gohel, Vina Gohel and my brother Nishank Gohel, you are the reason, motivation and support for what I am today.

LIST OF TABLES

Page

LIST OF FIGURES

LIST OF ABBREVIATIONS

Functional Magnetic Resonance imaging…….. (fMRI)

Resting State Functional Connectivity……. (RSFC)

Resting Stat Functional Magnetic Resonance Imaging…….. (rs-fMRI)

Blood Oxygen Level Dependent…… (BOLD)

Independent Component Analysis…….. (ICA)

Regions Of Interests……. (ROIs)

Montreal Neurological Institute…….. (MNI)

Default Mode Network……...……. (DMN)

Frontal-Parietal Network...…….. (FPN)

Resting State Networks…… (RSNs)

Positron Emission Tomography…….. (PET)

Low-Frequency Fluctuations…….. (LFFs)

Nuclear Magnetic Resonance……..…… (NMR)

Inter-class Correlation Coefficient…….. (ICC)

Time of Repetition…….. (TR)

Time of Echo…….... (TE)

Magnetically Prepared Gradient Echo…… (MPRGE)

Cerebral Spinal Fluid…….. (CSF)

White Matter…… (WM)

Gray Matter…….. (GM)

Fast Fourier Transformation…… (FFT)

Functional Connectome Project……... (FCP)

Frontal Eye Field……. (FEF)

Inferior Parietal Sulcus…… (IPS)

Middle Temporal Gyrus …….. (MTG)

Pre-Central Gyrus…… (PCG)

Lateral Parietal Cortex……. (LPC)

Medial Pre-Frontal Cortex……... (MPFC)

Posterior Cingulate Cortex…….. (PCC)

Attention Deficit Hyper-activity Disorder…….. (ADHD)

CHAPTER I

INTRODUCTION

Since its development in 1990's functional magnetic resonance imaging (fMRI) has been widely used to analyze changes in brain function under influence of various levels of cognitive conditions. Functional magnetic resonance imaging based on the principal of Nuclear magnetic resonance (NMR) uses the magnetic properties of H+ ions, abundantly present in Human body. Ogava and Colleagues based on the observation that the magnetic properties of deoxygenated hemoglobin are different than that of oxygenated hemoglobin developed an fMRI signal contrast dependent on the level of oxygen in the blood. This signal labeled as Blood Oxygen Level Dependent (BOLD) signal is based on the hypothesis that neuronal firing in human brain causes underlying changes in glucose consumption, further creating changes in blood oxygen level. These changes in blood oxygen level causes increase in blood flow, in turn causing changes in BOLD signal intensity. Earlier fMRI studies manipulated the level of cognitive load and in turn investigated the resulting effect on Blood Oxygen Level Dependent (BOLD) signal, and hence are labeled "task-based" fMRI studies.

As an alternative to task activation studies, Biswal and colleagues[1], performed BOLD fMRI experiments in the absence of any external explicit task condition, labeled as "resting-state" fMRI experiments. By taking a representative voxel's time course from the sensorimotor cortex and correlating with every other voxel time series in the brain, a significant pattern of correlation in the sensorimotor cortex, similar to that obtained during sensorimotor activation pattern during bilateral finger tapping paradigm was

observed. These resting state BOLD fluctuations have been shown to be highly correlated across spatially remote though functionally related brain regions predominantly in low-frequency range (0.01-0.1 Hz) commonly known as 'low-frequency fluctuations (LFFs) [1]. The correlations of temporally filtered BOLD time series between brain regions are thought to represent neuronal level functional integration and have been termed 'Resting State Functional Connectivity' (RSFC). Due to selective nature of RSFC, the human brain can be characterized into multiple networks using approaches such as seed based correlation[1] and independent component analysis (ICA) [2,3]. Functional integration between brain regions and various RSNs has also been established using other imaging modalities that doesn't involve temporal filtering such as Positron Emission Tomography (PET) [4]and structural connectivity[5] as well as non-imaging modalities that involves some kind of temporal processing such as electroencephalography (EEG) [6].

Electrophysiological signals obtained through single cell recordings and EEGs during resting state are known to be present across multiple frequency bands, and neuronal networks in mammalian brain demonstrate multiple frequency bands spanning up to 500 Hz[7,8]. Together, these observations imply that functional integration between neuronal processes occurs over a wide range of frequencies. Generally, BOLD fMRI fluctuations used to study functional integration between neuronal processes during rest are temporally filtered in low-frequency band (LFFs) (0.01-0.1 Hz)[1], predominantly to avoid influence of physiological noises (respiration (~0.2-0.3 Hz) and cardiac signal (~1.2 Hz)) present in BOLD fMRI data. This narrow fMRI frequency band overlaps with multiple frequency bands defined previously by electrophysiological studies: slow-5 (0.01-0.027 Hz), slow-4 (0.027-0.073Hz) and part of slow-3 (0.073-0.198 Hz) [7,9]. In

addition, due to hardware limitations preceding recent advances, the sampling rate for whole brain fMRI has been limited to about 2 seconds, resulting in a frequency bandwidth of fMRI typically between 0-0.25 Hz. This has limited further exploration of fMRI signal during resting state in frequencies higher than 0.1 Hz, which may relate to corresponding slow-3, slow-2 and slow-1 frequency bands.

1.1 Statement of the problem

Although known that, electrophysiological signals obtained through single cell recordings and EEGs during resting-state are known to be present across multiple frequency bands, and neuronal networks in mammalian brain demonstrate fluctuations in multiple frequency bands spanning up to 500 Hz, resting state fMRI signal, has been studied in low-frequency range (LFF) (0.01-0.1 Hz). This is based on consideration of noise characteristics, due to higher signal power contained in low-frequency range[1] and due to limitations of fMRI scanning protocol that has limited the fMRI bandwidth to 0.25 Hz. In addition, unlike EEG signal, BOLD signal in LFF is seldom divided and studied in multiple frequency bands, due to lower temporal resolution and similar power distribution between the frequency bands <0.1 Hz (slow-4 (0.027-0.073 Hz) and slow-5 (0.01-0.027 Hz)). This has limited exploration of BOLD signal in frequencies > 0.1 Hz as well as sub-bands of BOLD fMRI signal and possible role of such frequencies in cognition and various brain diseases.

1.2 Background of the problem

Previous studies have explored and quantified resting state fMRI signal and resting state functional connectivity in higher frequency bands. In one of the earlier

studies Cordes and colleagues have studied resting state BOLD fMRI signal using a low-spatial resolution but high temporal resolution data[10]. They showed significant differences in functional connectivity patterns across frequency bands. Similarly, Wu and colleagues have showed consistent RSFC across frequency bands[11]. These studies although, exploring the higher frequency BOLD fluctuations in the range (0.1 to 0.25 Hz), have not explored BOLD signal in even higher frequencies (than 0.25 Hz). Additionally, these studies have not explored the changes in RSFC and related network topologies at higher frequency BOLD fluctuations.

1.3 Objectives of the research

The primary goal of this dissertation is to investigate influence of BOLD signals frequencies on resting state functional connectivity. We devised three distinct objectives to study this primary goal. The first objective of the current research is to utilize recent advancements in multiband imaging sequences to quantify RSFC measures in BOLD signal frequencies higher than 0.1 Hz. The second objective of the current research is to identify and quantify changes in whole brain network topology as a result of changes in frequency bands based RSFC. The third and final objective of the current research is to study disruption of frequency based neuroimaging parameters in schizophrenia to understand the neurocognitive basis of BOLD signal frequencies.

1.4 Research questions

The first objective of the current research is to quantify effect of changes in BOLD signal frequencies on RSFC. We identified following research questions to accomplish the first objective.

1. Is the power distribution of various frequencies in known resting state networks change when considering wider BOLD signal frequency range?
2. Does the connectivity strength and spatial extent of resting state networks derived using Independent Component Analysis (ICA) and seed based correlation depend on the frequency band being studied?

The secondary objective of the current research is to quantify effect of frequency specific RSFC changes on whole brain network topologies. We identified two distinct research questions to quantify these changes.

3. Do changes in functional connectivity across frequency bands contribute to large-scale changes in whole brain network topology?
4. Do the hubs of whole brain network and corresponding modules of whole brain RSFC changes as a function of frequency bands?

The final objective of the current proposal is to quantify effect of schizophrenia on frequency specific resting state parameters. We compared BOLD signal power between the schizophrenia populations and healthy controls.

5. Is the effect schizophrenia on functional connectivity and resting state parameters, limited to low-frequency bands or is it consistent at higher BOLD signal frequency bands?
6. Is the difference in BOLD signal power between schizophrenia and healthy controls, frequency specifics?

1.5 Hypothesis

Based, on the previous literature, we derive following hypothesis with respect to each of the research questions.

(1) We hypothesize that power distribution of BOLD signal frequencies will be different between each of the known resting state network, though within a specific network; higher signal power will be observed in low-frequency BOLD fluctuations.

(2) We hypothesize that RSFC will be observed in frequency bands higher than 0.1 Hz though; wide scale differences in RSFC will be observed across frequency bands.

(3) We hypothesize significant differences in network topologies will be observed across BOLD signal frequencies. We also hypothesize that significant differences in whole brain network modules and network hubs will be observed with changes in BOLD signal frequencies.

(4) We expect to see similar disruption of BOLD signal power in schizophrenia in higher frequency range, as it has been well documented in low-frequency range. However, based on earlier EEG and MEG studies, we hypothesize significant interactions between group level differences and frequency band being studied.

CHAPTER II

LITERATURE REVIEW

2.1 Background of Functional Magnetic Resonance Imaging (fMRI) and Blood Oxygen Level Dependent (BOLD) signal

Magnetic Resonance Imaging is a popular, noninvasive imaging modality to study anatomy of brain or for that matter, any region with soft tissue. Unlike other imaging scanning modalities like CT-Scan or X-ray, it does not use either internal or external radiation and therefore does not create any long time radiation effects on subjects. It is a very useful tool in neuroimaging studies because of three main reasons. First, it provides very high spatial resolution, helpful in imaging minute structures of brain. Second, it provides very good tissue contrast by using different type of pulse sequence, which aids in automatic segmentation of different brain tissues. Third, as discussed above, is lack of radiation effects, which enables longitudinal studies including various clinical populations.

Magnetic Resonance Imaging (MRI) works on principle of Nuclear Magnetic Resonance (NMR) that in turn uses magnetization properties of ^{1}H ion abundantly present throughout the human body. Studies have shown a fundamental concept in Functional MRI (fMRI) that deoxygenated hemoglobin shows paramagnetic properties while oxygenated hemoglobin shows diamagnetic properties under the presence of external magnetic field. Based on prior knowledge that the presence of paramagnetic substance in blood, decreases spin de-phasing and thus decreases $T2^{*}$ parameter, Seigi Ogava and Colleagues[12] demonstrated use of this phenomenon to evaluate brain functions

based on concentration of deoxygenated hemoglobin present in blood. Increase in neuronal activity in specific regions of the brain typically results in increase of metabolic consumption that leads to vasodilation. Vasodilation leads to an increase of blood flow and the amount of oxygenated red blood cells is much greater than the metabolic need, this leads to an increase in concentration of oxygenated hemoglobin compared to the concentration of deoxygenated hemoglobin. This increase in blood flow causes decrease in concentration of deoxygenated hemoglobin causing net increase in signal from particular brain region during T2-T2* weighted imaging.[12,13] Ogawa and colleagues identified this phenomenon of changes in signal intensity in T2-T2* weighted imaging as a function of concentration of deoxygenated hemoglobin and oxygen in blood and dependent on brain functional activity, and labeled it as "Blood Oxygen Level Dependent" (BOLD) signal.

In the first study of using fMRI, Ogava and colleagues use this Blood Oxygen Level Dependent (BOLD) signal to quantify physiological changes occurring in visual cortex area during task related activation[12]. Since its development in 1990's fMRI has been widely used to analyze changes in brain's physiology under various task conditions. Bandettini et al[14] were one of the first groups to propose and develop basic processing steps for temporal filtering and for correlating each individual voxel from fMRI dataset to reference time series in order to find out activation for particular task. Similarly, Kiviniemi and colleagues were one of the first groups to apply blind source separation techniques to BOLD fMRI data[2].

2.2 Resting State fMRI and Resting state functional Connectivity in Low-Frequency Fluctuations (LFFs) of BOLD signal

In 1995, Biswal and colleagues, used fMRI techniques to study healthy subjects in the absence of an explicit cognitive task conditions. After filtering the fundamental and harmonics of the respiration and heart rates from the data collected using fMRI, they demonstrated significant temporal correlation of BOLD signal in low frequency range (0.01-0.1 Hz) between pixels in primary sensorimotor cortex (both intra- and inter-hemi spherically). These pixels were first identified as active during an independent finger-tapping paradigm performed in the same session. Only a few pixel time courses (<3%) from regions outside the sensorimotor cortex exhibited significant temporal correlation with time courses from pixels within the sensorimotor cortex[1]. Friston et al. had previously defined functional connectivity as the temporal correlation of a neurophysiological index measured in different brain areas[4,15]. These studies by Biswal and colleagues supported the hypothesis that low-frequency physiological fluctuations constituted such a neurophysiological index. These intra- and inter-hemispheric correlations among functionally related regions suggest that synchronous fluctuations may be a general cortical phenomenon representing the functional connection of cortical areas. Due to this reasons, phenomenon of synchronous low-frequency fluctuations between brain regions during rest condition was labeled as **Resting State Functional Connectivity (RSFC)**.

Following, the identification of RSFC, several groups has studied resting state functional connectivity in the brain, across human life-span, clinical populations, and animal models using various methodologies. One of the most commonly used methods to

derive RSFC is seed based correlation analysis that derives the functional integration between a single brain region and all the other brain regions. In order to perform a seed based correlation analysis, BOLD fMRI signal time series from a brain regions is correlated with BOLD signal time series from all the other brain regions and corresponding maps are thresholded to derive the RSFC maps for a particular seed region. Another widely implemented method to study the functional integration at whole brain is Independent Component Analysis (ICA) [2,3]. ICA is a blind source separation technique, which segments the whole brain in sets of regions that show selective frontal integration within themselves with little or no correlation with outside brain regions. These sets of brain regions are collectively labeled as Resting State Networks (RSNs). Recently, studies have segmented the whole brain in to set of brain regions. For each of these brain regions, an average rs-fMRI time series is extracted. A Pearson's correlation coefficient is calculated between each of these ROI pairs that describe the RSFC between all the possible pairs of ROIs in human brain. This particular method labeled as ROI based analysis results in a correlation matrix, which describes the functional connectivity on a whole brain level.

In one of the earlier studies of RSFC, Fox and colleagues using seed based correlation analysis identified two distinct brain systems, which showed anti-correlation with each other during a resting state scan[16]. Subsequent work by Hampson and Gore has also observed pixels within visual and within auditory cortex that behaves similarly where as low frequency fluctuations of BOLD signal are correlated within these regions but not outside of them[17]. These studies establish the foundation for functional integration using fMRI. Following, publication of the initial paper, these results have been replicated

and extended by other research groups. Xiong and Fox et al. analyzed resting state fluctuations and identified six areas of the motor system that exhibit significant inter-regional connectivity; primary motor cortex, premotor cortex, secondary somatosensory cortex, anterior cingulate cortex, and posterior cingulate[18]. These authors point out that analysis of resting-state connectivity reveals many more functional connections than the usual task-induced activation analysis. They suggested that task-induced activation maps underestimate the size and the number of areas involved in a task and that those are more fully revealed by resting-state fluctuation analysis.

One of the system consisting posterior cingulate cortex, lateral parietal cortex and medial prefrontal cortex, showed decreased in signal intensity in response to cognitive task and hence were labeled as task-negative / default-mode network (DMN). The regions showing positive activation with response to the cognitive tasks mainly consisted of bilateral inferior parietal sulcus, pre-central/post central gyrus and were labeled as part of various task positive networks[16]. Following discovery of group of brain regions showing higher correlation of resting state BOLD signal with each other and very little correlation with other brain regions, these groups of regions were identified as resting state networks (RSNs). Beckmann and colleagues, implemented ICA on low-frequency resting state BOLD signal to divide whole brain in to set of resting state networks namely, visual network, higher visual network etc[3].

In one of the first papers, studying the robustness and reliability of RSFC, Shehzad and colleagues, implemented Inter-class Correlation Coefficient (ICC) and observed very high intersession and intersession reliability of RSFC[19]. In one of the first large-scale neuroimaging studies, Biswal and colleagues used resting state data acquired

from 12 different institutions across the world to study the reliability of resting state[20]. One of the major limitations of these studies has been the low-temporal resolution of the fMRI due to hardware limitation of MRI. In addition, these studies have focused on low-frequency fluctuations (LFFs) of BOLD signal (0.01-0.1 Hz) due to the studies by Biswal and colleagues that have showed that the LFFs have highest power in BOLD signal and are least affected by cardiac and respiratory fluctuations.

2.3 Resting State Functional Connectivity in High Frequency Fluctuations (HFFs) of BOLD signal

As discussed in previous section, several researchers have studies functional integration between brain regions, during resting state fMRI. One common factor amongst most of these resting state fMRI studies is their focus on low-frequency fluctuations of BOLD signal (0.01-0.1 Hz). The primary reasons for the rs-fMRI studies to have focused on low-frequency BOLD is the observation that BOLD signal power is highly concentrated in the low-frequency of BOLD fluctuations by Biswal and colleagues[1]. The secondary reason for the focus on low-frequency fluctuations has been to minimize the effect of high frequency cardiac and respiratory noises on BOLD signal[21]. The tertiary reason for the focus on low frequency of BOLD fluctuations has been the temporal resolution of whole brain fMRI, which has limited the exploration of BOLD signal in frequency bands higher than 0.25 Hz. Despite of these limiting factors, previous studies have investigated resting state BOLD signal and RSFC in frequency bands higher than 0.1 Hz.

In one of the first studies of high frequency BOLD signal in resting state fMRI, Cordes and colleagues scanned healthy controls at a higher sampling frequency to investigate presence of RSFC at higher frequencies. Due to hardware limitations, Cordes and colleague didn't acquire the rs-fMRI data at whole brain level, rather acquiring it over only 4 slices in the area of motor cortex. They reported significantly higher contribution (~90%) of LFFs to the RSFC of the auditory, the visual and the sensory motor networks compared with 0.1 to 1.1 Hz[10]. In the same study, contribution of high frequency BOLD fluctuations to RSFC of auditory, visual and motor network, although smaller than LFF, was consistently significant. Additionally, in motor cortex, high-frequency BOLD fluctuations in range of 0.1-0.5 Hz, contributed ~20% to the correlation strength. These results suggest presence of RSFC at high-frequency BOLD fluctuations, as well as variable though significant contribution of high frequency BOLD fluctuations to RSFC between various brain regions.

Although, Cordes and colleagues explored the presence of RSFC at higher frequency BOLD fluctuations, the results were limited to motor cortex, auditory cortex and visual cortex, due to lower field of view acquired during the scanning session. In order to further investigate the RSFC in high-frequency BOLD fluctuations at whole level, Wu and colleagues acquired rs-fMRI data at whole brain level at the sampling rate of 1 image every two second (TR-2s, sampling frequency =0.5 Hz). This enabled investigation of RSFC in frequency bands from 0.1 to 0.25 Hz in various cortical brain networks, including default mode network, visual network, sensory motor network and limbic network including amygdala network and hippocampus network [11]. Wu and colleagues observed significant presence of RSFC in both cortical and limbic networks

across frequencies ranging from 0.01-0.25 Hz, though spatial extent of RSFC showed significant differences across networks. Additionally, significant differences were observed in frequency specific RSFC in cortical networks, compared to limbic networks, where limbic networks showed littler variations in RSFC compared to cortical networks. These results further validated the presence of frequency specific differences in RSFC as well as provided further information about subject specific variability in RSFC at higher frequency BOLD fluctuations. These studies although, investigating the whole brain RSFC across frequency bands, are limited in respect to the frequency band being studied, which remains smaller than that of other neuroscience techniques (EEG, MEG).

Recent advancements in data acquisition sequences and multi-band imaging techniques [22–24] have enabled whole brain fMRI scanning at sub-second temporal resolution. These advancements have significantly increased fMRI bandwidth from 0-0.25 Hz to 0-1Hz. Using similar acquisition methods, Lee and colleagues acquired whole brain rs-fMRI data at the temporal resolution of 100 ms to study the RSFC at frequency bands up to 1Hz. Lee and Colleagues observed sustained inter-hemispheric connectivity in the sensory motor cortex from BOLD fluctuations in higher frequency ranges (>0.25Hz) than traditionally used in resting state fMRI studies (0.01-0.1 Hz)[25]. In the same study, similar results were obtained in visual network, implying consistency of RSFC at higher frequency BOLD fluctuations. In a very recent study, Boubela and colleagues have shown the presence of the default mode and frontal-parietal networks by applying independent component analysis to BOLD fMRI data acquired at higher sampling rate (TR=354 ms, sampling frequency = 2.82 Hz)[26]. Although, these studies have described presence of different RSNs in higher frequency bands than LFFs (>0.1

Hz), these were mainly performed using a single approach to study RSNs [25,26]. Moreover, these reports focused on specific networks rather than on the entire collection of RSNs [25,26]. Finally, the BOLD signal frequencies >0.1 Hz were generally combined in a single frequency band to derive RSNs [25,26].

2.4 Graph theoretical properties of whole brain RSFC in LFFs and HFFs

A network can be described as a collection of nodes and connections between them. Some of the examples of real life networks are power grid lines, airport/airline distribution network. In terms of power grid lines, the power plants and houses are considered nodes of a network, while the cables connecting are considered connections between them, which are an example of physical connections between nodes. Similarly, the airline network is an example of a network where airports are considered nodes, while the airline routes are an example of virtual connections between the nodes. In addition, to consisting of virtual or physical connections, networks vary respect to topologies. Network topologies can be defined by studying the distance between nodes, the number of connections passing through a node, total number of connections, amongst other variables. One of the main properties to define a network topology is to quantify the measure of local integration. The measure of local integration is defined as clustering coefficient C. C is the average of the nodal clustering coefficients C_i over all nodes in a network, where C_i of the i^{th} node is defined as the number of existing connections among the neighbor nodes divided by all their possible connections, *i.e.* $C = 1/N \sum_{i=1}^{N} C_i$. The clustering coefficient provides a measure of local structure, and quantifies resistance to failure and the extent of the local density or cliquishness of the network. Similarly, Path

Length (L) defines the measure related to the connection length between the nodes. The characteristic path length L is the average of the local shortest path lengths L_i over all nodes, where L_i of i^{th} node is the average of the minimum number of edges d_{ij} that have to be traveled to go from node *i* to other nodes *j*, *i.e.*

$L = 1/N \sum_{i=1}^{N} L_i = 1/N(N-1) \sum_{i,j \in N, i \neq j} d_{ij}$. Thus L represents the extent of average connectivity or global routing efficiency of a network.

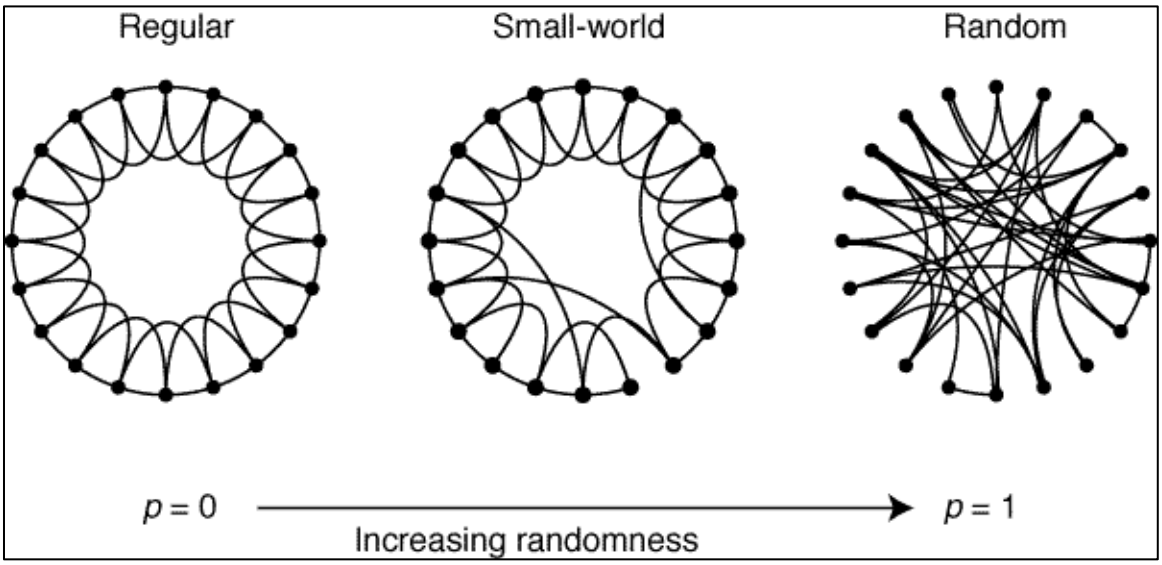

Figure 1: Types of Graph (reproduced from Watts and Strogratz et al., 27)

In one of the earliest studies of network topologies, Watts and Strogatz described three different types of various network topologies, a regular network, a random network and a small-world network. As described in figure 1 reproduced from the study by Watts and Strogatz[27], a regular network has higher clustering coefficient and higher path length. Increased clustering coefficient is associated with higher number of connections between each node and its immediate nodes. This causes a higher local integrations and increased

resistance to failure. In a regular network, absence of long-distance connections between nodes causes increased connection length between two nodes, resulting in increased path length. Increased path length is related to decrease in global efficiency. Random network topology is an opposite of regular network, with random long distance edges between two distance nodes. A random network can be described by decreased clustering coefficient and decreased path length. This types of network, although having high global efficiency and shorter connection length between two distant nodes has little local efficiency. Watts and Strogatz[27] defined a network topologies consisting of very high local connectivity with presence of a few long distance edges between the nodes. This type of network showed high local connectivity and local efficiency due high number of local connections as well as increased global efficiency and decreased connection length due to presence of long distance connections. Watts and Strogatz defined this type of network as "small-world network", where the network has higher local connectivity compared to random network and similar connection distance between two nodes as a random network. A small world network can also be described as having higher clustering coefficient than a random network and having equal path length as a random network.

Human brain is intrinsically organized in to large number of brain regions and even larger number of axonal connections between them only confined by the size of the cranium. In human brain, different brain regions in grey matter can be modeled as nodes in the network, while white matter tracts between these regions can be modeled as edges. This has enabled researchers to study the brain network topologies. Various researchers have observed small-world topological properties of structural brain connectivity. In one the first studies of Diffusion tensor imaging applied to human brain data, Iturria and

Colleagues identified brain regions as nodes and while matter tracts identified between regions using DTI as edges of the network. They observed a small-world architecture in the whole brain structural connectivity[28,29]. Figure 2 reproduced from the study by Sporns and Bullmore[30] describes various brain network topologies with respect to cost of connections and the efficiency of information transfer. As discussed earlier a lattice network topology that is representative of regular network topology as low- connection cost, combined with low- efficiency of global information transfer. On the contrary, a random brain topology has higher connection cost, along with higher global efficiency of information transfer. Sporns and colleagues described the brain network topologies as a complex topology, been constrained by the connection cost, and still wired to produce high global efficiency of information transfer similar to a small-world network[31].

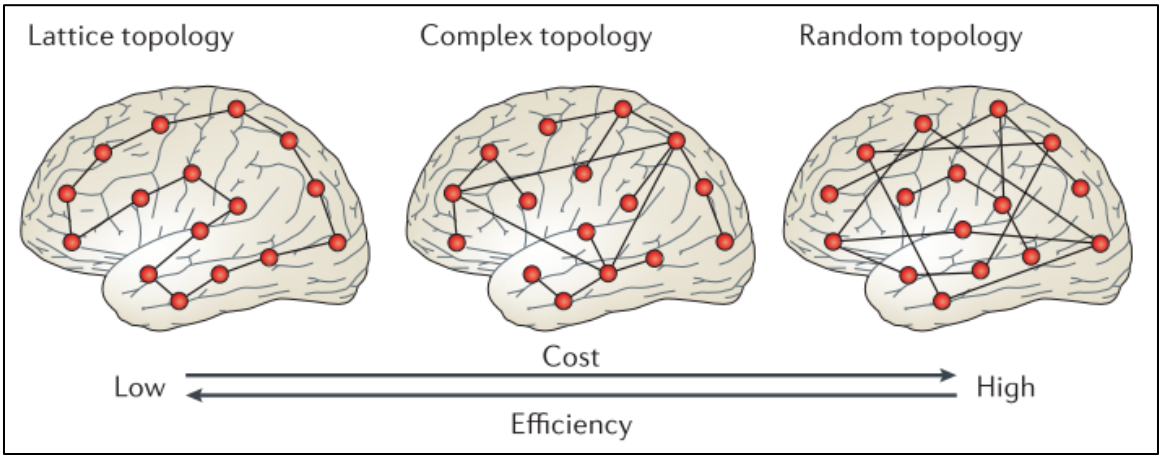

Figure 2: Examples of brain network topology (reproduced from Bullmore et al.,[30])

In addition to the structural connectivity defined by axonal projections between brain regions [32], temporal correlations between blood oxygen level dependent (BOLD) signals of brain regions are thought to represent intrinsic functional connectivity between

brain regions is termed as resting state functional connectivity (RSFC)[1]. One of the striking features of resting state functional connectivity is the selectivity whereas a set of brain regions shows high temporal dependencies of low-frequency BOLD fluctuations (LFF-0.01-0.1 Hz) with each other compared to other brain regions (such as left-right pre-central gyrus[1], posterior cingulate gyrus to Medial prefrontal cortex(MPFC)[16]). This selective functional connectivity between brain regions allows brain to be represented as a large-scale parsimoniously connected graph, where brain regions acts as nodes and the functional integration measures between them are described as edges[30,33–35]. These parsimoniously connected graphs of the brain are shown to have higher clustering coefficient and shorter path-length than a randomly connected graph with the same number of nodes and edges. Subsequently, numerous studies have described the benefits of brains small-world architecture with respect to global energy consumption[36,37], Information transfer[38], resistance to targeted node attacks[39], to name a few. In addition, this small-world network architecture of the brain has also been shown to be disrupted in the various neurological and psychiatric disorders implying importance of network architecture in healthy brain functions [40–42].

Although, numerous studies have described brain as a small-world network, one of the major limiting factors of these studies has been the definition of edge between the nodes. In most of the graph theoretical studies of whole brain RSFC, the edges of the brain network are defined as the Pearson's correlation between BOLD signal time series of two distinct region in the low-frequency range (0.01-0.1 Hz) [43] as a whole or sub-segments of the low-frequency range[39,44]. On the contrary, earlier EEG and MEG studies have focused on different brain network topologies across frequency bands in healthy

controls [45,46], though BOLD fMRI studies showing differential network topologies across frequency bands are sparse. In one of the earlier studies by Achard and colleagues have shown the presence network topologies across multiple frequency bands in an fMRI study where the higher frequency networks were found to be similar to the random network compared to the low-frequency networks[39]. Similarly in a very recent study Sasai and colleagues have shown differential network topological properties across various frequency bands, though the maximum frequency band studied by sasai and Colleagues is in the range 0.25 Hz[44].

2.5 Resting state fMRI and schizophrenia

Schizophrenia is a chronic, severe, and disabling mental disorder characterized by deficits in thought processes, perceptions, and emotional responsiveness (NIMH). According to an estimate, approximately 1.1% of U.S populations have the disorder that has profound effect on one's psychological and social behavior. Behavior symptoms of schizophrenia are broadly classified in three categories. "Positive" symptoms are defined as symptoms that are present/elevated in schizophrenia patients compared to controls (e.g. auditory and visual hallucinations). Negative symptoms are defined as psychotic behaviors that are absent/ deprecated in schizophrenic patients compared to healthy populations (e.g. empathy, day to day interactions). While positive and negative symptoms of schizophrenia can fluctuate, cognitive deficits remain relatively stable, and are already apparent in first-episode patients who have never received antipsychotic medicines[47,48]. In this regard, schizophrenia has largely been associated deficits in attentional, working memory, executive functions as well as auditory and visual hallucinations. These functions require acquisition, integration and analysis of complex

contextual information. These complicated cognitive tasks are related various brain networks comprised of multiple brain regions, which are thought to show disruptions at both regional level and in terms of integration between them.

Earlier studies on schizophrenia have characterized these disruptions at regional level specifically using anatomical MRI and CAT images. Schizophrenia has been characterized by large scale reductions in gray matter volume observed in medial temporal lobe, superior temporal gyrus, planum temporal pole (see Shenton et al. 2001 for a comprehensive review) [49]. These brain regions are known to be associated to auditory processing and specifically, simulations to the regions in superior temporal gyrus are known to result in auditory and hallucinations, hallmark symptoms of schizophrenia. In addition, studies have also shown abnormalities in frontal lobe of human brain, though these findings have not been consistent[49]. Anatomically these brain regions are thought to be part of heteromodal association cortex (HAC) that are thought be comprised of inferior parietal lobule, prefrontal cortex, planum temporal pole and broca's area[50].

In recent years, functional imaging studies have provided new insights regarding disruptions of functional integration between brain regions in schizophrenia and psychosis. There is now considerable evidence from resting state functional magnetic resonance imaging (rs-fMRI) studies that schizophrenia and associated psychotic disorders may be characterized by neurodevelopmental abnormalities involving loss of segregated systems and increased coherence between systems by young adulthood[51]. Several studies have reported disrupted functional integration in wide-spread brain areas, including, decreased connectivity amongst insular cortex, temporal lobe, prefrontal lobe

as well as increased connectivity between cerebellum and other brain regions[52]. Researchers have also studied the disruption of default mode network (DMN) in schizophrenia though the results are highly variable. Most of the studies have shown decreased connectivity of default mode network compared in schizophrenia patients compared to controls[53,54], while there has also been report of increased functional connectivity and activity of DMN in schizophrenic subjects and in first-degree relatives [55]. In addition, studies have also shown deficits in lower visual and auditory functioning in schizophrenic populations[56,57] that are known to be associated with auditory and visual hallucinations observed in schizophrenic populations. Similar to fMRI studies, EEG studies have also observed differential power distribution across brain regions and related disruptions in connectivity pattern in schizophrenic populations. Patients with schizophrenia are shown to have greater theta power during resting state conditions in frontal regions, but lower theta power in the frontal regions during attentional task performance [58]. Similarly, studies have also shown the presence of cross-frequency bindings between EEG rhythm and various resting state networks associated with schizophrenia that could conceivably disturb self-attentional processes[59]. In lieu of these results, the working hypothesis of neural network in schizophrenia is disintegrations between brain regions.

Despite the implications of such work, few studies to date have investigated different frequency bands within the low-frequency band of .01 to .1 Hz using rs-fMRI in schizophrenia, while no study has investigated BOLD frequency bands >0.1 Hz. In one of the earlier studies of BOLD signal power in schizophrenia, Hoptman et al [60] reported lower BOLD signal power in LFFs compared to matched healthy volunteers, in the

lingual gyrus, cuneus, and precuneus. They also observed greater BOLD signal power in the left parahippocampal gyrus within the sub-bands of LFFs (0.01-0.1 Hz). Similarly, Turner and colleagues observed, decreased BOLD signal power in posterior section of the brain in psychosis population and increased BOLD signal power in the frontal cortex regions compared to healthy volunteers, in a multisite psychosis study[61]. In contrast, Huang et al[62] reported that compared to healthy volunteers, antipsychotic drug-naïve first-episodic schizophrenia patients demonstrated significantly lower BOLD signal power within the range of 0.01–0.08 Hz in the medial prefrontal cortex and concomitant increases within the right and left putamen. More recently, Yu and colleagues [63] examined resting state fMRI activity in 3 different frequency bands including (1) slow-5 (0.01–0.027 Hz); (2) slow-4 (0.027–0.08 Hz); and (3) the standard band of 0.01–0.08 Hz in 69 patients with schizophrenia and 62 healthy controls. They reported that low frequency fluctuations in slow-4 were higher overall in the basal ganglia, cingulate cortex and fusiform gyrus, but lower overall in the middle temporal gyrus, lingual gyrus, inferior frontal gyrus and ventromedial frontal gyrus within slow-5. Moreover, these authors noted that several brain regions demonstrated significant frequency band x group interactions suggesting that spontaneous neural activity might be frequency dependent among patients with schizophrenia. Although, the results of these studies are somewhat consistent regarding the brain regions implicated in psychosis, they are inconsistent regarding the direction of the effect.

Summary

Based on the extensive literature review, we can establish that resting state functional magnetic resonance imaging is a well-established, reliable, robust and widely

used neuroimaging method to study changes in human brain function across various neuroclinical populations. One of the limiting factors of resting state fMRI is the focus on low-frequency (0.01-0.1 Hz) BOLD signal fluctuations, due to limitations of temporal resolution of fMRI. This has resulted in a knowledge gap with respect to possible neuro-cognitive implications of resting state BOLD signal in frequencies >0.1 Hz, its effects on whole brain network topologies as well as frequency band specific implications of resting state fMRI in neuro-clinical populations such as psychosis. Recent advancements in parallel imaging sequences, have drastically improved the temporal resolution of fMRI and there remains a unique opportunity to use this advancements to explore the frequency based resting state functional connectivity and its neurocognitive implications.

CHAPTER III

METHODOLOGY

In order to investigate presence of RSFC in higher frequency BOLD fluctuations, and to understand its effect on whole brain network topologies and in neuropsychiatric diseases, we designed three distinct projects pertaining to each of the research goals. In the first project, we aim to use the recently acquired, open-access, high temporal resolution data to estimate and quantify frequency specific RSFC at whole brain level. Based on the results obtained in the first project, we aim to study the effect of frequency specific RSFC on whole brain network topologies. In the third project, we aim to use the voxel-vise properties of BOLD signal power to study the effect of psychosis on resting state parameters across various frequency bands. By combining results from these three cohesive projects, we aim to establish a framework for interpretation of RSFC in frequency bands higher than 0.1 Hz.

3.1 Estimating and quantifying frequency specific RSFC

3.1.1 Subject recruitment

In order to study the resting state BOLD signal in the frequency bands higher than 0.1 Hz, one needs to acquire the whole brain resting state fMRI data at very high sampling frequency. Due to recent advancements in the parallel imaging procedures[22], it is possible to acquire the whole brain fMRI data with the temporal resolution of 500 ms. In the current study, we obtained these data from an open-access data sharing repository,

Enhanced Nathan Kline Institute-Rockland (NKI) Sample. Enhanced Nathan Kline Institute-Rockland (NKI) Sample[64] is an endeavor headed by Dr. Michael Milham (MD, PhD) aimed at creating a large-scale (N>1000) community sample of neuroimaging data across the human life-span from the participants of Rockland county in the state of New York. For this study, we used the resting state data and the anatomical MPRAGE data acquired from these subjects. The scanning parameters for Resting state scan are, sampling time/Time of Repetition (TR) =645 ms, field of view (FOV) =240x240 mm^2, matrix size/image size = 74 x 74, number of slices = 40, Time of Echo (TE) = 30 ms, number of time points/number of volumes = 900, with a spatial resolution of 3mm isotropic voxel. These scanning parameters resulted in resting state fMRI scan of ~10 minutes. For each of the subjects, a high-resolution T1–weighted magnetically prepared gradient echo (MPRAGE) image was also obtained (FOV=250x250 mm^2, TR=1900ms, TE=2.52ms, # of slices =176, voxels size=1x1x1 mm). Further information about subject scanning can be obtained from project website (http://fcon_1000.projects.nitrc.org/indi/enhanced/). We acquired a total of 129 subjects from the first release of NKI-Enhance Rockland sample. In order to create a homogenous sample from the community sample, we applied multiple selection criterion to the subjects obtained from the first release (further discussed in the results section).

3.1.2 Data processing

In the current study, we implemented a processing pipeline that was developed using AFNI [65], FSL[66] (http://fsl.fmrib.ox.ac.uk/fsl/fslwiki/FSL) and in-house developed MATLAB (MATLAB, 7.14, The MathWorks Inc., Natick, MA, 2000) programs [67]. Figure 3 displays various data processing steps and corresponding output filename. Data

pre-processing steps included discarding the first 20 time points (~13 s) to account for T1 relaxation effects, rigid body motion correction with respect to mean image and skull removal for anatomical MPRAGE images. For each of the subjects, motion parameters were calculated to reflect head motion in six directions with respect to the mean image. First order derivative of the motion parameters were also calculated. High resolution MPRAGE image were segmented into gray matter (GM), white matter (WM) and cerebral spinal fluid (CSF) and probability maps were created representing each of the three tissue types. Each of the subject's segmented probability images were down-sampled to match BOLD fMRI data and thresholded at $p > 0.95$ to create subject specific masks for CSF and WM. These masks were used to extract time-series from CSF/WM from pre-processed resting state BOLD fMRI data. Principal component analysis was performed on time-series extracted from CSF and WM masks. The first 5 principal components were extracted that may reflect signals due to physiological and thermal noises[68,69]. A total of 22 regressors time series (6 motion parameters, 6 first-order derivatives of motion parameters, first 5 principal components of CSF and WM signal) were regressed out from the BOLD fMRI data using a linear regression model. Prior to independent component analysis and seed based correlation; the resting-state functional images were normalized into MNI standard space using non-linear registration implemented using FSL-FNIRT. Subsequent data processing included spatial smoothing with 6 mm FWHM Gaussian blur.

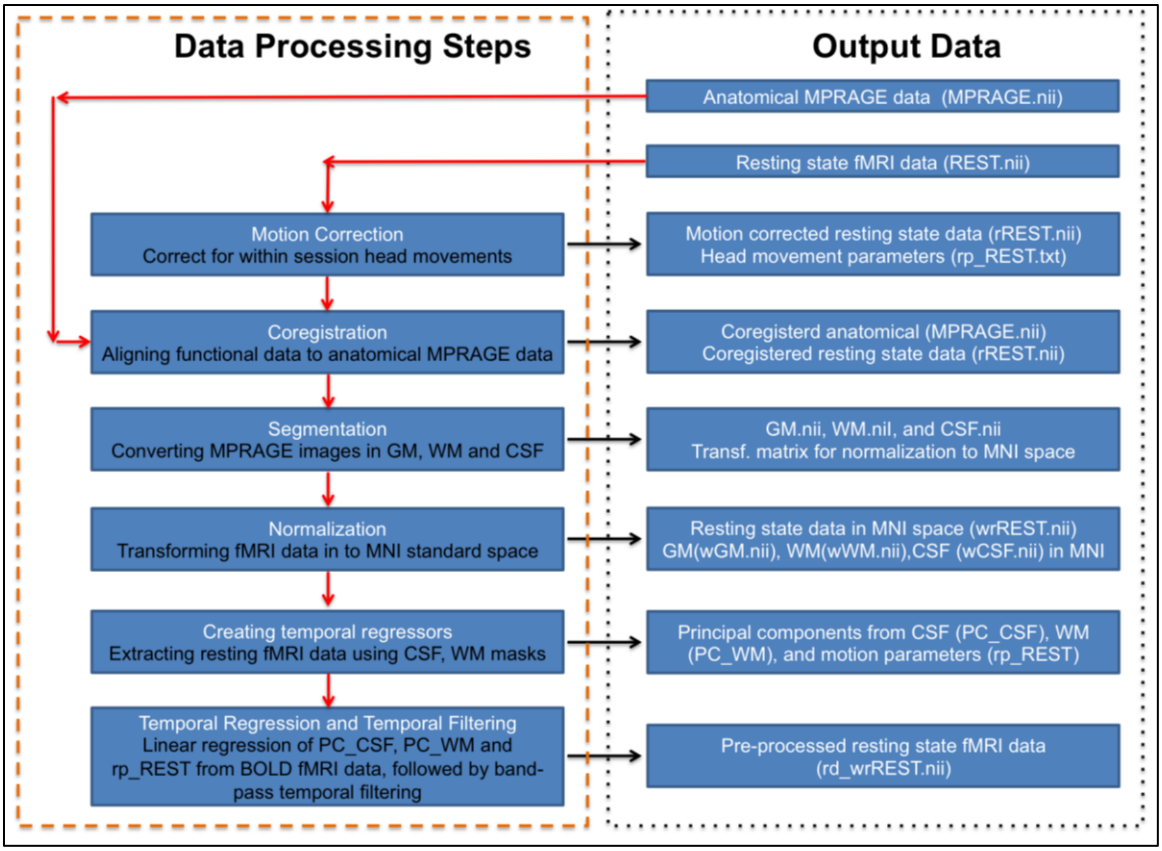

Figure 3: Data processing steps and corresponding output information

Following data pre-processing, BOLD fMRI data was temporally filtered into five distinct frequency bands in order to study frequency specific functional integration. These frequency bands were (1) slow-5 (0.01-0.027 Hz) (2) slow-4 (0.027-0.073 Hz) (3) slow-3 (0.073-0.198 Hz) (4) slow-2 (0.198-0.5 Hz) and (5) slow-1 (0.5-0.75 Hz), coinciding with frequency bands defined using electrophysiological [7,9] and fMRI studies[70]. The frequency bands slow-5 and slow-4 mainly represents the frequency range (0.01-0.073 Hz) widely employed in resting state BOLD fMRI studies. Slow-3 represented combination of both frequencies from classic frequency band (0.073-0.1 Hz) and from frequency band discarded through temporal filtering (0.1-0.198 Hz); while slow-2 represented BOLD fMRI fluctuations that were generally considered highly contaminated with respiration signal. Classically, slow-1 frequency band is defined by a bandwidth of 0.5-1.5 Hz but

due to limitation of sampling frequency in the current fMRI study, we have restricted slow-1 band between 0.5-0.75 Hz. In addition, pre-processed BOLD fMRI data without temporal filtering (though the series were demeaned, leaving the bandwidth as 0.01-0.75 Hz) were also used in subsequent analysis and will be referred as noFILT.

3.1.3 Data Analysis

Group Independent Component Analysis

The relative contributions of each frequency band to different RSNs, as well as frequency-specific characteristics of a given network, were studied using a data driven approach. To analyze the former, first probabilistic group ICA, using temporal concatenation approach in MELODIC software[3], was performed on unfiltered BOLD fMRI data. RSNs derived using this approach pertains to whole-frequency band (0.01-0.75 Hz). 40 independent components were derived. Spatial correlation was conducted between these group level IC maps and 1000-Functional Connectome Project (FCP) IC maps to identify and compute spatial overlap with RSNs[67]. For each of the identified RSNs, a corresponding group IC time series was obtained. Fast Fourier transformation (FFT) was performed on the group IC time series of each of the RSNs. The relative power contribution of each frequency band to the IC time series was calculated as the ratio of the power in the given frequency band to the total power contained in the entire bandwidth (0.01-0.75 Hz) (Figure 5). In order to study frequency specific characteristics of various RSNs, group ICA was also performed on each of the five sets of temporally filtered BOLD fMRI data. Similar to above mentioned analysis, spatial correlation

followed by visual comparison with group IC maps from FCP-1000 dataset was used to identify RSNs (figure 6).

Seed based correlation

We conducted seed based correlation using the seven seed regions as defined by Fox et al., [16], Wu et al.,[11]and Biswal et al.,[20] Seed regions from the frontal eye field (FEF; 25, -13, 50 MNI space), inferior parietal sulcus (IPS; -25,-57, 46), middle temporal gyrus (MTG; -45, -69, 2) and pre-central gyrus (PCG; -45,-9,39) were selected from task positive networks, while seed regions lateral parietal cortex (LPC; -45,-67,36), medial prefrontal cortex (MPF; -1, 47, -4), posterior cingulate cortex (PCC; -5, -49, 40) were from task negative networks. For each seed, a 5mm sphere was created in Montreal Neurological Institute (MNI) standard space. The average time series of each seed region was extracted and correlated with all brain voxels to derive subject-level, seed based correlation maps for a specific seed. This map was converted into z-score values using Fisher's r-z transformation. MELODIC mixture modeling was also applied to z-score images in order to account for the temporal smoothness and increased degrees of freedom introduced due to use of multiband imaging sequence[22]. Group level correlation maps were calculated for each of the seven seed regions by performing one-sample t-tests ($p<0.05$, FDR corrected). This process was repeated for each of the five frequency bands and for each of seven seed regions resulting in 35 group level correlation maps. This group level correlation maps were visualized with the BrainNet Viewer[71] (http://www.nitrc.org/projects/bnv/) (figure 7). In order to quantify spatial extent for each of this group level correlation maps, a spatial extent fraction for each of the maps was

defined as number of GM voxels passing the statistical threshold ($p<0.05$, FDR corrected) divided by total number of GM voxels in MNI space (figure 8).

Functional connectivity strength for each seed region was calculated on first level subject specific maps. To avoid biases due to differences in spatial extent observed across frequency bands, RSFC strength was calculated from a set of ROIs defined based on FCP-1000[20] group level connectivity maps. FCP-1000 group level connectivity maps included six out of seven seed regions used in current study with exception of PCG, hence group level IC map representing motor network from FCP-1000 was used for PCG. Each of the group level seed based correlation map/IC maps from FCP-1000 project was divided in to brain regions that showed positive and negative correlation with the seed region. MNI coordinates of the voxels showing maximum positive/negative correlation were extracted from this brain regions and 5 mm sphere was created surrounding this coordinates in MNI space. Mean positive and negative connectivity strength was calculated from each of these ROIs for a subject and for a specific frequency band. This process was repeated for each of the seven seed regions for each of the 5 frequency bands across 21 subjects. Group level RSFC strength was calculated by taking mean across subjects for each of the frequency bands and for all the seven seed regions. Table 1 lists the ROI coordinates derived for positive and negative connectivity strength. Figure 4 displays the ROIs on the glass brain surface.

Table 1: MNI coordinates (LPI) for the ROIs defined for calculation of connectivity strength.

Seed Name	X	**Y**	Z	ROI Name
Lateral Parietal Sulcus (LPC)				
Positive connectivity				
	3	**42**	**33**	**Left Cingulate Gyrus/ BA 31**
	45	66	36	Left Angular Gyrus
	39	-18	48	Left Superior Frontal Gyrus/ BA 8
	-51	63	36	Right Angular Gyrus
Negative connectivity				
	-42	-9	-3	Right Insula/ BA 13
	-6	-15	36	Right Cingulate Gyrus
	42	-6	0	Left Insula
	-63	30	27	Right Inferior Parietal Lobule / BA 40
	12	90	30	Left Cuneus / BA 19
	60	30	21	Left Superior Temporal Gyrus
Medial Prefrontal Gyrus (MPF)				
Positive connectivity				
	-3	-48	-3	Right Medial Frontal Gyrus/ BA 32
	0	21	36	Left Cingulate Gyrus
Negative connectivity				
	-21	69	51	Right Precuneus
	21	66	51	Left Precuneus / Left BA 7
	54	63	-9	Left Middle Occipital Gyrus/ BA37
	-54	57	15	Right Superior Temporal Gyrus/ BA22
	-51	-9	30	Right Inferior Frontal Gyrus
	48	-6	24	Left Inferior Frontal Gyrus
	-27	0	60	Right Middle Frontal Gyrus/ BA 6
Posterior Cingulate Cortex (PCC)				
Positive connectivity				
	6	48	39	Left Cingulate Gyrus
	51	60	27	Left Middle Temporal Gyrus / BA 39
	-51	57	27	Right Superior Temporal Gyrus
Negative connectivity				
	-42	-3	0	Right Insula
	42	-3	0	Left Insula /BA 13
	-60	27	48	Right Post-central Gyrus
	-6	-9	51	Right Superior Frontal Gyrus/ BA 6

	-48	-45	3	Right Inferior Frontal Gyrus
	-54	60	-12	Right Fusiform Gyrus / BA 37
	57	33	51	Left Post-central Gyrus
	51	69	-9	Left Middle Occipital Gyrus
Frontal Eye Field (FEF)				
Positive connectivity				
	-24	12	51	Right Pre-central Gyrus
	24	9	57	Left Middle Frontal Gyrus
Negative connectivity				
	0	42	36	Left Cingulate Gyrus
	51	60	42	Left Inferior Parietal Lobule/ BA 39
	-51	54	36	Right Supramarginal Gyrus
	-33	-63	3	Right Superior Frontal Gyrus/ BA 10
	36	-63	3	Left Middle Frontal Gyrus/ BA 10
Inferior Parietal Sulcus (IPS)				
Positive connectivity				
	24	57	45	Left Superior Parietal Lobule/ BA 7
	24	57	45	Left Brodmann area 7
	-27	60	48	Right Superior Parietal Lobule
	51	60	-12	Left Fusiform Gyrus / BA 37
	48	-6	27	Left Inferior Frontal Gyrus / BA 9
	-51	54	-15	Right Fusiform Gyrus / BA 37
	27	0	51	Left Middle Frontal Gyrus
Negative connectivity				
	0	-57	3	Left Middle Frontal Gyrus
	-6	51	27	Right Cingulate Gyrus
	-57	60	30	Right Supramarginal Gyrus
	57	63	33	Left Supramarginal Gyrus / BA 39
Middle Temporal Gyrus (MTG)				
Positive connectivity				
	45	69	-3	Left middle occipital gyrus
	-48	66	-6	Right middle occipital gyrus
	-24	60	54	Right Superior Parietal lobule
	27	54	57	Left Superior parietal lobule
Negative Connectivity				
	0	-39	33	Left middle frontal gyrus
	0	36	36	Left Cingulate gyrus
	-51	60	45	Right inferior parietal lobule
	51	57	45	Left inferior parietal lobule
	-42	-21	45	Right middle frontal gyrus
	45	-18	45	Left middle frontal gyrus / BA 8

Pre-central gyrus (PCG)				
Positive connectivity				
	-60	9	33	Right pre-central gyrus
	57	9	33	Left pre-central gyrus
	3	6	54	Left medial frontal gyrus / BA 6
	0	18	54	Left medial frontal gyrus
	-27	30	60	Right post-central gyrus / BA 3
	30	30	60	Left pre-central gyrus
Negative Connectivity				
	-39	78	33	Right superior occipital gyrus
	0	75	48	Left precuneus
	57	45	42	Left inferior parietal lobule/ BA 40

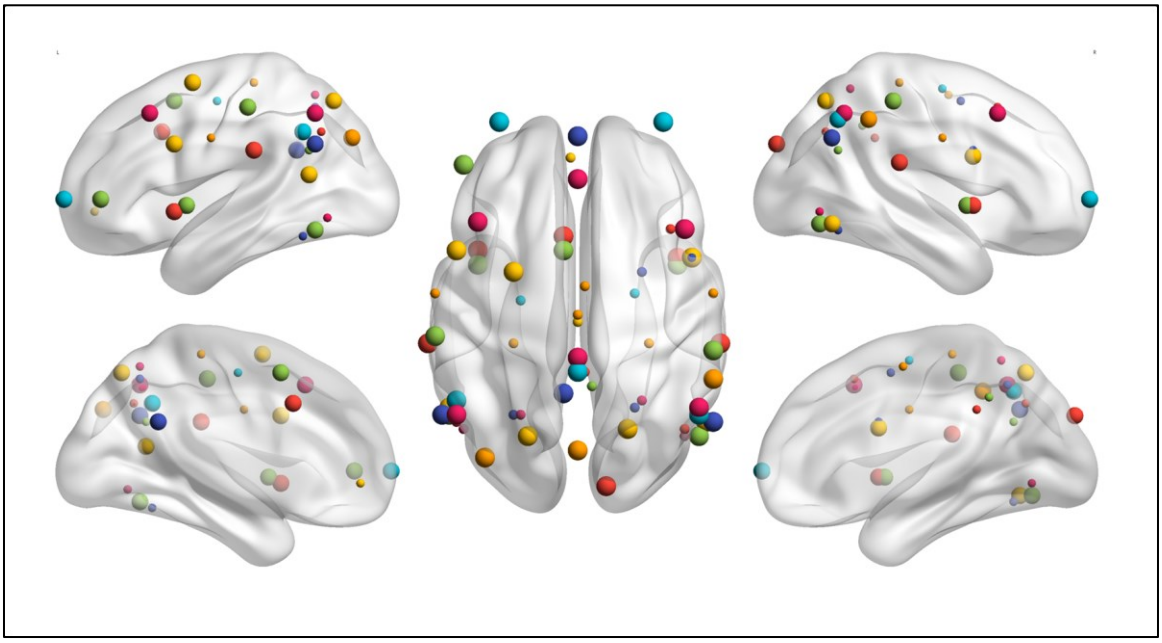

Figure 4: Regions of interests implemented for connectivity analysis overlaid on the glass brain surface.

Inter-subject covariance of BOLD signal power

In a recent study, Taylor and Colleagues[67] have shown that brain regions in a given network, has high synchronicity of amplitude of BOLD signal in low-frequency

bands. Using a large-scale resting state fMRI data (n=198 subjects), they observed significant correlation between amplitude of BOLD signal power, between regions of resting state networks across subjects, though these results were only pertaining to low-frequency BOLD fluctuations. In order to study the inter-subject covariance of power of BOLD signal fluctuations in different frequency bands, we calculated measure called similar to the index, 'Amplitude of Low-frequency Fluctuations' as defined by Zhang and Colleagues[72]. We define 'Amplitude of Frequency Fluctuations (AFF)' as a generalized term representing BOLD signal amplitude in a particular frequency band. For each of the subject, pre-processed BOLD fMRI data was temporally filtered in one of the five-different frequency bands (slow-1 to slow-5). Fast Fourier transformation was applied to this temporally filtered time series to derive voxel-vise power spectrum for the given frequency band. Square root of this power spectrum was calculated to derive voxel-vise amplitude measure. Average amplitude was calculated to derive voxel-vise map of amplitude measures pertaining to each frequency band. Amplitude value at each of the voxel was divided by whole brain average amplitude measure. This process was repeated for each of the five-frequency bands.

These voxel-wise BOLD signal amplitude measures were further used to study functional covariance networks as a means of deriving functional integration between brain regions using voxel-vise measure. Briefly, covariance networks identify a set of brain regions that display higher inter-subject variance specific to a BOLD signal parameter[67]. In the current study, signal amplitude in five different frequency bands was used a voxel-vise measure. For a given frequency band, average BOLD signal amplitude was calculated for 23 ROI masks as defined by group ICA (Table 1). These average

amplitude measure is treated as a variable while the individual subjects are treated as observations. Pearson's correlation coefficient was calculated for each of the 253 ROI pairs (n*(n-1)/2, n=23 ROIs). These resulted in a 23x23 dimension symmetrical correlation matrix. Significant inter-subject correlation were identified ($p<0.1$, FDR corrected) and displayed on a whole-brain surface maps using BrainNet Viewer [71] (figure 9). This method was repeated for each of the five frequency bands (slow-1 to slow-5) to derive frequency specific covariance matrices across subjects for each frequency band.

Time-frequency analysis for BOLD signal

Recent studies have shown that resting state BOLD signal, although studied as a stationary signal, has time varying characteristics. Chang and Glover used wavelet analysis to study changes in BOLD signal power across the scanning duration[73]. In order to study the changes in frequency content of BOLD signal across the scanning time, we performed time frequency analysis on seven different seed regions time series as mentioned earlier. We extracted mean time series from each of the seven seed regions for each of the subjects using unfiltered resting state BOLD fMRI data. We performed time-frequency analysis on this seed regions time series using the wavelet analysis toolbox as performed by Chang et al[73](figure 10). In addition, we also implemented cross-wavelet coherence analysis to study the presence of coherence between seed regions across different frequency bands (figure 11).

3.2 Effects of frequency based RSFC on whole brain network topology

3.2.1 Subject recruitment

Similar to the project 1, studies of frequency based changes in RSFC and their effect on whole brain network topology requires resting state BOLD fMRI data collected at high temporal resolution. To this end, we use the same online data repository as used in the first project. In the second project, we obtained the data from the second release of NKI-enhanced Rockland sample that contained a total of 170 subjects' resting state BOLD fMRI and anatomical MPRAGE data. The scanning parameters for Resting state scan are, TR =645 ms, field of view (FOV) =240x240 mm^2, matrix size/image size = 74 x 74, number of slices = 40, TE = 30 ms, number of time points/number of volumes = 900, with a spatial resolution of 3mm isotropic voxel. These scanning parameters resulted in resting state fMRI scan of ~10 minutes. For each of the subjects, a high-resolution T1–weighted magnetically prepared gradient echo (MPRAGE) image was also obtained (FOV=250x250 mm^2, TR=1900ms, TE=2.52ms, # of slices =176, voxels size=1x1x1 mm). Further information about subject scanning can be obtained from project website (http://fcon_1000.projects.nitrc.org/indi/enhanced/). In order to create a homogenous sample from the community sample, we applied multiple selection criterion to the subjects obtained from the first release (further discussed in the results section).

3.2.2 Data processing

A data processing scheme similar to the one implemented in our earlier publication was implemented[74,75]. For each of the subjects, first 20 time-points (~13 s) were removed to account for T1- relaxation effects. In the next step, motion correction

was performed on each of the functional images by registering functional images to the mean image using 'realign' function in SPM. Later, each of the functional images was co-registered to the anatomical MPRAGE image. Anatomical images were segmented in to three different tissue probability maps GM, WM and CSF using 'new segment' tool in spm8 and corresponding deformation fields were derived. In the next step, these deformation fields were used in normalization process to transform each of the functional images in to MNI standard space. The tissue probability maps derived in the segmentation step were thresholded at probability level 0.95 and binary mask representing CSF and WM were created. These binary maps were used to extract BOLD time series from resting state fMRI data and principal components analysis was performed on these CSF/WM time-series. A general linear model based regression analysis was performed on the BOLD fMRI data to minimize the effect of physiological noises. The regression model consisted of 34 regressors time series containing 5 principal components of WM, 5 principal components of CSF, and 24 motion time series based on Friston 24-model[76,77] (6 raw motion time series defining subjects motion during the resting state scan, 6 quadratics of raw motion time series, 6 auto regressive time series of motion parameter and 6 quadratics of the auto regressive motion time series). Following linear regression, the residual time-series were temporally filtered in to five distinct frequency bands, slow-1 (0.5-0.75 Hz), slow-2 (0.198-0.5 Hz), slow-3 (0.073-0.198 Hz), slow-4 (0.027 Hz -0.073 Hz) and slow-5 (0.01-0.027 Hz) using 3dBandPass function in AFNI. Each of the filtered BOLD fMRI dataset was spatially smoothed using 6mm FWHM Gaussian kernel.

3.2.3 Data analysis

Graph-theoretical analysis

A graph typically consists of a set of nodes and connections between them defined as edges. In order to study whole brain graph theoretical analysis, 160 nodes were defined in the brain based on coordinates defined by Dosenbach and colleagues[78]. Edges between any 2 nodes were defined as Pearson's correlation between the filtered resting state BOLD time series of the specific nodes. For each of the nodes, 6 mm sphere was created around the center coordinate defined by Dosenbach and colleagues in MNI standard space. For each of the ROIs the average BOLD time series was extracted from filtered BOLD fMRI data. A 160x160 symmetric correlation matrix was calculated by performing Pearson's correlation between average time series of each of the 12720 ROI pairs. This process was repeated for each of the subjects and for each of the five frequency bands resulting in 135 unique connectivity matrices. Each of these matrices was converted in to Z score using fisher's r to z transformation and absolute values were derived to study whole brain connectivity. In order to study, differences in graph theoretical properties of whole brain functional connectivity across frequency bands, graphs were created at both subject level and also at group level. In order to create group level graphs, the average correlation matrix was calculated across subjects for each of the five frequency bands (figure 12).

In order to create binary, un-directed graphs, each of the correlation matrices was thresholded at fix sparsity values that ranged from 0 to 1 (0-100%) with interval of 0.01. Sparsity can be defined as the ratio of number of edges in the adjacency matrix to the

total number of edges in the network. Although, earlier studies have mentioned small-world range to be present between sparsity 0.1 to 0.5, in the current study we have implemented the sparsity from 0-1 to completely review the changes in graph theoretical properties for whole brain connectivity across frequency bands. By applying sparsity threshold to each of the correlation matrices, we created binary, un-directed graphs for each of the subjects at each of the frequency band across all the sparsity values. These graphs although may have different Pearson's threshold across different subjects, have the same number of connections at a particular sparsity value.

For each of the graphs, we calculated graph theoretical properties using two openly available toolboxes, (1) Brain connectivity toolbox (BCT)[79]and (2) gephi (GEPHI)[80]. In the first step, we aim to determine whether the whole brain network displayed small –world properties across different frequency bands. To this end, we calculated a set of global parameters that describes the small-world properties of the whole brain network. These global parameters included clustering coefficient (C_{orig}, clustering_coef_bu.m, BCT), characteristic path length (L_{orig}, charpath.m, BCT), global efficiency (E_{glob}, efficiency_bin.m, BCT) and local efficiency (E_{local}, efficiency_bin.m, BCT). In addition, we also calculated a total of 100 random networks preserving the same number of nodes, edges, and degree distribution as the real networks at each of the sparsity range (randmio_und.m, BCT). For each of the random networks, we calculated clustering coefficient (C_{rand}) and characteristic path length (L_{rand}) describing whole brain network architecture. Normalized clustering coefficient (γ) was calculated by taking ratio of C_{orig} to C_{rand} (C_{orig} / C_{rand}) and normalized path length (λ) was calculated by taking ratio of L_{orig} to L_{rand} (L_{orig} / L_{rand}) at each of the sparsity values. A network is said to be small-

world network at a sparsity value if the Gamma is higher than 1 and Lambda is equal to 1[27]. We calculated the ratio of gamma to lambda (gamma/lambda) across the 100 sparsity values to determine the sparsity range where each of the networks showed small-world properties. We observed that the whole brain functional connectivity displayed small world properties at sparsity range from 0.1 to 0.5. Based on this result, further analysis was focused in this narrow 0.1-0.5 sparsity range (figure 13 and figure 14).

Synchonizability

In order to calculate synchonizability parameter, similar to the one used by Basset and colleagues[81], we created a subject-wise adjacency matrix at sparsity 30 and also calculated degree for each of the nodes in the network at the same sparsity value. We derived a normalized Laplacian matrix by replacing edge between nodes i and j by the value M where

$M = \frac{-1}{\sqrt{(D_i \times D_j)}}$ Where D_i and Dj are the degrees of node j and i respectively.

We replaced the diagonal in the Laplacian matrix by 1. We calculated Eigen values of this Laplacian matrix for each of the five frequency bands across all the subjects. We calculated the ratio of the second smallest eigenvalue and the highest Eigen values to derive synchonizability (S) for each of the frequency bands.

Nodal properties

In addition, we also calculated a set of nodal parameters, describing graph theoretical properties for each of the nodes. For each of the node, we calculated degree (D, degrees_und.m, BCT); between centrality (BC, betweenness_bin.m, BCT) and Eigen

vector centrality (EC, eigenvector_centrality_und.m, BCT) across the sparsity range 0.1-0.5. One of the aims of the current study was to identify differences in the nodal properties across frequency bands and to identify whether network architecture differences observed across the frequency bands are centered on specific brain regions. To this end, we identified hubs of a given brain network based on three different nodal properties.

In order to determine the hubs of the whole brain network, we used subject based connectivity matrices. We use three different nodal properties of degree, between centrality and eigenvector centrality for deriving hubs in the whole brain network. We calculated hubs at the sparsity of 30. For a given nodal property X_{node}, in the first step, we derived nodal property at the sparsity of 0.3 for each of the subjects. This results in 160 distinct values for each of the node for each of the subject (X_{node_s30}). In the next step, we calculated mean of X_{node_s30} across subjects resulting 160 mean nodal properties for each of the node in network ($X_{mean\_node\_s30}$). Each of this mean nodal property ($X_{mean\_node\_s30}$) was converted in to z scores. A specific node was identified as hubs if the z score of the particular node was higher than 1.5. Based on this analysis, we identified three different sets of hubs pertaining to degree, betweeness centrality and Eigen centrality (figure 15-18).

Modularity architecture

One of the important aspects of network architecture is the group of nodes that show higher number of connections to nodes within the group compared to the nodes outside the group. These groups of nodes are referred as modules. In order to study

differences in modularity architecture between the frequency bands, we calculated the modularity using the average correlation matrix for each of the frequency bands. For each of the five distinct correlation matrixes, we calculated modularity quotient (Q) using the Louvain algorithm (modularity_louvain_und.m, BCT) across the whole sparsity range. In order to display the modular architecture, we extracted the graph for each of the five frequency bands at sparsity of 30. This graph was further analyzed with the open source software (GEPHI) to derive and display the modular architecture across the frequency bands. In order to display, the nodes belonging to each of the module distinctly, each node was color coded to a specific module and displayed using the BrainNet Viewer (figure 21)[71].

In order to assess the effect of distance between two regions on the frequency specific RSFC strength, we calculated Pearson's correlation between the Euclidian distances between the two ROIs and the RSFC strength (defined as correlation of BOLD signal in specific frequency bands). Euclidian distance between the two ROIs was defined as

$$D_{ij} = \sqrt{(X_i - X_j)^2 + (Y_i - Y_j)^2 + (Z_i - Z_j)^2}$$

Where (X_i, Y_i, Z_i) and (X_j, Y_j, Z_j) represent the three-dimensional MNI coordinates for ROI j, and i respectively.

In order to avoid cross-hemispheric connections that may underestimate the actual distance between two ROIs, Euclidian distance was calculated for left and right hemisphere separately. Euclidian was calculated for each of the 12720 ROI pairs and

correlated with mean RSFC strength between each of the ROI pairs for each of the frequencies (figure 22).

3.3 Disruption of frequency specific BOLD signal power in schizophrenia

3.3.1 Subject recruitment

In order to study the disruptions of frequency band specific power in psychosis, it is very important to acquire the high temporal resolution resting state BOLD fMRI data in such population. Unfortunately, there is no publicly available data of psychosis patients using multi-band imaging sequences. In this regard, we use the open-access data repository- The Center of Biomedical Research Excellence (COBRE) to acquire data from schizophrenia patients and corresponding healthy controls. A total of 98 subjects' BOLD fMRI and anatomical MPRAGE data was acquired from this repository. The scanning parameters for the rs-fMRI scan were TR=2.0s, TE: 29 ms, matrix size=64x64, 32 slices, voxel size=3x3x4 mm^3, and an anatomical MPRAGE scan was obtained with TR/TE/TI = 2530/[1.64, 3.5, 5.36, 7.22, 9.08]/900 ms, matrix = 256x256x176, voxel size =1x1x1 mm. Individuals were instructed to keep their eyes open during the scan. Further information about the specific scanning paradigm for the COBRE dataset can be obtained from http://fcon_1000.projects.nitrc.org/indi/retro/cobre.html. Similar to previous projects, we applied multiple selection and motion thresholding criteria to create a homogeneous sample of subjects (further discussed in results sections 4.3.1).

3.3.2 Data processing

Data processing was the same for all individuals regardless of disease condition and used SPM 8 (http://www.fil.ion.ucl.ac.uk/spm/), FSL 5.0 [66],

(http://fsl.fmrib.ox.ac.uk/fsl/fslwiki) and AFNI [65] (http://afni.nimh.nih.gov/afni/). In the first step the first 5 time-points (10s) were removed from the rs-fMRI data to eliminate T1-relaxation effects. In the second step, we performed motion correction using SPM's realign function to align each individual's BOLD fMRI data to the mean of the images. During motion correction, head movement was recorded in 6 directions and used to exclude individuals with significant motion (as defined above) and to regress out the effects of motion on BOLD signal. Following motion correction, individuals' rs-fMRI data were coregistered to the anatomical image. Each anatomical image was later segmented into GM, WM and CSF probability maps using the 'New Segment' function in SPM8 while deriving a deformation field. Following segmentation individuals' BOLD fMRI data were transformed to MNI standard space using the deformation field derived during the segmentation step. For all individuals, probability maps for cerebrospinal fluid and white matter were thresholded at $p>0.95$ to create CSF and WM masks respectively. Using these masks the BOLD time series was extracted from the resting state dataset and the first five principal components were derived. A COMPCORR and friston-24 based GLM model was implemented to reduce the effect of physiological noise and motion time series from the BOLD fMRI data using FSL. The GLM model thus included a total of 34 regressor time-series (5 principal components of white matter, 5 principal components of cerebrospinal fluid, 6 motion parameters, 6 autoregressive motion parameters, and 12 quadratic models of the motion parameters). Residual time-series were extracted for each voxel following regression and used in subsequent analyses.

3.3.3 Data analysis

Following regression, each individual's BOLD time-series was temporally band-pass filtered in low- frequency bands (0.01-0.1 Hz) using AFNI's 3dBandPass program. Following temporal filtering, group independent component analysis was performed using a temporal concatenation approach available in FSL melodic and 20 independent components were extracted. Each of the 20 independent components was compared with the independent components derived from FCP-1000 maps[20] using software developed in-house[67] to identify 14 meaningful resting state networks. Each of the 14 resting state networks in this study was segmented in to 1-7 noncontiguous clusters using AFNI program 3dClustSim (see figure 23). For each of the cluster, the peak voxel coordinates were derived. A 6 mm sphere was placed around the peak coordinates to create the regions-of-interest. A total of 47 regions-of-interest (see Table 2) were used in this study. For each of the region-of-interest we extracted power in the BOLD signal for each individual in each of the 3 frequency bands as described below.

Frequency-Specific Amplitude of BOLD Signal Fluctuations

We segmented the overall BOLD frequency band from 0.0-0.25 Hz (TR-2 s, sampling frequency-0.5 Hz) into 3 distinct frequency bands including slow-2 (0.199-0.25 Hz), slow-3 (0.072-0.198 Hz) and slow-4 (0.027-0.073 Hz) based on earlier studies [70,74]. For each of these three distinct frequency bands, we computed power of the BOLD signal based on methods defined by Zhang and colleagues[72] using the "3dRSFC" AFNI command [82]. Briefly, we computed voxel-level fast Fourier transformations for individuals' BOLD fMRI time-series across the whole frequency band to derive power at

each frequency. The square-root of power at each frequency band was obtained to derive frequency specific amplitude measures. This frequency specific amplitude was averaged across the frequency bands slow-2, slow-3 and slow-4 to derive voxel-level frequency band specific amplitude measures. For each individual, amplitude at each voxel was normalized by mean amplitude across the whole brain to derive a measure similar to mALFF for each frequency band. These measures are similar to the ones used in earlier studies describing frequency based amplitude differences in schizophrenia [60,63]. In contrast to earlier studies that focused on BOLD fluctuations in traditional low-frequency bands (<0.1 Hz), we also investigated the power of BOLD fluctuations in higher frequency bands. As the term ALFF traditionally applies to the power of BOLD fluctuations in only low-frequency bands (<0.1 Hz), here we define AFF (**A**mplitude of **F**requency **F**luctuations) as a general term to describe the amplitude of various BOLD frequency fluctuations. Additionally, we did not utilize fractional measures given that fALFF measures traditionally calculate the ratio of power in low-frequency bands to the power in the whole BOLD frequency band [83]. Thus, to calculate a fAFF (Fractional Amplitude of Frequency fluctuation) measure similar to fALFF for the current study, one needs to divide AFF in any given frequency band with the combination of other frequency bands. This implies that decreased fAFF in one of the brain regions can be due to either decreased AFF of numerator frequency band or increased AFF of either one or both of the denominator frequency bands. Similarly, increased fAFF can be attributed to either increased AFF of numerator or decreased AFF of denominator or both. In addition, if the psychosis groups and the healthy volunteer groups differ in terms of network x

frequency interaction, in combination with the above mentioned mechanism would lead to a confound in the interpretation of study results.

ROI analyses

For each of the 14 networks, we calculated average mAFF by taking the mean across the respective ROIs for a given network in each of the 3 frequency bands. Average mAFF scores for the 14 networks were imported into SPSS (version 16) and we used repeated measures ANCOVA to specifically test the group x region x frequency interaction with alpha set to < .05. The between subjects factors included group (patient, healthy volunteer) and sex. The within subjects factor was network score (14 networks) and mAFF for the three frequency bands (Slow-2, Slow-3, and Slow-4). Age and site were included as statistical covariates. Given the assumption of sphericity was violated we used Greenhouse-Geisser correction to adjust degrees of freedom. Post-hoc investigation of specific frequency ranges that were significant between groups was conducted using alpha set at .05.

Table 2: List of Independent Components and Corresponding ROIs and MNI coordinates

			X	Y	Z	Name
IC01	Lingual Gyrus	ROI01	-12	67	7	Right Cuneus
IC03	Salience network	ROI02	-6	-23	31	Right Cingulate Gyrus
		ROI03	30	-41	31	Left Superior Frontal Gyrus
		ROI04	-30	-44	28	Right Superior Frontal Gyrus
		ROI05	-33	-17	4	Right Insula
		ROI06	33	-17	1	Left Insula / Left BA 47
IC05	Left FPN	ROI07	45	-20	34	Left Pre-central Gyrus /Left BA 9
		ROI08	36	67	49	Left Superior Parietal Lobule
		ROI09	39	-50	-2	Left Middle Frontal Gyrus
		ROI10	9	-29	46	Left Superior Frontal Gyrus
IC06	Insular Cortex	ROI11	36	19	1	Left Claustrum
		ROI12	-45	10	1	Right Insula
IC07	Right FPN	ROI13	-39	-17	52	Right Superior Frontal Gyrus/BA 8

		ROI14	-51	49	46	Right Inferior Parietal Lobule
		ROI15	-39	-53	-5	Right Middle Frontal Gyrus
		ROI16	-6	-29	46	Right Medial Frontal Gyrus/ BA 8
		ROI17	48	55	46	Left Inferior Parietal Lobule/BA40
IC08	Basal Ganglia	ROI18	-15	-5	7	Right Lentiform Nucleus
		ROI19	18	-2	7	Left Lentiform Nucleus/ Putamen
IC09	DMN	ROI20	6	64	34	Left Precuneus / BA 7
		ROI21	36	64	46	Left Superior Parietal Lobule/BA 7
IC10	Temporal Gyrus	ROI22	-57	49	16	Right Superior Temporal Gyrus
		ROI23	54	55	22	Left Superior Temporal Gyrus
		ROI24	6	52	40	Left Precuneus
		ROI25	3	-53	28	Left Superior Frontal Gyrus/ BA 9
		ROI26	-54	-26	7	Right Inferior Frontal Gyrus/BA45
		ROI27	-9	-29	61	Right Superior Frontal Gyrus
		ROI28	51	-23	10	Left Inferior Frontal Gyrus/ BA 45
IC12	Fusiform gyrus	ROI29	33	61	-14	Left Declive
		ROI30	-33	58	-14	Right Declive
		ROI31	24	-5	-14	Left Subcallosal Gyrus / BA 34
		ROI32	-24	-8	-17	Right Inferior Frontal Gyrus/BA47
IC13	Higher vis cortex	ROI33	-21	94	1	Right Cuneus
		ROI34	21	94	1	Left Cuneus
IC16	Dorsal Attention	ROI35	-39	37	64	Right Post central Gyrus
		ROI36	48	28	40	Left Post central Gyrus/ BA 2
		ROI37	48	64	-2	Left Inferior Temporal Gyrus
IC17	Middle Front. Gyr.	ROI38	6	-47	10	Left Medial Frontal Gyrus/ BA 10
		ROI39	9	-29	58	Left Superior Frontal Gyrus
IC19	Motor Cortex	ROI40	-57	4	28	Right Pre-central Gyrus
		ROI41	57	4	25	Left Precentral Gyrus
IC20	Inf Front. Gyrus	ROI42	-48	-17	25	Right Inferior Frontal Gyrus/ BA 9
		ROI43	-33	-26	-8	Right Inferior Frontal Gyrus
		ROI44	45	-17	25	Left Inferior Frontal Gyrus / BA 46
		ROI45	33	-26	-11	Left Inferior Frontal Gyrus
		ROI46	-33	55	49	Right Superior Parietal Lobule
		ROI47	-3	-20	55	Right Superior Frontal Gyrus/ BA 6

Voxel-wise analysis

We also used voxel-wise analysis to complement the region-of-interest analyses. We compared all patients vs. healthy volunteers to investigate frequency specific group level differences. Primary analyses focused on comparing all patients compared to

healthy volunteers with ancillary analyses focused on the comparison of first-episode and chronic patients with healthy volunteers and group comparisons by site. To reduce any residual effect of motion on mAFF differences we included individuals mean frame-wise displacement in the group level analysis as a covariate[77,84,85]. Group level statistics maps were thresholded at $p<0.01$ with correction for multiple comparisons performed using "3dClustSim." These group level differences were overlaid onto the surface level maps using BrainNetviewer[71] (figure 26).

CHAPTER IV

RESULTS

4.1 Estimating and quantifying frequency specific functional connectivity

4.1.1 Subject exclusion results

We applied multiple selection criteria to create a homogeneous sample from a total of 129 subjects available in the first release of NKI-RS. First, we excluded those with known history of neurological, psychological and physiological disorders (e.g. high or low blood pressure) yielding a remaining sample size of 84. Then, only subjects between the ages of 18 to 35 years were included (n=31). Lastly, we discarded subjects with large head motion (> one voxel edge) in any direction. In total, 21 subjects (mean: 24 years, std: 4 years, 12 female) were included for further analyses.

4.1.2 Hypothesis test results

In the first project, we aim to answer the first three research questions and test corresponding hypothesis.

Independent component analysis

12 different RSNs were identified in the group ICA output. Each of the 12 spatial IC maps, along with the corresponding (total) power spectrum, is shown in Figure 5: visual networks (VIS1-3, figure 5A-C), the default mode network (DMN1, figure 5D), the left-frontal parietal network (LFP, figure 5E), the dorsal attention network (DAN, figure 5F), the right-frontal parietal network (RFP, figure 5G), the default mode network

(DMN2, figure 5H), the superior temporal gyrus (STG, figure 5I), the salience network (SAL, figure 5J), the pre-central gyrus (PCG1, figure 5K) and the inferior frontal gyrus (figure 5L). Figure 5 also displays the relative contribution of power in each of the five frequency bands to the total power for each of the identified RSN. In 9 out of 12 identified RSNs, frequency band slow-4 (0.027-0.073) represented highest power (~30%) compared with other frequency bands. Slow-3 frequency band displayed highest power in the temporal gyrus (33%), the higher visual cortex (30%) and the inferior frontal gyrus (38%) while the slow-5 band accounted for highest power in the default mode network. Slow-2 accounted for ~5% power across all the RSNs with highest relative contribution observed in the salience network (15%). The (partial) slow-1 frequency band studied here (0.5-0.75 compared to 0.5-1.25 Hz) represented relatively less (<5%) of the total power in frequency band across all the RSNs. The contribution of slow-4 and slow-3 frequency bands was found to be highly similar across all the RSNs (figure 5N).

Figure 6 displays various RSNs derived using group ICA performed on filtered BOLD fMRI data in five different frequency bands. All the RSNs were consistently observed across 3 different frequency bands (slow-5, slow-4 and slow-3) though frequency band specific differences can be observed for each of the networks. Spatial maps representing the motor networks, the IFG and the DMN showed decreased spatial extent in frequency band slow-2 though the left/right frontal-parietal network (figure 6E, G) and the temporal gyrus were consistently present. Group ICA performed on slow-1 frequency band resulted in noisy maps for various RSNs.

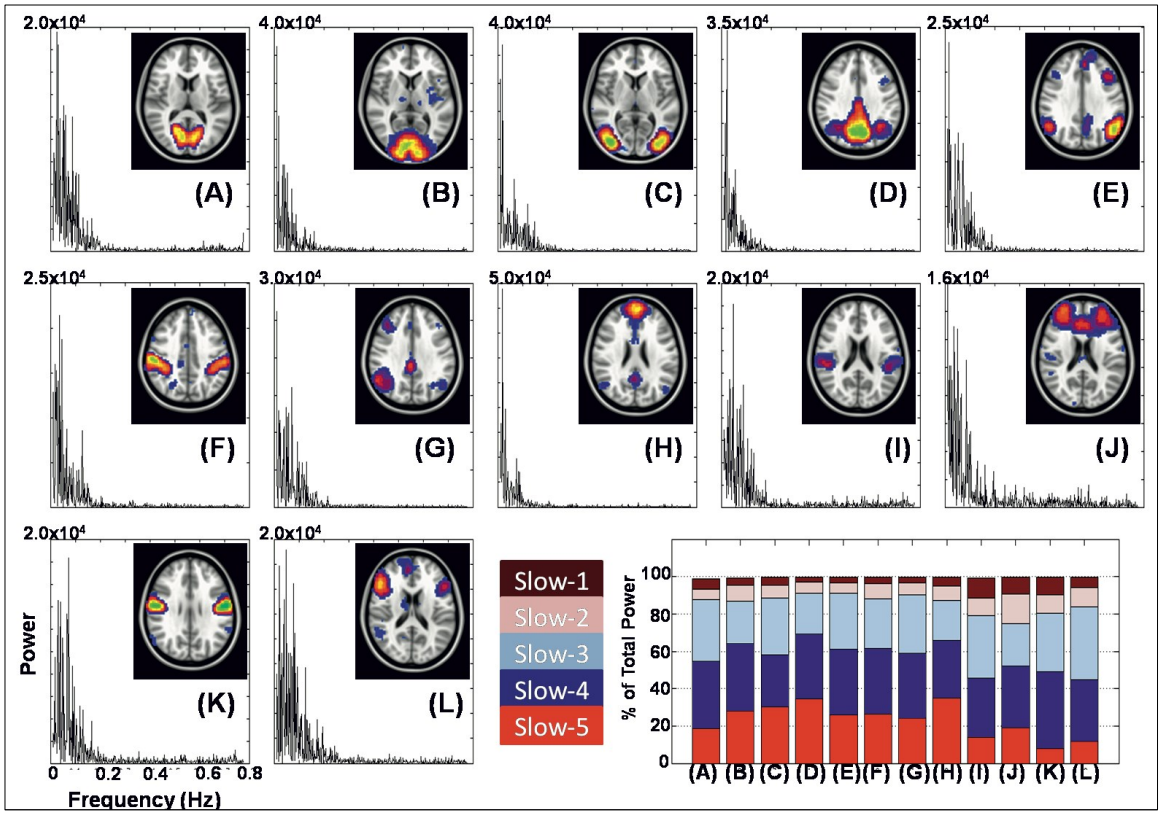

Figure 5: Power spectrum analysis on group level independent component time series from 13 resting state networks (A-C) Visual cortex (VIS 1-3), (D) default mode network (DMN) (E) Left frontal-parietal network (LFP), (F) dorsal attention network (DAN), (G) right frontal parietal network (RFP), (H) anterior default mode network (a-DMN), (I) superior temporal gyrus (STG), (J) Salience network (SAL), (K) pre-central gyrus (PCG), (L) Inferior Frontal gyrus (IFG). Bar plot represents percentage of power explained by each of the frequency bands for various networks.

The results obtained from these analysis supports the hypothesis that power distribution of BOLD signal in across resting state networks is heavily tailored towards low-frequency fluctuations (slow-4 and slow-5), though higher BOLD signal frequencies specifically, represented by slow-3 and slow-2 contribute significantly to BOLD signal power across various RSN. In addition, the RSFC pattern derived across RSN was found to be quite similar supporting the hypothesis at RSFC is present at multiple frequency bands and is not limited to LFFs.

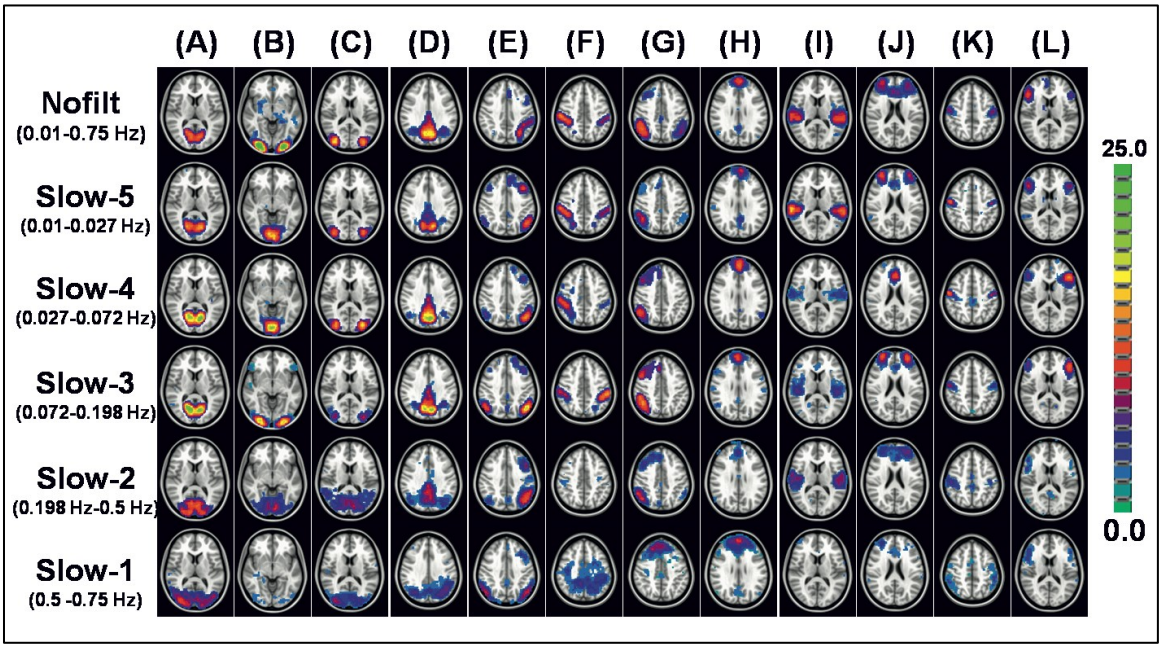

Figure 6: Group Independent Component Analysis maps from 1000 FCP project and corresponding group ICA maps derived from different frequency bands (LF- HF6) where IC01-IC03 (visual network), IC06 (default mode network), IC08 (left frontal parietal network), IC11 (right frontal parietal network), IC16 (Temporal Gyrus), IC17 (salience network), IC19 (motor network).

Seed based correlation

Figure 7 displays group level seed based correlation maps derived using seven different seed regions for each of the five frequency bands (slow-5 to slow-1) ($p<0.05$, FDR corrected). Known patterns of RSNs for each of the seed regions were observed across all the frequency bands, though frequency specific differences in spatial extent were observed. With an increase in BOLD signal frequency band from slow-5 to slow-1, little difference was observed in positively correlated brain regions while negatively correlated brain regions decreased across all the group level correlation maps. Specifically, connectivity patterns in slow-5, slow-4 and slow-3 bands were quite similar

for all the seed regions with the exception of the FEF. Across different frequencies, consistent inter-hemispheric connectivity was observed between a seed regions and corresponding brain region on contralateral side (Figure 7). The Spatial extents of MTG, LPC and MPF regions were found to be highly similar in slow-3 frequency band (0.073-0.198 Hz) and slow-4 frequency bands, while other seed regions displayed highest spatial extent in slow-4 frequency band (0.027-0.073 Hz). Spatial extent at slow-3 frequency bands was found to be higher than slow-5 frequency band for all the seed regions. Spatial extent of group level maps for all the seed regions, although decreased considerably at slow-2 and slow-1 frequency band, significant correlation was observed between a seed region and the corresponding brain region on contralateral side. Group level correlation maps for FEF displayed largest differences in spatial extent across frequency bands while IPS and MPF displayed smallest differences (figure 8).

Similar to spatial extent, frequency specific differences were also observed in mean positive/negative connectivity strength across various seed regions. LPC and MPF displayed stronger positive connectivity in slow-3 frequency band compared to other frequency bands while FEF, IPS and MTG displayed stronger positive connectivity in slow-4 frequency band.

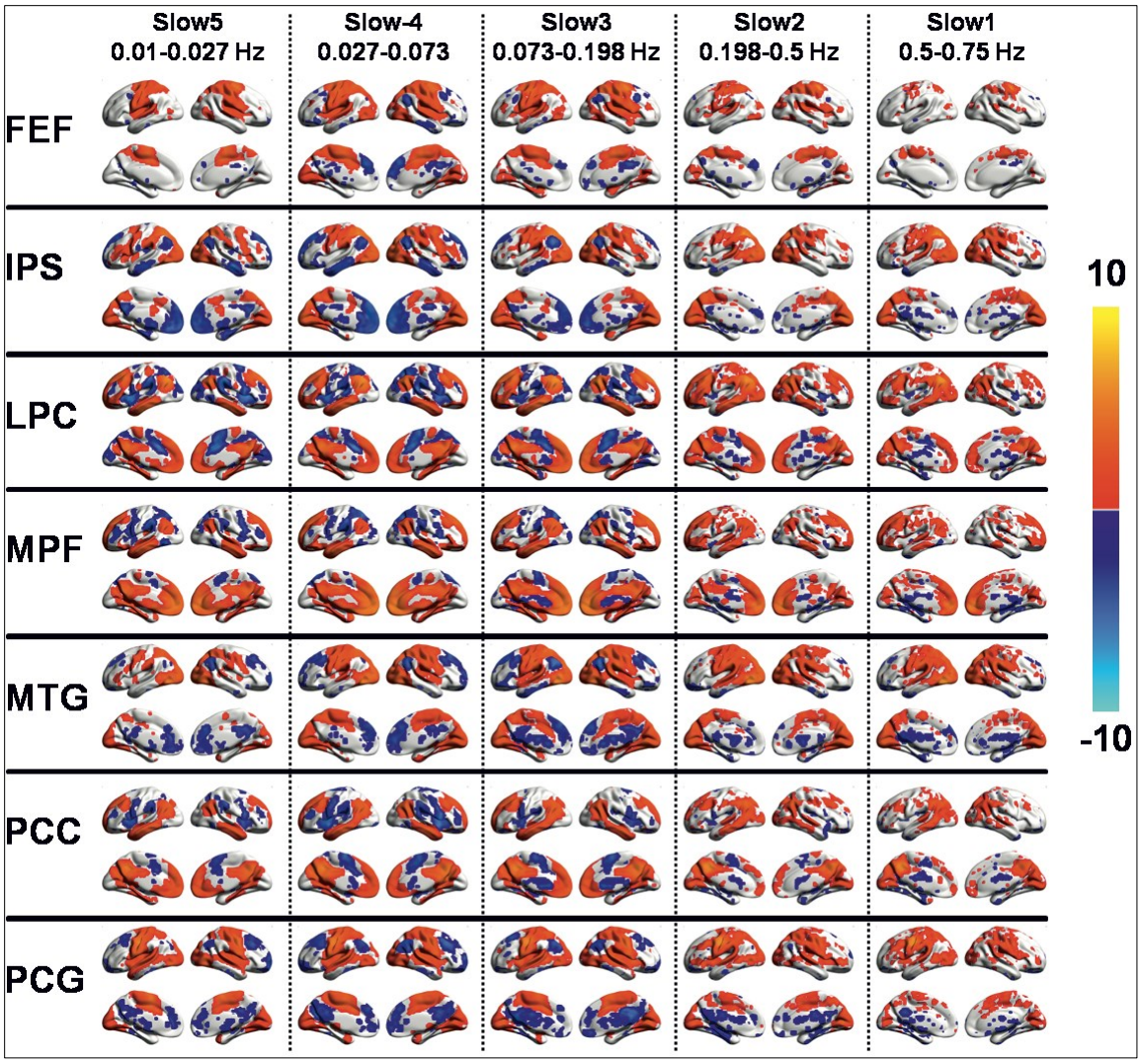

Figure 7: Group level seed based correlation maps for each of the 5 specific frequency bands slow-5, slow-4, slow-3, slow-2 and slow-1 for 7 different seed regions, FEF (Frontal eye field), IPS (Inferior parietal sulcus), LPC (Lateral parietal sulcus), MPF (Medial prefrontal gyrus), MTG (Middle temporal gyrus), PCC (Posterior cingulate), PCG (Pre-central gyrus). One-sample t-test results are thresholded at $p<0.05$ with FDR correction.

Positive connectivity strength for slow-2 and slow-1 frequency bands was highly similar across seed regions and was found to be weaker than low-5 frequency band at all the seed regions except for MPF and PCG. Connectivity strength at slow-4 and slow-3 frequency bands was found to be higher than slow-2 and slow-5 frequency bands.

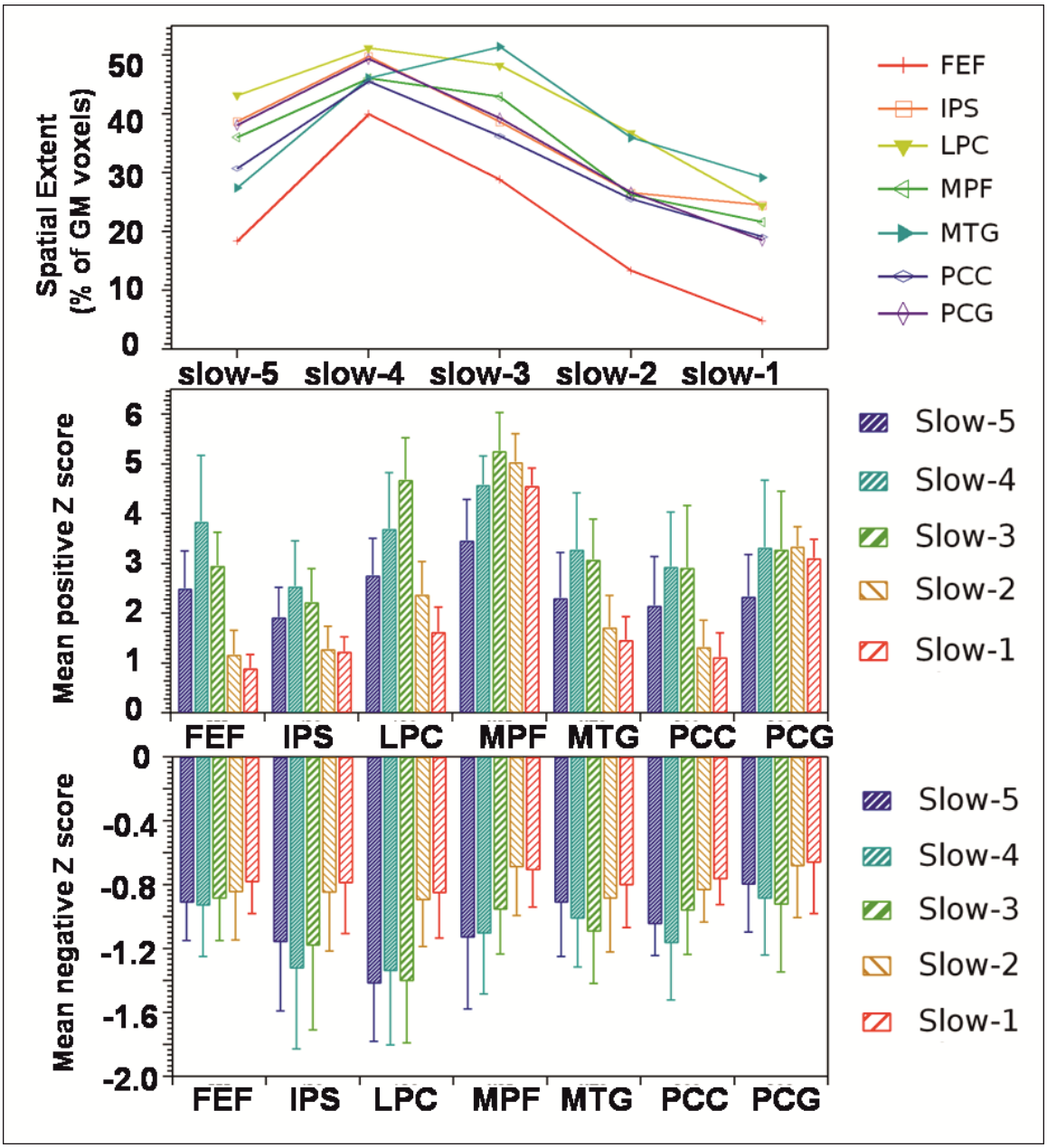

Figure 8: Frequency specific effects on spatial extent of group level seed based correlation maps (top panel), mean positive connectivity strength (middle panel) and mean negative connectivity strength (lower panel) for 7 different seed regions, FEF (Frontal eye field), IPS (Inferior parietal sulcus), LPC (Lateral parietal sulcus), MPF (Medial prefrontal gyrus), MTG (Middle temporal gyrus), PCC (Posterior cingulate), PCG (Pre-central gyrus). One-sample t-test results are thresholded at $p<0.05$ with FDR correction.

Compared to positive connectivity strength, negative connectivity strength was found to be consistent and weaker across all the frequency bands for each of the seven seed regions. Negative connectivity was found to be stronger in slow-3 frequency bands for PCG, MTG, and LPC while IPS and PCC displayed stronger negative connectivity in slow-4 frequency band. In summary, using ICA and seed based correlations; although slow-4 and slow-5 frequency bands largely affect RSNs, BOLD fluctuations in slow-3, slow-2 and slow-1 frequency bands also contribute significantly to RSFC (figure 8).

Compared to group ICA, frequency bands specific differences in seed based connectivity were widespread and mainly affected the spatial extent of the RSNs. In addition, we observed consistent negative correlation between brain regions belonging to two different types of networks across multiple frequency bands implying possible importance of these higher frequency BOLD fluctuations on inter-network communications. These results support the hypothesis that changes in BOLD signal frequency has larger effect on RSFC derived using seed based correlation analysis. In addition, these results also provides proof regarding possible role of higher frequency BOLD fluctuations in between network communications.

Figure 9 displays inter-subject correlation for each of the five frequency bands. Only significant connectivity pairs are reported ($p<0.1$, FDR corrected). Connectivity between ROIs belonging to same networks is displayed by dotted edges. Hot colored edges represent significant positive inter-subject correlation in BOLD signal amplitude while cold colored edges represent negative correlation. Higher number of connections was observed in high frequency BOLD fluctuations (slow-1 and slow-2) compared to low-frequency BOLD fluctuations (slow-3 to slow-5). Left-right, pre-central gyrus

displayed consistent positive inters-subject correlation of BOLD signal amplitude across all the frequency bands except in the slow-1 frequency bands. Part of left and right frontal parietal networks displayed positive correlation with DAN ROIs in slow-4 and slow-3 frequency bands while positive connectivity between lingual gyrus ROIs was consistently present at all the frequency bands except slow-5.

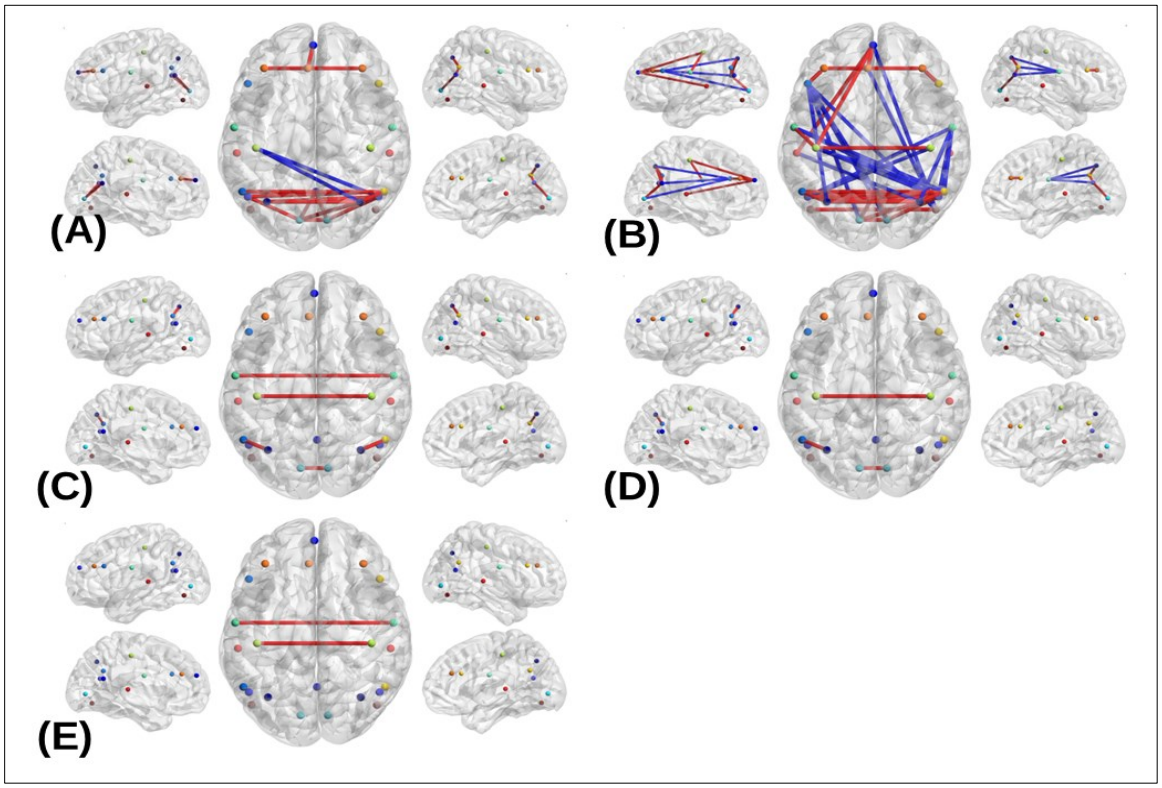

Figure 9: Inter-subject correlations for BOLD signal amplitude contained in specific frequency band for ROIs defined using group level ICA (A) slow-1 (B) slow-2 (C) slow-3 (D) slow-4 (E) slow-5. Results are thresholded at $p<0.1$ with FDR correction.

Highest number of connections was observed in slow-2 (0.198-0.5 Hz) frequency band followed by slow-1 frequency band. Regions of interest from default mode network, dorsal attention network, visual network and salience network displayed higher stronger correlation within the network in slow-2 frequency band. Right frontal-parietal network ROI displayed stronger positive correlation with default mode, dorsal attention, left

frontal parietal network and negative correlation with pre/post central gyrus. Pre/post central gyrus displayed strong negative correlation with ROIs from DMN and DAN network.

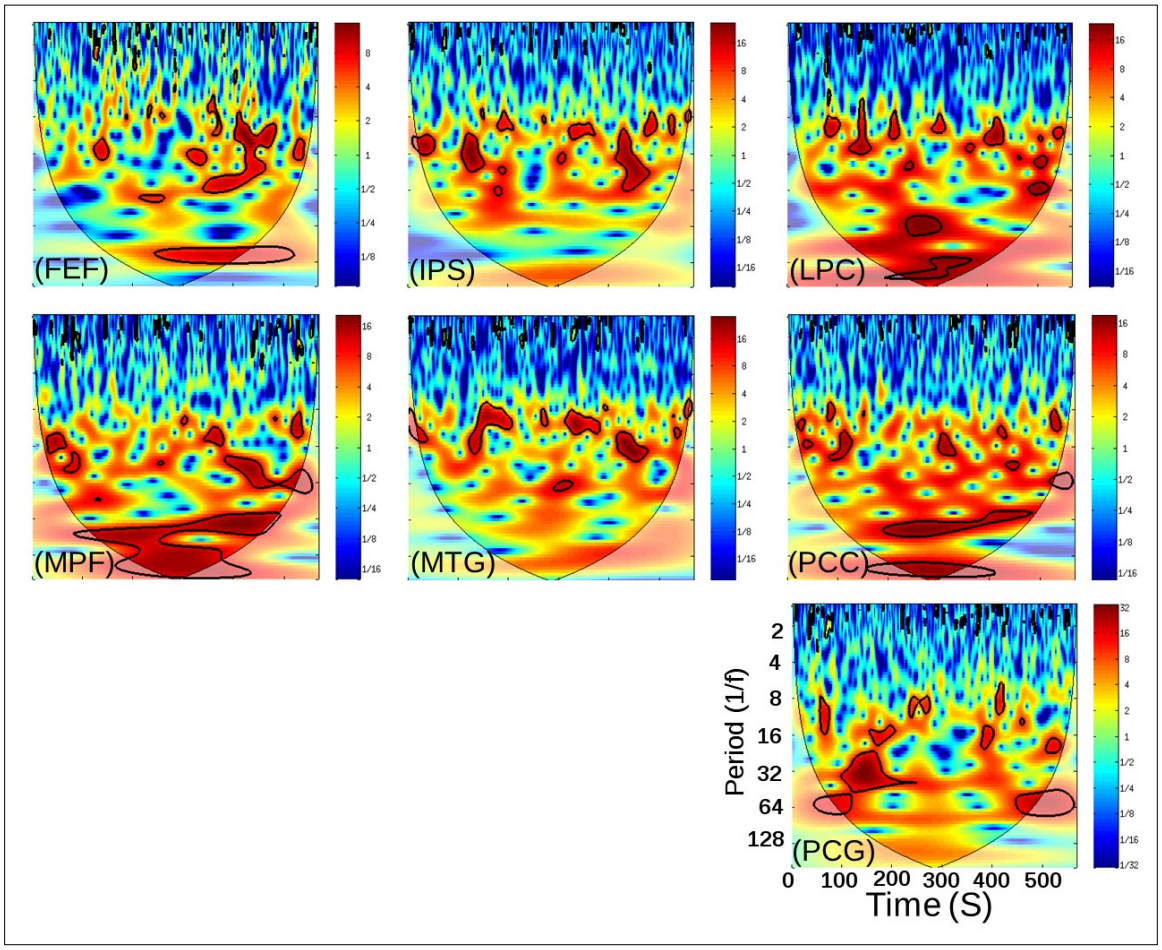

Figure 10: Time-frequency analyses on the un-filtered resting state time series from 7 distinct seed regions, Frontal Eye Field (FEF), Inferior parietal sulcus (IPS), Lateral parietal cortex (LPC), Medial prefrontal cortex (MPF), Middle temporal gyrus (MTG), Posterior cingulate cortex (PCC), pre-central gyrus (PCG).

Figure 10 displays the wavelet spectrogram for one representative subject for each of the seven seed region. The x-axis displays the scanning time in seconds while y-axis displays the period of the signals. Seed regions belonging to task negative networks, such as medial prefrontal cortex, posterior cingulate cortex, and lateral parietal cortex showed higher power in low-frequency range while regions from task positive regions such as

inferior parietal sulcus, frontal eye filed and middle temporal gyrus showed higher power in relatively higher frequency range.

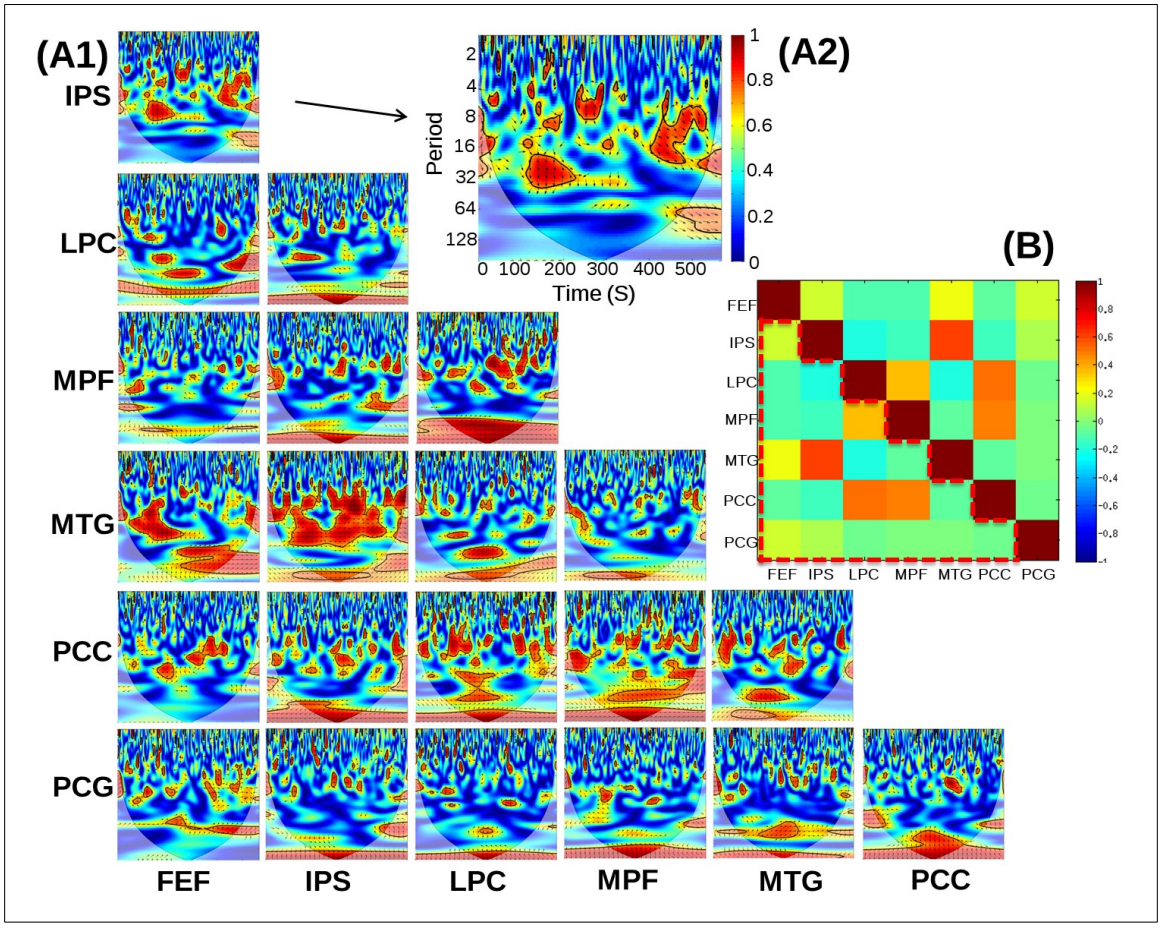

Figure 11: Cross-coherences analysis between all the pairs for 7 distinct seed region time-series, Frontal Eye Field (FEF), Inferior parietal Sulcus (IPS), Lateral parietal cortex (LPC), Medial Prefrontal Cortex (MPF), Middle Temporal Gyrus (MTG), Posterior Cingulate Cortex (PCC), Pre-central Gyrus (PCG)

Based on the results obtained in wavelet analysis, we performed a wavelet coherence analysis to determine interaction between brain regions as a function of time and frequency. Figure 11 displays the wavelet coherence maps for each of the 21 different seed pairs (n*(n-1)/2, n=7 seed regions. Similar to results obtained in figure 8, seed regions belonging to same type of network (task positive or task negative) showed higher power in low-frequency band while regions belonging to two different types of

networks (task positive or task negative) showed higher power in higher frequency range. Figure 11 A1 shows cross wavelet coherence analysis maps for each of the ROI pair while figure 11A2 shows only one of the coherence maps representing the axis. Figure 11B shows the structure of the correlation matrix of where each cell represents a cross-wavelet coherence map. These results support the hypothesis that frequency specific power distribution in BOLD fMRI signal changes across scanning session length. The results obtained in cross wavelet analysis further support the claim that functional integration between brain regions from distinct network is high in high-frequency bands compared to low-frequency bands and is dependent on the networks being studied.

4.2 Effects of frequency based RSFC on whole brain network topology

4.2.1 Subject exclusion results

We applied multiple selection criteria to create a homogeneous sample from a total of 170 subjects available in the second release of NKI-Enhanced Rockland Sample. First, we excluded those with known history of neurological, psychological and physiological disorders (e.g. high or low blood pressure) yielding a remaining sample size of 100. Then, only subjects between the age range of 18 to 35 years were included (n=40). Lastly, we discarded subjects with large head motion (> one voxel edge) in any direction. In total, 27 subjects (mean: 25 years, std: 3 years, 14 female) were included for further analyses.

4.2.2 Hypothesis test results

Figure 12 displays the group level mean correlation matrices for each of the five frequency bands. As visible from figure, the correlation matrices across frequency bands

show distinct RSFC connectivity pattern. The RSFC at slow-4 and slow-5 frequency bands is more segregated in to multiple networks compared to the slow-1 and slow-2 frequency bands. In addition, as can be seen adjacent frequency bands display similar patterns of connectivity across ROI pairs (slow-1and slow-2, slow-4 to slow-5), though connectivity pattern between slow-1 to slow-4 and slow-5 was different.

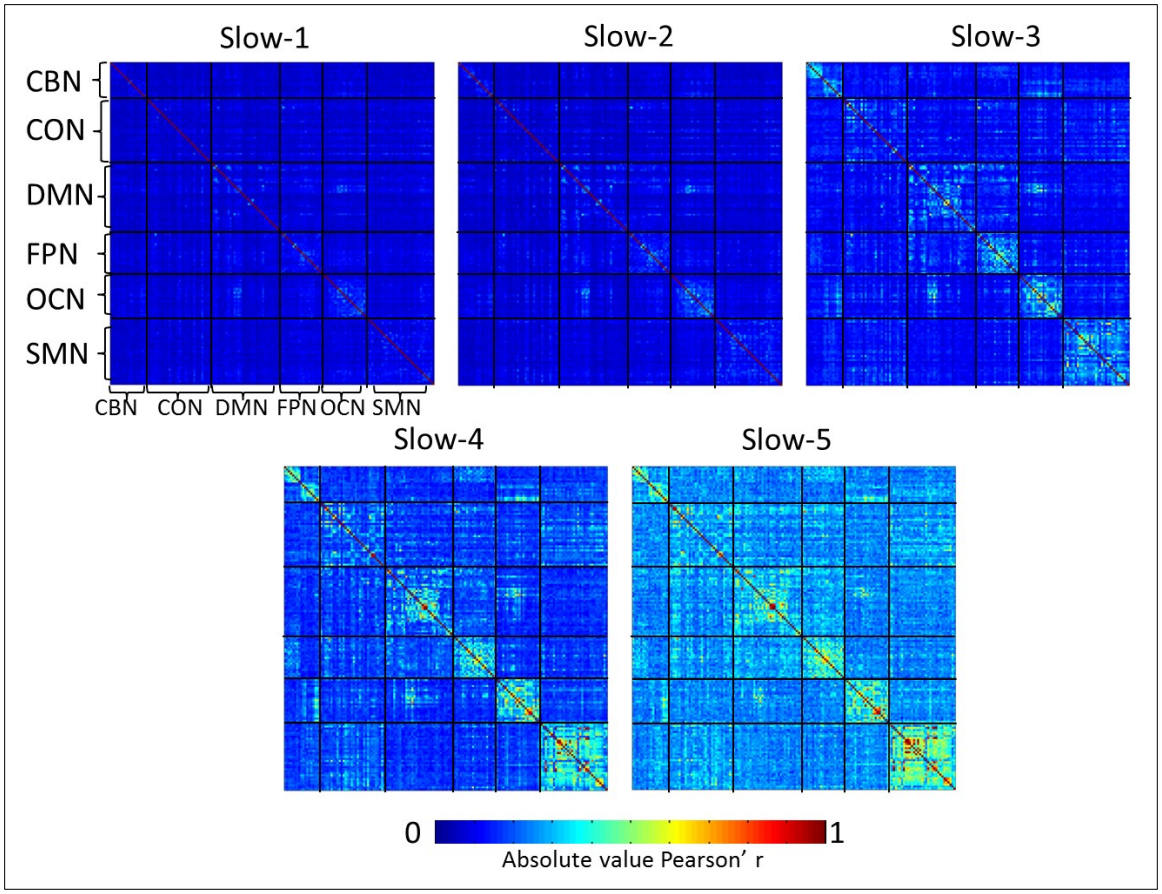

Figure 12: Mean Functional Connectivity matrix derived from a total of 27 subjects, across 5 different frequency bands. The six different network studied are: CBN-cerebellum network, CON-cingular-opercular network, DMN- default mode network, FPN-frontal-parietal network, OCN- occipital network, and SMN-sensory motor network.

Global properties of graph theoretical analysis

In the current study, our first goal was determine differences in graph theoretical properties of whole brain RSFC across different frequency bands. To this end, we calculated global graph theoretical properties (clustering coefficient and path length) across the whole sparsity range (0-1) for both the real networks and matched random networks for each of the subjects. We observed similar trends of clustering coefficient and path length across frequency bands. Clustering coefficient (CC) at frequency bands slow-1 and slow-2 was high similar and was lower compared to CC at slow-3, slow-4 and slow-5 bands. In addition, slow-1 and slow-2 displayed the minimal path length compared to slow-3, slow-4 and slow-5 (figure 13).

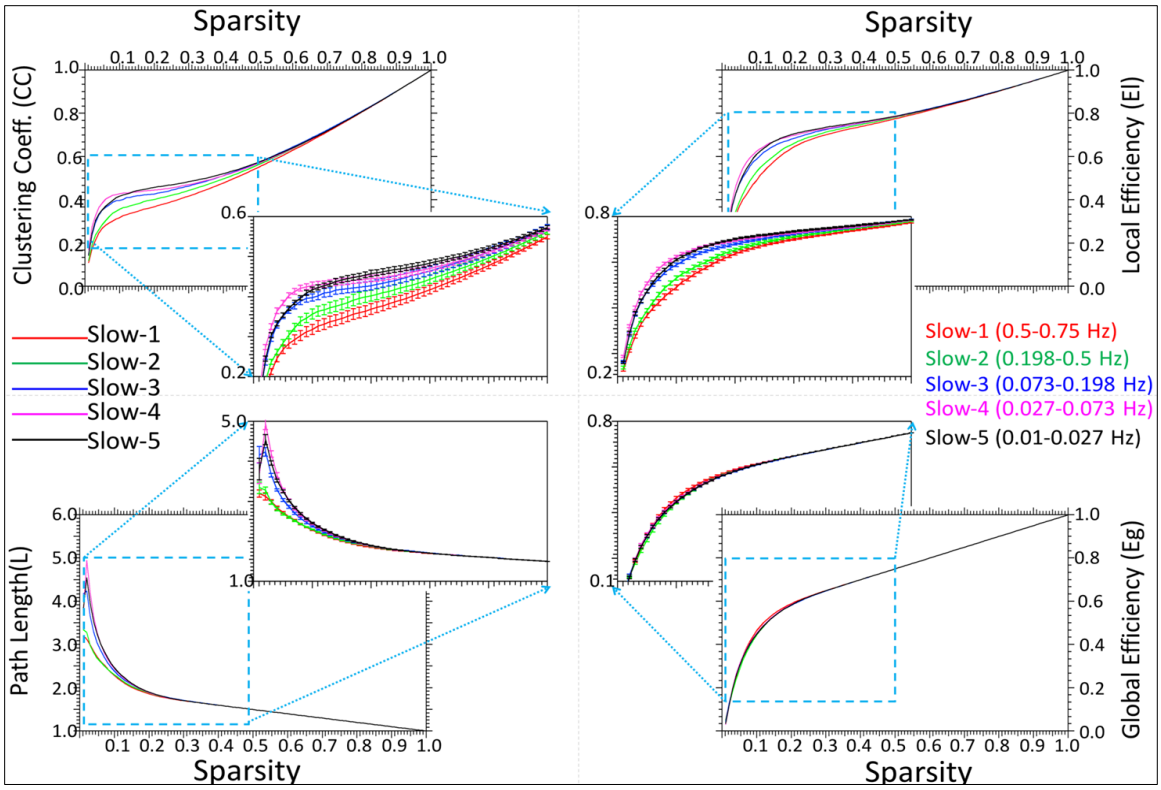

Figure 13: Graph theoretical properties of clustering coefficient, local efficiency, path length and global efficiency for five distinct frequency bands (slow-1, slow-2, slow-3, slow-4 and slow-5)

We also observed that global efficiency across the frequency bands was quite similar while the local efficiency was quite different. Local efficiency was found to be similar in slow-4 and slow-5 frequency bands and was higher compared to other frequency bands slow-1 and slow-2. Slow-3 frequency bands displayed local efficiency higher than slow-1, 2 but lower than slow-4, and slow-5.

As seed in figure 14, we observed that gamma was higher than 1 across the sparsity range 0-50, for each of the frequency bands while lambda was found to be equal to 1 across the sparsity range 10-50 for all the five frequency bands. These results imply that functional brain connectivity across all the frequency bands represent a small-world architecture, where the clustering coefficient for the brain network is higher than random

network while the global path length is quite similar to that of random network. Whole brain RSFC at each of the frequency band was organized in to small-world architecture, but small-world indices for slow-4 and slow-5 frequency bands were higher compared to slow-3, slow-2 and slow-1 frequency bands in that order.

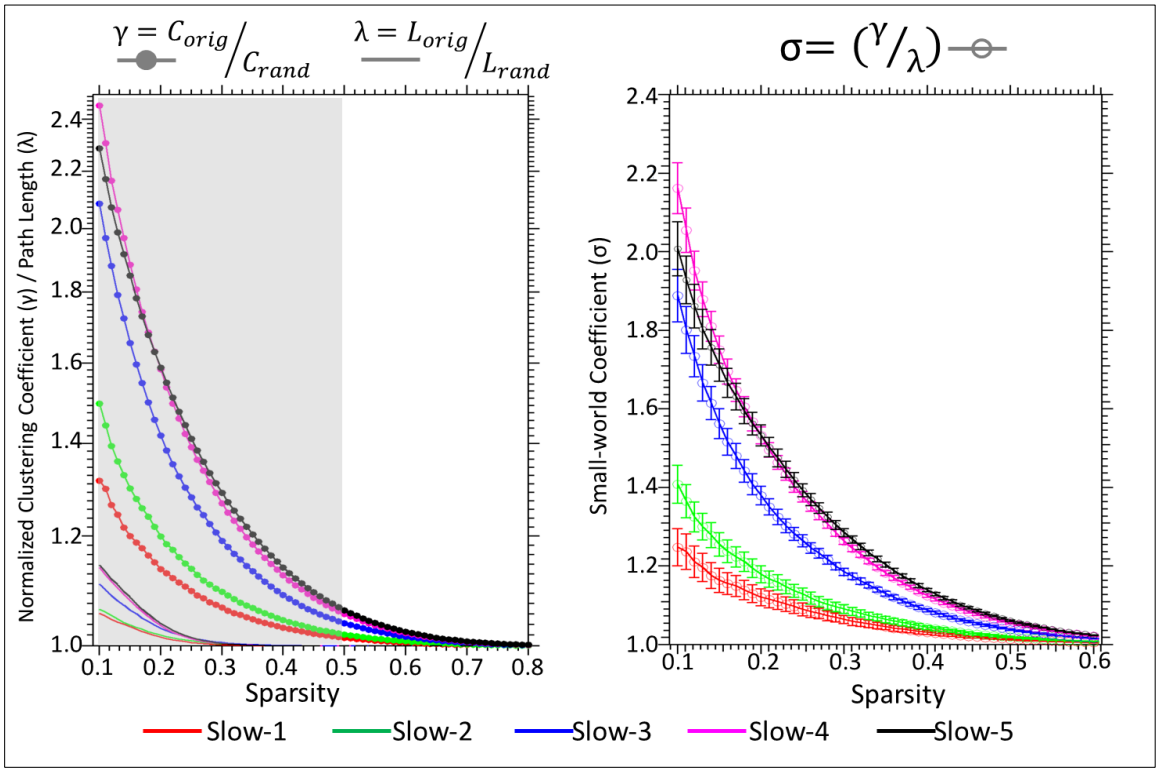

Figure 14: Normalized clustering coefficient (gamma) and normalized path length (lambda) for five distinct frequency bands (left side) and small-world index (sigma = ration of gamma to lambda) for five distinct frequency bands (right side).

Nodal properties of RSFC across frequency bands and hubs of the networks

Hubs of global brain connectivity: In order to derive the hubs of functional brain topology across frequency bands, we calculated each of the nodal properties of degree, betweenness centrality and Eigen vector centrality at the sparsity of 30. Figure 15 displays the distribution of these three different nodal properties. For each of the nodal properties, hubs were defined as brain regions showing higher than 1.5 SD distance from

the mean. As seen in figure 15, the hubs of slow-1 and slow-2 frequency bands were located in the posterior section of the brain and mostly contained posterior cingulate cortex and visual regions. On the contrary, the hubs of slow-5 and slow-4 network were located near the central sulcus of the brain and mostly consisted of pre-/post-central gyrus, inferior frontal gyrus and posterior cingulate cortex.

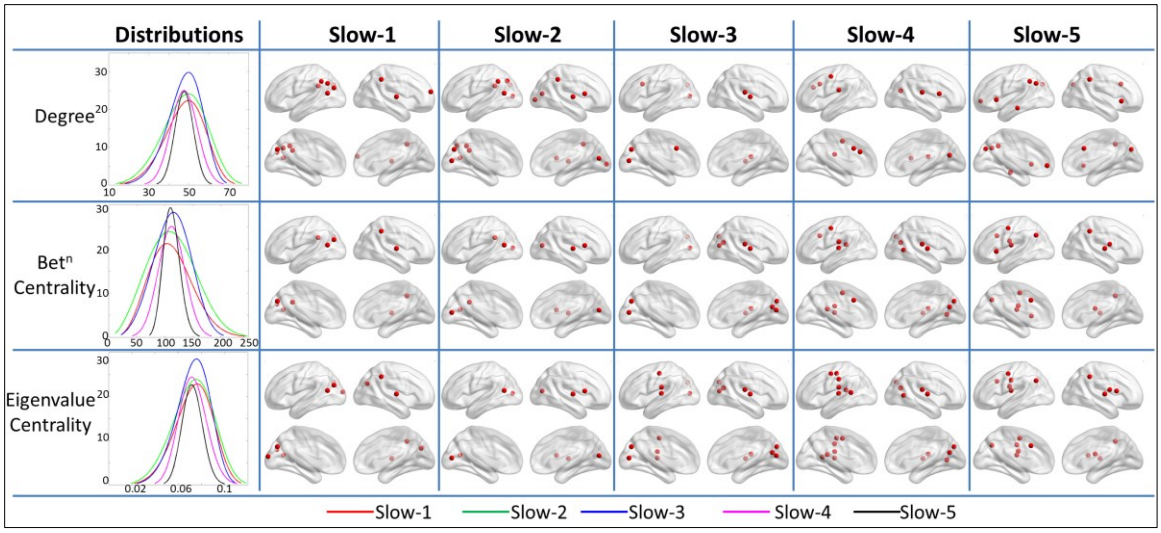

Figure 15: Distribution of degree, betweenness and Eigenvalue centrality of all the brain regions at the sparsity of 30. Glass brain figures display the hubs of the brain identified using three distinct nodal measures for five frequency bands

Differences in nodal properties across frequency bands

In order to study differences nodal graph theoretical properties for each of the nodes, we first studied changes in distribution of each of the nodal properties across frequency bands. We observed significant differences in the nodal distribution across frequency bands for each of the three nodal measures. Due to differential degree distribution observed between the frequency bands for each of the nodal properties, hubs of brain network were defined by extracting the top 5% (8 ROIs) for each of the nodal properties across the frequency bands. Figure 15 displays the fitted histogram for each of

the nodal distribution and corresponding hubs for each of the frequency bands and each of the nodal properties. Increased in the variability of nodal properties was observed in higher frequency bands (slow-1 and slow-2) compared to the low frequency bands (slow-4 and slow-5).

We observed the degree distribution to be narrower in slow-4 and slow-5 frequency bands while for slow -1 and slow-2 frequency bands the degree distribution was wider and skewed towards higher degree. Hubs for slow-1 and slow-2 frequency bands were mainly located in occipital and parietal cortex while no hub ROIs were located in frontal cortex. Comparatively, slow-3 displayed hubs in occipital cortex, insula and in supplementary motor area. The hub ROIs for slow-4 and slow-5 frequency bands were located in the motor cortex and basal ganglia regions (figure 16).

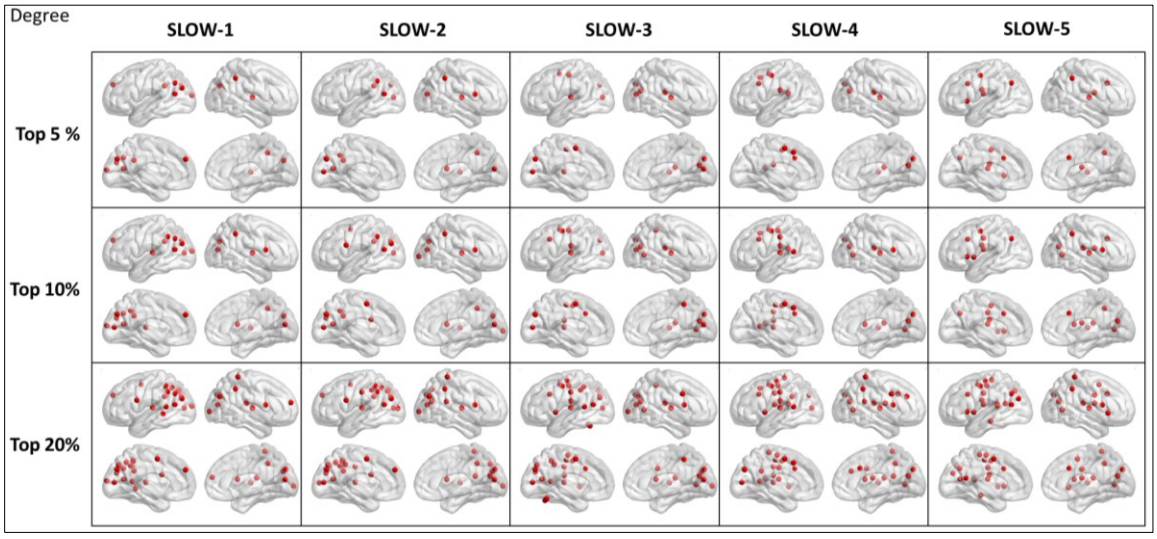

Figure 16: Nodes with in top 5, 10 and 20 percentiles degree across five frequency bands

We observed differential betweenness centrality distribution across frequency bands. The hubs ROIs for slow-1 frequency bands were mainly located in parietal cortex

while one of the hubs was also located in medial pre-frontal cortex. The hub ROIs were quite similar between slow-1 and slow-2 frequency bands. The hub ROIs for slow-3 frequency bands were located in temporal cortex and basal ganglia regions. Slow-4 hubs ROIs were mainly situated in ACC and frontal regions while the hubs in slow-5 frequency bands were mainly situated in temporal gyrus and insula. We also observed presence of at least one of the occipital ROIs as hubs across all the frequency bands (figure 17).

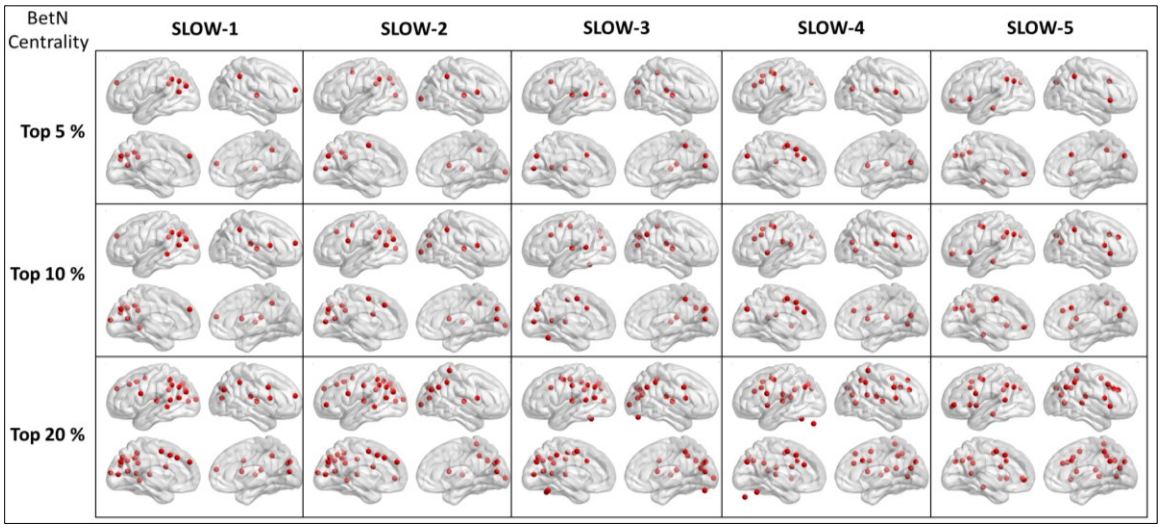

Figure 17: Nodes with in top 5, 10 and 20 percentiles betweenness centrality across five frequency bands

The distribution of Eigen vector centrality was found to be very similar across the frequency bands. The hubs for slow-4 and slow-5 frequency bands were mainly located along the pre-central and post-central gyrus. While hubs for slow-1, slow-2 and slow-3 frequency bands were quite similar to the hub regions identified using nodal degree (figure 18).

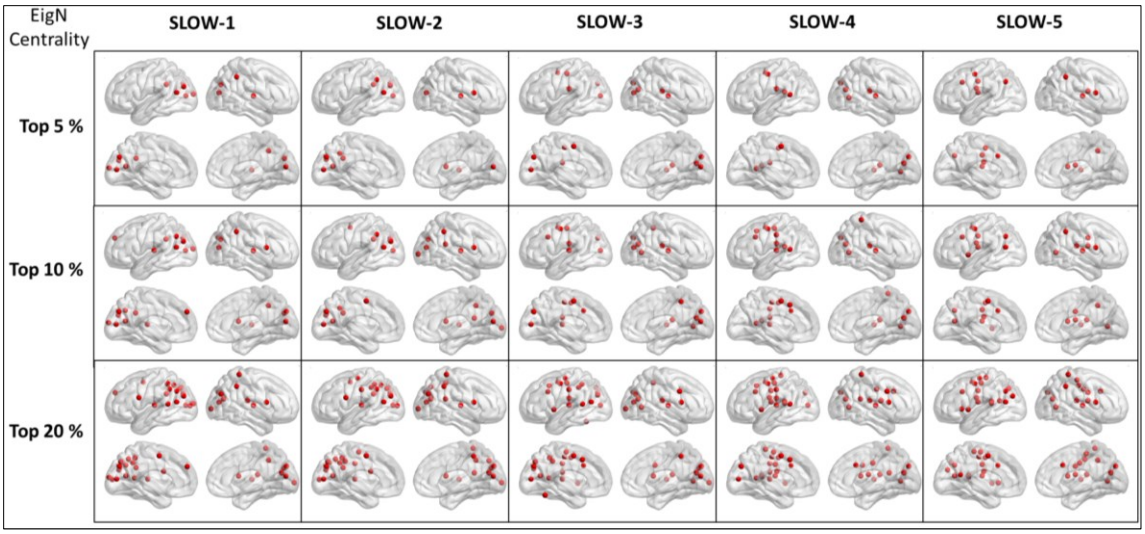

Figure 18: Nodes with in top 5, 10 and 20 percentiles Eigenvector centrality across five frequency bands

In order to further classify, the similarities and differences in hub architecture between the frequency bands, we also derived regions showing degree in top 10 percentile. Based on these regions, we identified the brain regions showing consistently higher degree across the frequency bands and the regions showing high degree in one of the unique frequency bands. Figure 19 displays the brain regions showing higher degree across all the frequency bands and mainly consist of regions in posterior cingulate cortex, temporal gyrus and insula. In addition, SMA is also one of the regions showing higher degree across frequency bands. Figure 20 displays the brain regions showing uniquely higher degree across frequency bands. We observed higher number of unique hubs in slow-5 frequency bands compared to other frequency bands, additionally, all the hubs in slow-5 bands were located in the central sulcus of the brain. In addition, the hubs of slow-1 and slow-2 frequency bands were located in the posterior section of the brain.

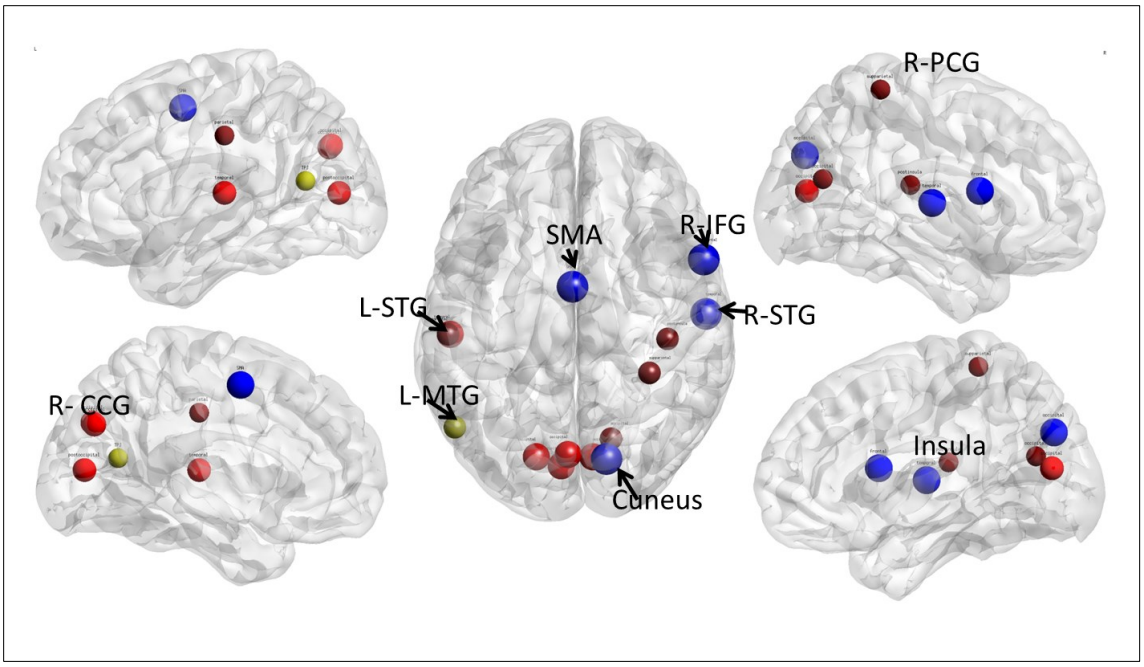

Figure 19: Nodes of the whole brain network that show consistently higher degree across frequency bands and hence are important irrespective of the frequency bands studied.

Modularity

We observed significant decrease in modularity as slow-1 and slow-2 frequency bands compared to slow-3, slow-4 and slow-5 frequency bands. Frequency band slow-4 displayed highest modularity while slow-1 displayed lowest modularity. Across all the frequency bands, we observed three distinct modules that represented frontal lobe, parietal/temporal lobe and occipital lobe thought connectivity between these modules varied significantly across frequencies. The three modules in slow-1 frequency bands we highly inter-connected (figure 21A). The Frontal module also had connections in PCC and superior parietal regions, while the occipital and cerebellar ROIs formed a distinct module. The modules at slow-2 frequency bands displayed similar connectivity pattern as seen in slow-1 frequency band though higher number of ROIs in temporal and parietal lobe showed increased connectivity the frontal module (figure 21B). With decrease in

frequency bands, slow-3 displayed highly modular network structure, where the connectivity within modules was stronger compared to between network modules.

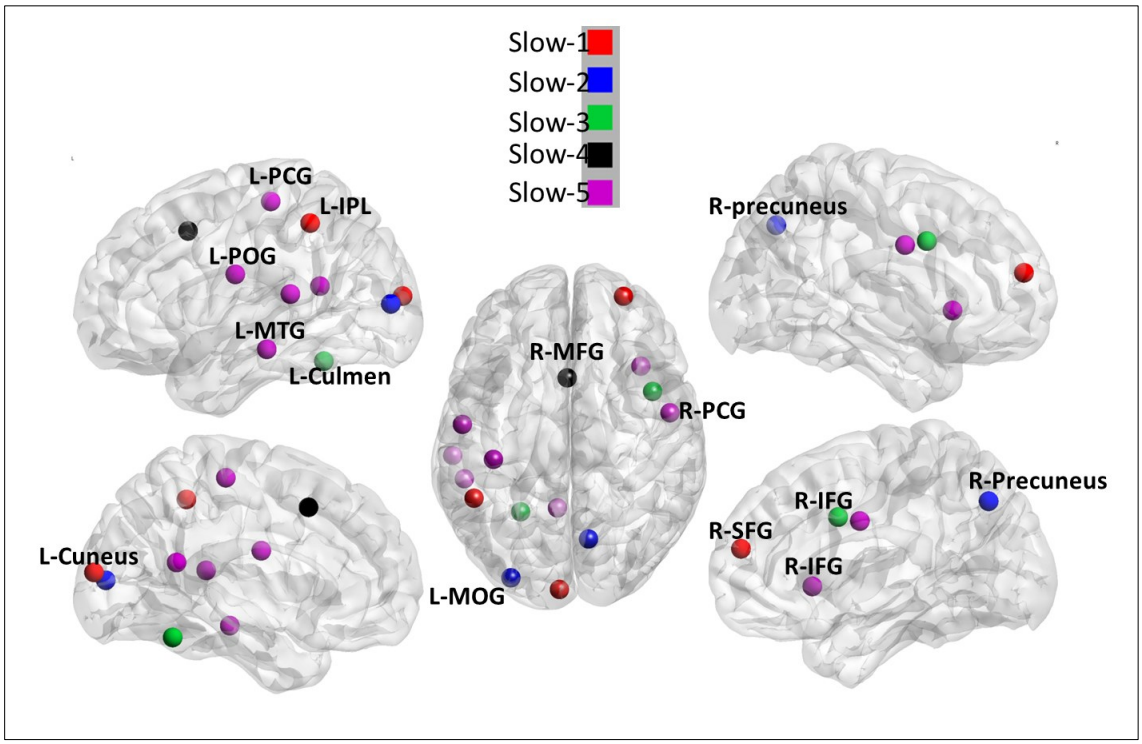

Figure 20: Nodes of the whole brain networks that show consistently higher degree in any one of the bands but not in any other frequency band

As seen in the surface level maps, the spatial distribution of modular architecture was highly intertwined with ROIs in default mode network were represented in the same module. We also observed similar modularity property for slow-4 frequency band, where the higher visual cortex regions formed a complete module (figure 21D, red), one module resembles default mode network (figure 21D, blue) and the green module represented motor/ attention network. Similarly, in the frequency band slow-5 the ROI modules were highly segregated compared to slow-1 and slow-2 frequency bands but showed less

segregation compared to slow-4 and slow-5, thought the ROIs resembled similar modular architecture as seen in slow-4 frequency band (figure 21).

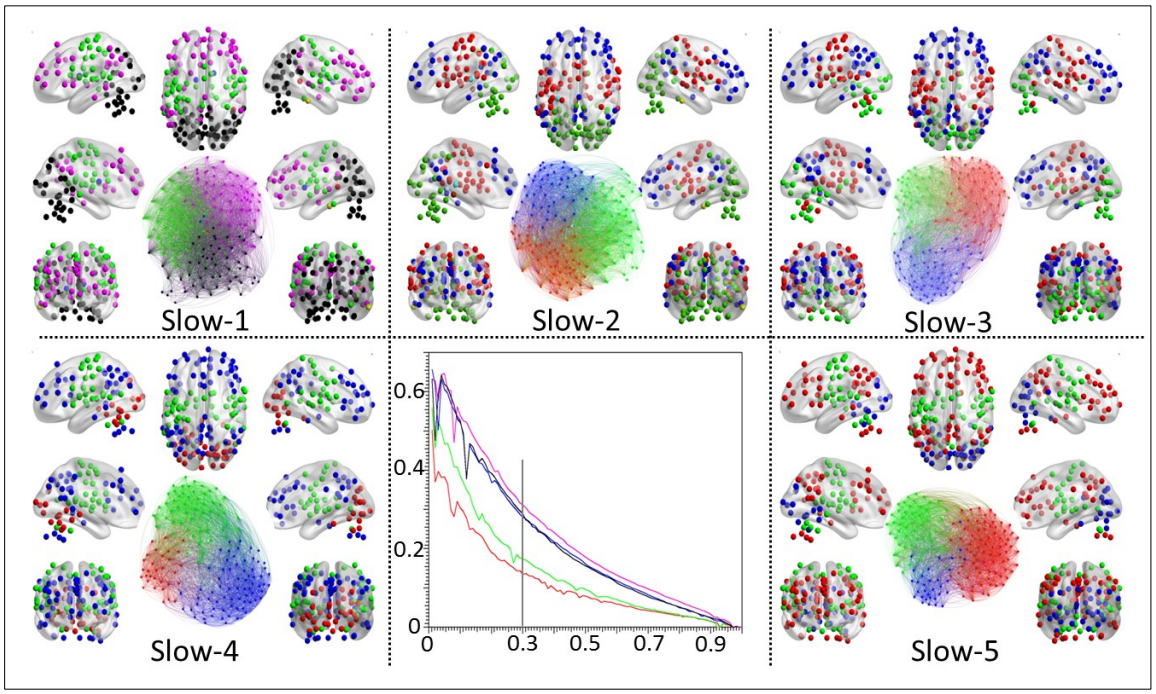

Figure 21: Modularity for five distinct frequency bands across the sparsity range (central figure). The modules identified at sparsity of 0.3 are displayed to explain interaction between them and to associate which module each of the ROI belongs.

In addition, to understand whether the differences in the modularity can be associated with Euclidian distance between the brain regions, we calculated Euclidian distance between for each of the 12720 ROI pairs. The distance was calculated separately for left and right hemisphere to avoid the inter-hemispheric connectivity. Figure 22 displays the scatterplots between Euclidian distance and functional connectivity between brain regions. As expected, we observed a negative relationship between RSFC strength between two regions and Euclidian distance between two regions, although the relationship was stronger in slow-5 and slow-4 frequency bands compared to slow-1 and slow-2 frequency bands.

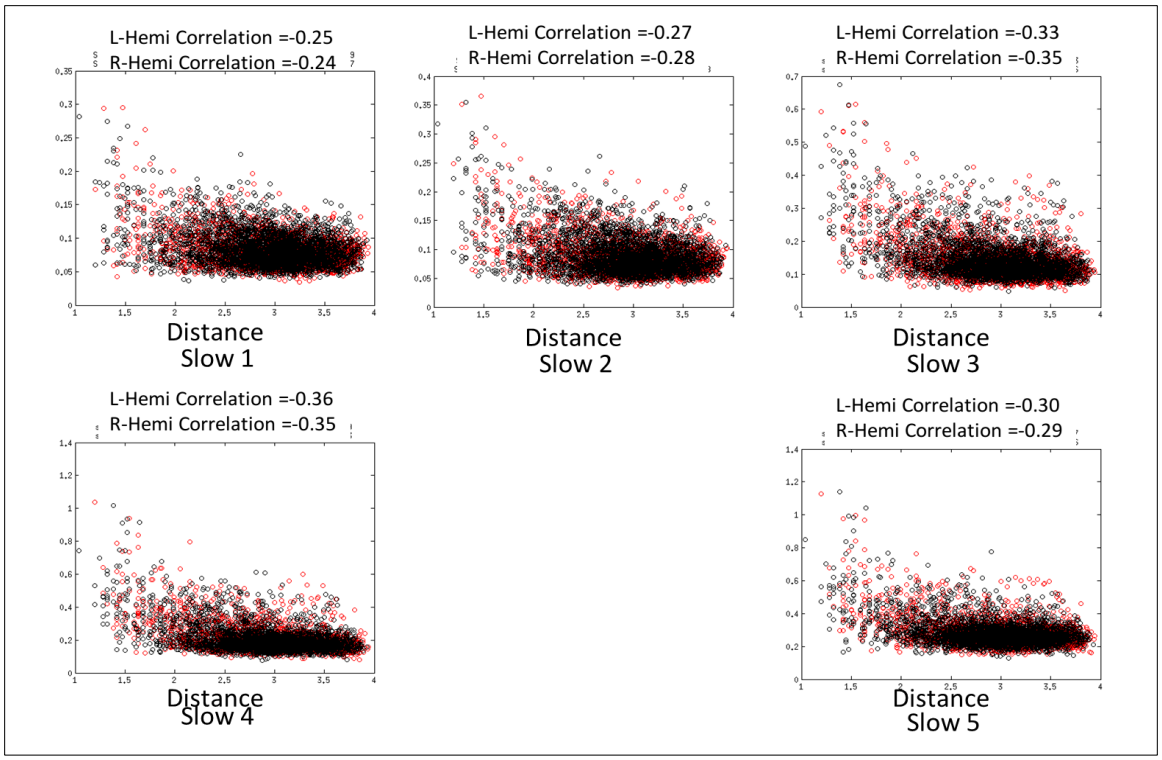

Figure 22: Relationship between functional connectivity in different frequency bands and the Euclidian distance between the two ROIs. Euclidian distance is calculated separately for left (red dots) and right hemisphere (black dots)

These results obtained from graph theoretical analysis shed light on the changes in the whole brain network topologies across various frequency bands and describe the effect of frequency based RSFC changes on whole brain network topologies. Specifically, we observed that brain network topologies at slow-2 and slow-1 is more similar to random network topology that supports high global efficiency of information transfer. In addition, these slow-2 and slow-1 networks showed significantly higher synchonizability implying the network being in the critical dynamic state that may support the wide scale changes in network topologies in response to external stimuli. Additionally, we observed that although network hubs of the whole brain connectivity frequency dependent, brain regions in temporal gyrus, sensory motor network and posterior cingulate cortex have higher degrees, irrespective of the frequency bands. These

results support the hypothesis that large-scale changes in brain network topologies are observed across various BOLD signal frequency bands.

4.3 Disruption of frequency specific BOLD signal power in schizophrenia

4.3.1 Subject exclusion results

We used several motion thresholding criteria to reduce its effect on the BOLD fMRI data. First, consistent with our prior study, we only included individuals demonstrating < 1 voxel maximum motion in any direction[74]. In addition, for each subject we computed frame-wise displacement as defined by Jenkinsons and colleagues[86] and only individuals demonstrating mean frame wise displacement less than 0.5 mm were included in the analysis. The exclusion of individuals based on frame-wise displacement is a relatively recent technique that has been more widely implemented due to recent studies demonstrating a relationship between micro-movements (<1mm) and resting state functional connectivity. In the current study, our goal was to study changes in BOLD signal power at frequencies higher than 0.1 Hz, which imply faster changes in this signal. Although no studies to date have examined the relationship between frame-wise displacement and BOLD signal power higher than 0.1 Hz, based on results of low frequency fluctuations[84], higher frame-wise displacement could conceivably affect BOLD signal power >0.1 Hz. We therefore implemented a stricter frame-wise displacement threshold in the current study. A total of 31 patients (mean age = 36.0; std = 14.1; 24M/7F) with schizophrenia and 50 healthy controls (mean age = 33.8; std = 11.4; 34M/16F) survived the motion threshold and hence were used in further analysis.

4.3.2 Hypothesis test results

Group independent component analysis

There were no significant differences between patients and healthy volunteers in distributions of age, sex and motion. Based on comparison with the FCON-1000 ICA maps, we identified 14 independent components. Figure 23 displays the group level independent component maps and the corresponding regions-of-interest derived for this study are highlighted in the figure. The resting state networks in this study included (A) visual cortex, (B) salience network, The resting state networks in this study included: (A) visual cortex; (B) salience network; (C) left-frontal parietal network; (D) insular Cortex; (E) right frontal-parietal network; (F) basal ganglia network; (G) default-mode network (posterior part); (H) default mode network (Anterior section); (I) fusiform gyrus; (J) higher visual network; (K) dorsal attention network; (L) frontal gyrus; (M) motor network and (N) inferior frontal gyrus. Table 2 lists the MNI coordinates for all regions-of-interest and corresponding resting state networks.

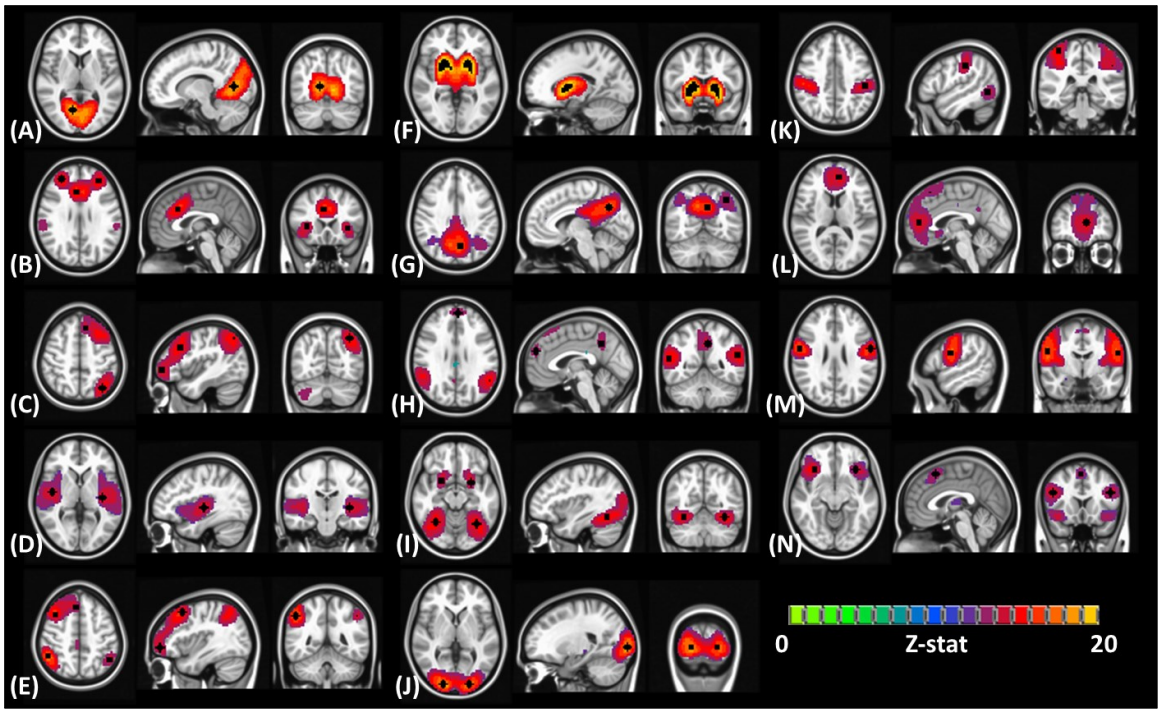

Figure 23: Group IC maps and corresponding ROIs. (A) IC01: visual, (B) IC03: salience, (C) IC05: left frontal parietal network, (D) IC06: insular cortex, (E) IC07: right frontal parietal network, (F) IC08: basal ganglia, (G) IC09: default-mode network (posterior section), (H) IC10: default-mode network (anterior section), (I) IC12: fusiform gyrus, (J) IC13: higher visual network, (K) IC16: dorsal attention network (L) IC17: frontal gyrus, (M) IC19: pre-central gyrus and (N) IC20: inferior frontal gyrus and anterior cingulate cortex.

Repeated measures ANCOVA revealed a significant interaction of group by IC ($F = 4.98$, $DF = 6.39$, $p < .001$). Post-hoc analyses indicated significant main effects of group for visual cortex ($F = 9.11$, $DF = 76$, $p = .003$), dorsal attention ($F = 7.76$, $DF = 76$, $p = .006$) and motor cortex ($F = 8.89$, $DF = 76$, $p = .003$) such that healthy volunteers had higher scores compared to patients across the 3 frequency ranges. Significant main effects of group were also evident for the salience ($F = 4.03$, $DF = 76$, $p = .046$) and frontal gyrus ($F = 5.75$, $DF = 76$, $p = .017$) networks such that psychosis patients had higher mAFF scores compared to healthy volunteers across the 3 frequency ranges. Bar-plots illustrating mAFF for each of these 5 resting state networks within each frequency band are provided in figure 24.

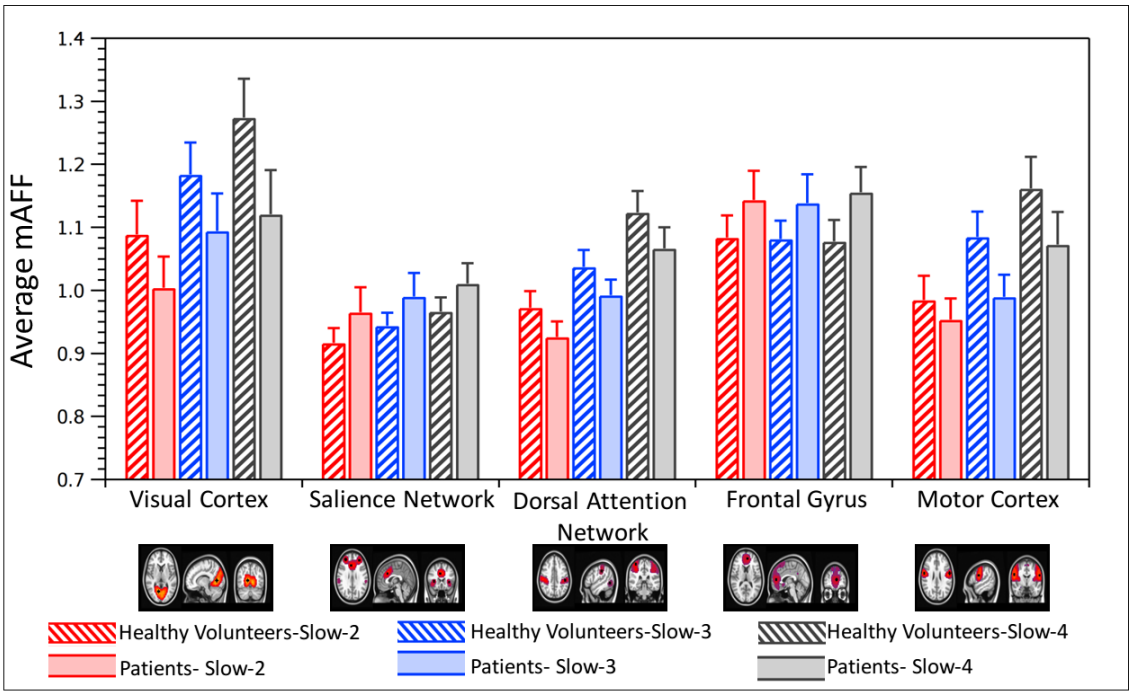

Figure 24: Group by frequency interaction for AFF value for five distinct networks

In addition, the group x IC x frequency interaction was significant (F = 1.75, DF = 13.53, p = .042) and thus, we investigated group x frequency interactions for each of the ICs in post-hoc analyses. There was a significant group x frequency interaction for visual cortex (F = 3.57, df = 1.72, p = .038) with significant group differences evident in slow-2 (t = 2.20, df = 79, p = .023; partial eta-squared = .023) and slow-3 (t = 2.24, df = 79, p = .024; partial eta-squared = .024), but with the greatest effect size in slow-4 (t = 3.20, df = 79, p = .002; partial eta-squared = .047). In addition, the group x frequency interaction was significant for the motor cortex (t = 4.10, DF = 1.63, p = .025) with the largest effect size evident in slow-3 (t = 3.33, DF = 79, p =0.001; partial eta-squared = .051) and to a lesser extent slow-4 (t = 2.38, DF = 79, p = .018; partial eta-squared = .027).

There were also significant main effects of frequency for the dorsal attention (F = 23.17, DF = 1.57, p < .001) and motor (F = 6.63, DF = 1.57, p = .003) networks such that

slow-4 was significantly higher than slow-3, which, in turn, was significantly higher than slow-2. A significant ($F = 9.49$, $DF = 1.57$, $p < .001$) main effect of frequency for frontal gyrus was evident, but there were no significant differences in frequency across groups. Neither the main effect of sex nor interactions with sex were statistically significant.

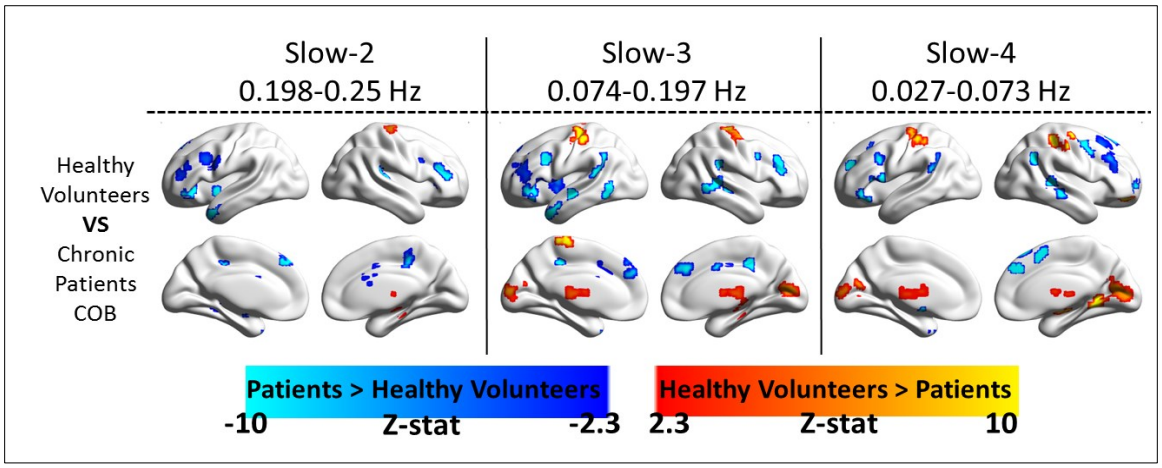

Figure 25: Frequency specific differences in mAFF across frequency bands

Figure 25 provides the group level comparisons for voxel wise analyses in each of the frequency bands ($p<0.01$, corrected for multiple comparisons using 3dClustSim). Consistent with the significant interaction effects from the region-of interest analyses we observed lower mAFF in the slow-3 frequency band within the bilateral motor cortex in all patients compared to healthy volunteers with the most robust effects observed in slow-3. We also observed significantly lower mAFF in the visual cortex in all patients compared to healthy volunteers within the slow-2, slow-3 and slow-4 frequency bands that were most robust in slow-4 again consistent with the region-of-interest analyses. These results support the hypothesis of disruption of BOLD signal power in both low and high frequency BOLD signal in psychosis populations. The results from significant group x frequency interactions also suggest, significantly higher effect of psychosis on high

frequency BOLD fluctuations in slow-3 and slow-2 compared to low-frequency fluctuations in slow-4.

CHAPTER V

DISCUSSIONS

5.1 Estimating and quantifying frequency specific RSFC

5.1.1 Interpretation of the findings

In the current study, we used whole brain resting state functional MRI data acquired using short repetition time (645 ms) to investigate functional integration between brain regions during rest at multiple frequency bands. Various RSNs that have been commonly derived by BOLD signal in frequency bands slow-5 and slow-4 were consistently present at other BOLD frequency bands: slow-3, slow-2 and slow-1. These slow-3 to slow-1 frequency bands represent higher frequencies (0.073-0.75 Hz) compared with near-standard "low-frequency fluctuations" (0.01-0.073 Hz) represented by slow-4 and slow-5. Although, earlier studies have derived the default-mode, the fronto-parietal, the sensory motor and the visual networks using BOLD fluctuation in high-frequency range (>0.1 Hz)[11,25,26]; the current work expands this notion to multiple other RSNs including the dorsal attention, the salience and the higher visual networks. Consistent significant connectivity between a seed region and its contra lateral hemispheric ROIs was also observed at all the frequency bands (slow-5 to slow-1). In addition, connectivity within regions from task-positive networks varied considerably across frequency bands while connectivity between regions from task-positive and task-negative networks was similar across frequency bands.

Electrophysiological studies have suggested that the human brain operates over a wide range of frequencies, characterized as 'slow' bands (<1.5 Hz), EEG bands (1.5 to 80 Hz) and 'fast' bands (80-600 HZ)[9,87]. Even though EEG and fMRI signals represent different aspects of underlying neuronal activity (e.g., direct v/s indirect measures respectively), studies have associated multiple RSNs as identified by fMRI with one or more EEG rhythms[88–90]. In the current study, RSNs were derived based on BOLD fMRI signals temporally filtered in the each of the "slow" frequency bands as defined in electrophysiological studies. Current reports of consistent RSFC between network ROIs at various frequency bands along with results from previous fMRI and EEG studies imply that RSFC is a multi-frequency band phenomenon. The frequency band definitions used in the current study were based on the study by Penttonen and colleagues, who argued that different frequency bands in brain oscillations follow a natural logarithmic function[9]. Helps and colleagues on the other hand have suggested that these distinct frequency bands might not represent the frequency bands of natural neuronal oscillations[91]. This can imply that BOLD signal when studied in specific frequency bands may represent addition/subtraction effects of individual neuronal fluctuations and not a single process. In addition, earlier studies have shown that multiple neuronal processes can co-exist in the same cortical areas and that slower neuronal processes may modulate faster processes[7]. Thus, studying BOLD signal in specific frequency bands can relate to studying integration between these individual neuronal processes. Study and interpretation of each individual neuronal process would require deeper understanding of underlying neurophysiological mechanism and better methods to represent these neuronal fluctuations.

Spatial extent of ICA-derived RSNs was found to be highly variable across frequency bands. RSNs such as the default mode, the visual and the sensory motor networks displayed greatest spatial extent in slow-4 frequency band (0.027-0.073 Hz), while other RSNs such as the dorsal attention, the left-right frontal parietal and the salience networks displayed highest spatial extent in slow-3 and slow-2 frequency bands. Decrease in spatial extent of the visual and the sensory motor network in slow-3 to slow-1 frequency bands (>0.1 Hz) has been reported in earlier studies[11,25]; in the current work, this property was extended to several other networks. Moreover, this is the first study to display frequency specific differences in spatial extent and RSFC strength of different RSNs. These frequency specific differences in spatial extent can imply presence of some common neuronal oscillations in the regions of the same networks that are specific to a particular network. Earlier electrophysiological studies have shown significant correspondence between a specific RSN and specific EEG rhythms[90,91]; supporting the claim that connectivity within a RSN may be tailored to a specific frequency band. Alternatively, frequency specific differences in spatial extent with ICA could also be attributed to non-homogeneous presence of physiological noise across the brain in the specific frequency bands that are also known to reduce power of RSFC between brain regions[21].

Intra-network RSFC strength derived based on seed based correlation analysis for both task positive and task negative seed regions was found to be positive across all the frequency bands. Seed regions from task-positive network are known to be positively correlated with other task-positive brain regions and task-negative seed regions are known to be positively correlated with other task-negative regions in low-frequency band

(0.01-0.1 Hz)[16]. Similarly, in the current study, this positive connectivity within task positive and task-negative networks was observed at each of the frequency bands, though it was highly variable across seed regions and across frequency bands. Consistent positive inter-hemispheric connectivity between task-positive regions such as the left/right pre-central gyrus and visual cortex in BOLD frequencies higher than LFFs has been reported earlier using sliding-window approach[25] which is similar to the consistent positive connectivity observed for PCG in current study for all the frequency bands. In addition, task-positive seed regions (FEF, IPS, and MTG) displayed stronger positive connectivity in slow-4 frequency band while task-negative seed regions (LPC, MPF, and PCC) displayed stronger connectivity in slow-3 frequency band. This distinct connectivity pattern for task positive and task negative networks may suggest presence of two distinct neuronal processes represented by these networks. Earlier 'resting' EEG studies have observed presence of a 'default mode-like network' in slow-3 frequency bands[91] which is consistent with higher connectivity observed in slow-3 frequency band for task-negative network seed regions in current study. The same study also reported stronger associations between the EEG power in the slow-3 frequency band and self-reported inattention in ADHD patients compared to controls within 'DMN' network but no differences were observed outside the network. This suggests that the frequency band specific differences observed in the current study for task-positive and task-negative networks may reflect underlying cognitive states and needs to be studied in detail with neurobehavioral measures.

Task-positive and task-negative networks are known to be anti-correlated[16]. While in a particular class of cases this strong negative correlation is likely attributed to data

processing methodology that involves global signal regression[92], other studies have confirmed presence of anti-correlated networks in human brain[77]. In the current work, no global signal regression was implemented, hence as expected connectivity between task positive and task negative networks was found to be weaker compared to connectivity within network. In addition less variation in negative connectivity strength was observed across different frequency bands compared to positive connectivity for all the seed regions. These results suggest that, unlike within-network functional integration that may be frequency band specific, between-network functional integration may occur over a wider range of frequencies. Earlier studies have shown significant effects of 2-choice RT task v/s rest conditions on EEG power both within a 'default mode like network' (task negative) and outside of a 'default mode like network' (task-positive)[91]. Specifically, EEG power within default mode network channels has been shown to be higher in 'rest' compared to 'task' condition in slow-3 and slow-2 frequency band while channels outside the default mode network displayed the inverse pattern associated with task-switching. This implies a coupling between task-positive and task-negative network associated with rest/task switching process for goal directed behavior to be present across multiple frequency bands. In combination with earlier EEG studies, current results of consistent negative correlation observed between task positive and task negative network brain regions imply functional integration between networks to be present at wider-frequency band.

In the analyzed data, resting state BOLD signal was found to have significant power contribution from each of the frequency bands with exception of slow-1 frequency band. This is expected because sampling frequency used in the current study although

higher than tradition fMRI sampling frequency (1.5 Hz compared to 0.5 - 0.33 Hz in tradition MRI), cannot cover the whole–frequency band of slow-1 fluctuation (0.5-1.5 Hz). In the current study, resting state BOLD fluctuations from slow-5 (0.01-0.027 Hz), slow-4 (0.027-0.073 Hz) and slow-3 (0.073-0.198 Hz) frequency bands accounted for similar amount of power in the BOLD signal across various networks. Although, traditional fMRI bandwidth can measure BOLD fluctuations in slow-3 frequency band, resting state fMRI studies have temporally filtered BOLD signal in slow-5 and slow-4 frequency bands to avoid effects of respiratory signal in RSFC analysis and due to power contained in this frequency band[1]. This respiration signal, known to be present at ~0.3 Hz [21] may overlap with hemodynamic response due to underlying neuronal fluctuations in slow-3/slow-2 frequency band. This implies that regressing CSF/WM signals out from the data (thought to be highly contaminated by respiration signal) may also reduce the power of BOLD signal in slow-3/slow-2 frequency bands. In addition, the BOLD signal is known to be inherently low frequency signal due to slow hemodynamic response to neuronal firings acting as a low-pass filter. This implies that multi-frequency band neuronal oscillations in the brain will be low-pass filtered with higher power in low-frequency band and decreased power in high-frequency band. This could explain limited power contained in slow-2 frequency band (0.198-0.5 Hz). The results from the current study show that the BOLD signal in higher-frequency bands even though not sampled completely (slow-1) and be attenuated through hemodynamic response (slow-3, slow-2 and slow-1), is still highly correlated across brain regions and displayed RSNs similar to BOLD fluctuations in low-frequency range (slow-5, slow-4). This implies that these BOLD fluctuations in slow-3, slow-2 and slow-1 frequency bands has significant

presence of neuronal fluctuations and may provide more information about functional integration in brain.

The noise sources in the BOLD signal are typically thought to comprise of the respiration signal (0.2-0.3 Hz) and cardiac signal (1 Hz). Using a high temporal sampling rate that results in higher frequency resolution, we have been able to correctly sample the main respiration signal, though the aliasing of the cardiac signal could not be avoided. Earlier studies have used RETROICOR to remove effects of physiological noises from BOLD fMRI data, which requires explicitly recording cardiac and respiratory signal[93]. Due to the lack of physiological measurements for subjects in current study data, RETROICOR could not be implemented. Other studies have also used the regression of time series from CSF/WM as a means of removing effects of physiological signals from resting state fMRI data. In a recent study, Chai and colleagues used five principal components from CSF/WM time series to regress effects of physiological noises from the data [68]. Here, similar to this method we have used principal components of CSF/WM time series and derivatives of motion parameters to regress effects physiological noises and head motion effects out from the data. Future studies involving specifically recorded physiological signals would help improve the robustness and reliability of RSFC in multiple frequency bands.

5.1.2 Limitations and future directions

One of the major limitations of current study is the lack of higher sampling frequency that can cover the whole slow-1 frequency band. It may be possible that with further technical advancement, the sampling rate can be increased, then one can study the

whole ‘slow’ frequency band (up to 1.5 Hz). This may enhance similarities between findings from electrophysiological studies focusing on ‘fast’ neuronal processes and fMRI studies focusing on ‘slow’ neuronal processes. In addition, current study used regression of CSF/WM time series to reduce the effect of physiological noises from BOLD signal. Future studies using direct measurements of physiological noises source (respiratory signal and cardiac signal) can improve reliability and robustness of the results obtained in current study. It may be possible that by using higher sampling frequency and by greatly reducing effect of physiological noises sources, one can better define this functional integration between brain regions leading to other resting state networks, which may reflect equally, or more important neuronal processes.

5.2 Effects of frequency based RSFC on whole brain network topology

5.2.1 Interpretation of findings

In the current study, we investigated network topological properties of resting state functional connectivity across multiple frequency bands ranging from 0.01 to 0.75 Hz, using a multiband high temporal resolution (TR=645 ms) open-access data. This is the first study to systematically investigate network properties across multiple frequency bands higher than the low-frequency range (0.01-0.1 Hz). We observed that functional brain connectivity across various frequency bands is organized in small world architecture, though large-scale differences are observed in small world parameter, modularity index and hub distribution, across frequency bands. On the contrary global efficiency of information transfer was found to be quite similar across the frequency bands.

In the current study, we segmented the whole frequency band from 0-0.75 Hz in to five distinct frequency bands based the studies by Buzsaki and Colleagues[7,87]. Although, these studies are based on the EEG and LFP, in a recent study by Achard and c colleagues[39], using wavelet transform on BOLD fMRI data, found similar frequency bands. In addition, recent studies have shown the presence RSFC in these very distinct frequency bands (slow-1 to Slow-5) implying that these slow-1- to slow-5 frequency bands representative of underlying neuronal fluctuations. [74,94] This implies that the BOLD signal fluctuations can also be studied in the frequency bands defined using EEG and LFP literature and share a common underlying neuronal mechanism. Additionally, similar to the current results, MEG studies have shown similar pattern of changes in clustering coefficients across frequency bands[95] implying that various MEG frequency bands that are related to different cognitive functions are representative of various network connectivity pattern. In addition, connectivity properties in only part of EEG bands show small-world architecture implying that small-world properties are highly dependent on synchronization and cognitive functions rather than power in given signal. Although, in the current study the small world architecture was observed across all the frequency bands, changes in clustering coefficient, small-world coefficient and modularity point to differential connectivity pattern across frequency bands that may be based on cognitive roles of each of this frequencies and needs to be studied in detail.

The RSFC at slow-4 and slow-5 frequency bands was found to be stronger than the RSFC at slow-1 and slow-2 bands. In accordance with our hypothesis, whole brain resting state functional connectivity was organized in small world architecture in frequency bands higher than low-frequency range (0.01-0.1 Hz). In addition, small world

indices were found to be frequency dependent where as small world indices decreased with increase in frequency bands. Functional connectivity pattern at higher bands were found to be closer to random network patterns compared to slow-4 and slow-5 implying that the higher frequency bands have large number of high-density local connections while the lower frequency bands have stronger long-range connections. Earlier studies have shown that strength of synchronized oscillations in a neuronal network is increased by inclusion of long distance axonal projections, which mediate global topological shortcuts between spatially remote oscillators[7] which are in accordance with stronger functional connectivity observed in the current study in the low-frequency range. In an earlier study by Basset and colleagues, similar pattern of the functional connectivity topology has been observed[81], where lower frequency bands show higher small world indices compared to higher frequency bands, although in the MEG setup. These results imply that the differential small world architecture across frequency bands observed in the current study is based on underlying neuronal fluctuations as observed in earlier MEG /EEG studies.

Studies have shown that the brain metabolic costs are very high but are kept as low-as possible for a function and much of the metabolic costs are attributed to maintaining the electro chemical gradient required to support signaling and coordination between neuronal activity between distinct brain regions[36,37]. A common consensus in neuroscience literature exists that brain networks are often functionally reconfigured less expansively in order to reduce metabolic costs in response to external stimuli. In addition, topology of brain networks is thought to be in critical state that enables rapid and robust large-scale reconfiguration of functional networks between regular and random networks

in response to external stimuli [34,81,96]. MEG studies have shown that the brain networks remain in a critical state, close to phase transition between regular and random networks, and are reconfigured in response to the task paradigm with high efficiency and higher long distance inter-modular edges which are rapidly reconfigured (in the order of milliseconds) to higher clustering and higher modularity networks [34,96]. Specifically, Basset and colleagues in MEG data have shown that finger-tapping task is associated with long-range stronger connections at higher frequencies and that task performance is associated with reconfiguration of high-frequency networks to favor long distance connections. Basset and Colleagues propose that brain networks are topologically and dynamically contained in a narrow window of permissible global parameters but diversity functions are supported by the reconfiguration of set of interregional connections from the global network architecture. Basset and colleagues used the measure of synchonizability to define a brain networks that are in on the verge of critical dynamics that would favor rapid, adaptive reconfiguration in the face of change demands. Synchonizability of high frequency networks was found to be much higher than low frequency networks in MEG network. In the current study, we observed that synchonizability of whole brain network is higher at high-frequency BOLD networks (slow-1 and slow-2) compared to low-frequency BOLD networks (slow-4 and slow-5). These results imply that similar to MEG studies, the high-frequency BOLD networks are on the verge of critical dynamics that would favor adaptive reconfiguration in presence of external stimuli and needs to be studied in detail.

In the current study, we observed highly segregated network with long-range connection at slow-4 and slow-5 but less segregation and short ranged network in slow-1

to slow-2. Higher small-world values at slow-4 and slow-5 frequency bands implies that the whole brain RSFC is more segregated in small communities with long range connections between them, while lower small world coefficient for slow-1 and slow-2 frequency bands imply, higher clustering coefficient and bigger communities and short range connections among them. This implies that functional brain connectivity in high frequency band consists of higher number of connections to be reorganized. It can be argued that the cost associated with building, maintain and the speed of signal transmission increases with increases with length of the distance between inter-neuronal connections[97,98]. In addition, high frequency connections are less energy efficient compared to low-frequency connections, implying that inclusion of low-frequency long-range connections may decrease the brain's metabolic costs. In a recent study, Salvador and colleagues have shown that that inter-hemispheric connectivity between same brain regions is higher at low frequencies while the functional coherence between asymmetric ROI pairs is higher at high frequency [99]. This can imply that the functional connectivity within a particular network is modulated by low-frequency fluctuations while the functional connectivity between any two networks is modulated by high frequency fluctuations. In the same study, higher frequency graphs were found to be locally connected with short edges while lower-frequency graph were globally connected with long-distance edges in the network. These results are consistent with the higher number of long range connections observed in the current study for the low-frequency networks compared to the lower number of long range connections observed at higher frequency bands. This results could suggest a neural efficiency hypothesis where long-distance connections are maintained at low-frequency for energy perseverance while short

distance between network connections are maintained at higher frequency to allow rapid task switching [81] but needs to be studied in detail in various task conditions.

In the current study, we observed large-scale changes in network hubs for various frequency bands. Specifically, OCN and CBN network has high correlation across bands and have hub ROIs across slow-1 to slow-3. SMN has stronger connectivity in slow-4 and slow-5 and has hub ROIs in the motor cortex. In addition, nodal property distribution (Eigen value centrality, betweenness centrality and degree distribution) varies across bands, where slow-1 and slow-2 lower peak and longer tails compared to short tailed distribution observed for slow-4 and slow-5 frequency bands. These results imply that the hubs identified in current analysis are ROIs that are important to whole network organization irrespective of analysis methods. At slow-4 and slow-5 narrow distribution with shorted tails, imply each ROI are tailored to different type of connection. For example, higher Eigen vector centrality in SMN in slow-4 and slow-5 mean that these ROIs are connected to other important ROIs (in SMN,) similarly higher degree and betweenness centrality in visual ROIs in slow-1 and slow-2 imply higher number of connection for those brain regions. Studies have shown that targeted node attacks on network hubs may cause large-scale disruptions in the functional connectivity topology. This implies that low-frequency brain networks that are highly segregated and have fewer number of regions as hubs are more susceptible to the target node attack. The functional connectivity topology of high frequency connectivity on the other hand can have more networks and thus may have higher resilience to the targeted node attack as there are more regions with higher degree and highly connected in the higher frequency bands compared to low-frequency bands, though further studies are needed to understand the

effect of targeted node attacks on network topological properties at high-frequency bold fluctuations.

Community structure of brain can be defined as hierarchy of modules that consists of highly connected nodes sharing the functional specialization. One of the major frequency based differences were observed in the modular architecture observed for various frequency bands which was in accordance with the small-world results obtained in the current study. Earlier studies have shown the similar effect but only in the low-frequency fluctuations but the current study expand this notion to higher frequency bands [100]. Modularity was found to be significantly lower in slow-1and slow-2 compared to slow-3 to slow-4 and slow-5 frequency bands. Specifically the whole brain network was divided in to three major components mainly (frontal, parietal and occipital) though inter-connection between three major modules was different across frequency bands. In the current study we used the 160 regions of interest defined by Dosenbach and colleagues, which have been categorized in to 6 different networks, though the results of modularity analysis revealed presence of three major modules across the frequency bands. Specifically, functional connectivity of the ROIs in cerebellum and visual network were part of the same modules in the slow-1, slow-2 and slow-3 frequency bands while in slow-4 and slow-5 frequency bands the ROIs in cerebellum were part of the module that contained DMN ROIs as well. DMN ROIs were organized in a single module in the low-frequency bands (slow-4 and slow-5) compared to higher bands (slow-1, slow-2, slow-3). In addition, we observed that the ROIs from frontal parietal network were mostly split in to two different modules where parietal ROIs were in the same module as motor network ROIs. Studies have suggested that brain regions show higher clustering owning to higher

number of connections to neighborhood ROIs who have similar functional specifications and often belong to the same module. In the current study, ROI belonging to known resting state networks were found to be associated with ROIs from other RSNs as a function of frequency bands, where the association was higher at low-frequency bands compared to higher frequency bands. In addition, ROIs involved in lower level cognitive processes such as visual, motor and auditory processing were found to be in the same module across the frequency bands compared to higher level cognitive processes such as executive and default mode network that were found to be distinctively present in lower frequency bands. These results imply that resting state networks defined as clusters of brain regions are dependent on BOLD frequency fluctuations. These results also imply that the functional and cognitive specialization of a set of brain regions, often described by their association with known brain networks is frequency dependent.

5.2.2 Limitations and future directions

One of the major limitations of results obtained in this project is the lack of neurocognitive testing scores or task-based fMRI data. With inclusion of such data, one can associate differences in network topological properties with task performance, which may provide novel insights in to the cognitive basis of BOLD signal fluctuations in various frequency bands. In addition, in the current study, the functional connectivity between brain regions defined as Pearson's correlation between filtered BOLD signal time series was converted in to absolute values. Negative correlations of BOLD signal of various brain regions, may imply inhibition mechanism, and though separate studies of positive and negative RSFC between brain regions and their effect on network topologies is out of the scope of current work.

5.3 Disruption of frequency specific BOLD signal power in schizophrenia

5.3.1 Interpretation of findings

The results of this study provide new data regarding the role of frequency bands in rs-fMRI abnormalities in the neurobiology of psychosis. Specifically, we assessed power in 3 distinct frequency bands including slow-4 (0.027 - 0.073 Hz), slow-3 (0.074 - 0.198 Hz) and slow-2 (0.199 - 0.25 Hz), between patients with psychosis and healthy volunteers within 14 resting state networks. We observed a significant group x frequency interaction for the visual and motor cortical networks, with the most robust group differences (patients < healthy volunteers) assessed from effect size measures in slow-4 and slow-3, respectively. Moreover, main effects of group were evident in the visual cortex, dorsal attention and motor cortex networks such that healthy volunteers had higher mAFF compared to patients across the 3 frequency bands with opposite effects (patients > controls) observed within the salience and frontal gyrus networks. Our findings also support the hypothesis that the interaction and main effects were evident in patients with psychosis and expand prior findings to the investigation of higher frequency bands (slow-3, slow-2). Strengths of the current study include the use of large cohorts, highly stringent motion criteria applied in the analysis and investigation of higher frequency BOLD fluctuations not investigated previously.

We identified higher overall rs-fMRI activity across the 3 frequency bands in visual cortex, dorsal attention, and motor cortex networks compared to healthy volunteers, but the opposite pattern (patients > controls) was observed in the salience and frontal gyrus networks. The identification of lower visual cortex activity and higher frontal cortex activity across frequency bands was particularly robust in the current study.

In this regard our findings are highly consistent with the results from [60,61]. Specifically, Hoptman et al[60] (2010) reported lower ALFF in patients compared to healthy volunteers in occipital regions within slow-4, and Turner et al [61](2013) reported that patients demonstrated higher rs-fMRI low frequency power in frontal cortical regions, but less power in posterior regions than healthy volunteers, albeit in the narrower frequency bands (0.01–0.08Hz) compared to the current study. Our results are also consistent with those from Huang et al [62] who reported lower power of bold signal fluctuations in the low-frequency range in patients with schizophrenia compared to healthy controls in posterior brain regions, but stand in contrast to their report of lower ALFF within the range of 0.01–0.08 Hz in the medial prefrontal region and those of Lui et al [101] who reported that antipsychotic drug-naïve patients with first-episode schizophrenia demonstrated lower ALFF values in ventral medial frontal regions, although it should be acknowledged that the precise regions showing higher AFF in the current study are different. These observed differences may be due, in part, to different data processing methods. For example, in the current study we implemented a linear regression model to better characterize and reduce effects of physiological noise from the data whereas both Lui and Colleauges[101] and Huang and Colleagues[62] have not implemented such regression.

In contrast to the current findings, He et al [102] reported lower fALFF in the medial prefrontal and orbital frontal cortex in patients compared to healthy volunteers. It should be acknowledged, however, that the current study analyzed the amplitude of frequency fluctuations in 3 distinct frequency bands, while the fALFF measure used by He and colleagues was derived by taking ratios of power in the low-frequency band (0.01-0.08

~slow-4 (0.028-0.073)) to the overall frequency band (slow-2, slow-3 and slow-4). Thus a decreased fALFF in psychosis observed by He and Colleagues could be attributed to either the decreased amplitude in low- frequency bands (0.01 -0.1 Hz~slow-4) or increased amplitude in the high frequency bands (>0.1 Hz ~slow-2 + slow-3). There also exists a possibility that BOLD signal power is significantly increased in the patient populations compared to controls, though larger changes are observed in the high frequency bands compared to low frequency bands. In addition, in our prior work, we have shown that various frequency bands contribute different amount of power to known resting state networks [74]. Specifically, the combination of slow-2 and slow-3 frequency bands represents similar amount of power as slow-4 in default mode network, salience network and visual network. Thus, a direct comparison between increased mAFF observed in the frontal cortex of the brain in current study and decreased fALFF observed by He and Colleagues is not feasible. Further studies that cover the whole frequency band of slow fluctuations (0-1.2 Hz) are required to study how increased mAFF in one frequency band can affect the fAFF values across the brain.

The identification of lower rs-fMRI activity in the visual cortex and higher rs-fMRI activity in the frontal cortex has now been reported in multiple studies and across different frequency ranges [60,61] and thus appears to be a relatively robust finding in the literature. Similarly, Anticevic et al [103] reported higher rs-fMRI activity in the prefrontal cortex in early course schizophrenia, which predicted symptom severity. In addition, using the amplitude of low-frequency fluctuation Zou and colleagues [104] reported that frontal regions predicted working memory task activation and deactivation, which was most pronounced at the highest working memory loads suggesting that intrinsic

prefrontal rs-fMRI activity can predict "efficiency" of brain functioning. The identification of rs-fMRI abnormalities in occipital regions in patients with schizophrenia is consistent with reports of visual processing deficits in patients in the identification of visual contours[105] (Feigenson et al 2014), motion perception[106] and smooth pursuit eye movements [107]. Moreover, abnormalities in occipital regions were observed using voxel-mirrored homotopic connectivity rs-fMRI analysis in patients with schizophrenia compared to healthy volunteers [108] and disturbances in rs-fMRI activity within primary sensory areas could have potential downstream effects including visual hallucinations [109]. It should also be noted that integrated dysfunction between frontal and occipital pathways has been reported in the neurobiology of psychosis [110,111], which have been linked to positive symptoms among individuals with nonclinical psychosis [112].

Our findings are also broadly consistent with the results of EEG studies, which have demonstrated power distribution differences in schizophrenia. Patients with schizophrenia have greater theta power during resting state conditions in frontal regions, but lower theta power in the frontal regions during attention task performance [58]. Taken together, these results suggest that failures to increase oscillatory activity while performing a cognitive task may be influenced by high oscillatory activity while in a resting state. Along these lines Winterer and colleagues[113] have shown greater "noise" in patients with schizophrenia compared to controls where noise was defined as the proportion of EEG activity not time-locked to an event. In the current study, we also observed a higher power of bold signal fluctuations during the rs-fMRI in the frontal cortex of the brain, which may imply higher 'noise' in patients. Similarly, studies have also shown the presence of cross-frequency bindings between EEG rhythms and various

resting state networks associated with schizophrenia that could conceivably disturb self-attention processes [59].

Few studies to date have investigated possible interaction effects between frequency bands ranging from .01 to .1 Hz using rs-fMRI in psychosis and associated disorders and thus, it is difficult to compare our findings with prior work. In the study by Yu and colleagues[63] rs-fMRI activity was assessed in 3 different frequency bands including slow-5 (0.01–0.027 Hz), slow-4 (0.027–0.08 Hz) and the standard band of 0.01–0.08 Hz with significant interactions of region-by-frequency band. Specifically, these authors reported significantly larger ALFF in the slow-4 band compared to the slow-5 bands in the cingulate cortex, fusiform gyrus, basal ganglia, and midbrain regions. In contrast, they observed larger ALFF in slow-5 (compared to slow-4) in the lingual gyrus, middle temporal gyrus, inferior frontal gyrus and ventromedial frontal gyrus. It is also noteworthy that in the current study, we also identified significant main effects of frequency for the dorsal attention and motor networks such that slow-4 was significantly higher than slow-3, which, in turn, was significantly higher than slow-2. To our knowledge such a "gradient effect" of decreased power from lower to higher frequencies has not been reported previously in the literature. Higher power in lower bands compared to higher bands could conceivably be related to differential energy consumption among brain regions, although further studies using a higher sampling rate are required to study a wider frequency distribution.

5.3.2 Limitations and future directions

There were a number of study limitations that should be acknowledged that preclude firm conclusions. Although we did not examine functional integration among brain regions across frequency bands, differential patterns of AFF across brain regions, imply difference in frequency of neuronal fluctuations across regions that may give rise to disruptions in functional integration between brain regions. In the current study, we combined data across 2 sites and thus differences in machine manufacturer as well as task instructions[104] (Zou et al 2015) could affect study findings. We did, however, include site as a covariate in the analyses and additionally conducted separate analyses by site. Additionally, in the current study, we didn't include the frequency bands (slow-1 (0.5-1.2 Hz)) and slow-5 (0.01-0.027 Hz), given our inability of examine frequency higher than 0.25 HZ (TR-2s, sampling frequency-0.5 Hz) and to effectively remove slow scanner drifts that may resemble the slow-5 frequency bands fluctuations

CHAPTER VI

SUMMARY AND CONCLUSIONS

In conclusion, the work presented in this dissertation is intended to provide evidence of presence of resting state functional connectivity in BOLD fMRI signal in frequencies higher than traditionally studied range of 0.01 to 0.1 and to quantify these RSFC in higher frequency bands. In order to accomplish this goal, we acquired multiband fMRI data with high temporal resolution (TR=0.645 s) compared to generally acquired fMRI data with temporal resolution of 2s. In order to systematically study the presence of RSFC across various frequencies, we segmented the whole frequency bands of resting state BOLD signal in to five distinct frequency bands, slow-1 (0.5-0.75 Hz), slow-2 (0.198-0.5 Hz), slow-3 (0.073-0.198 Hz), slow-4 (0.027-0.073 Hz) and slow-5 (0.01-0.027 Hz) based on earlier EEG and LFP studies. In order to estimate RSFC in each of this frequency bands, we implemented independent component analysis and seed based correlation as two distinct methods to determine RSFC. RSFC was found to be present in all the five frequency bands, including slow-3, slow-2 and slow-1 that included BOLD signal in higher frequencies than traditionally studies using resting state fMRI. In addition, we observed significant differences in spatial extent and RSFC strength of various networks across frequency bands. We also observed significant differences in BOLD signal power distribution across all the RSNs.

In order to further classify the differences observed in RSFC strength across frequency bands, we performed graph theoretical analysis on whole brain RSFC on each of the frequency bands. As expected, we observed large-scale differences in network

topologies across frequency bands, where RSFC in slow-1 and slow-2 frequency bands showed lower local connectivity compared to slow-4 and slow-5 frequency bands. Although different, network topologies across all the frequency bands showed small-world architecture. This small-world architecture of brain has been observed in earlier studies of RSFC, though we are the first study to show this phenomenon in high-frequency BOLD fluctuations. Lastly, to identify neurocognitive basis of this BOLD signal fluctuations in slow-1, slow-2 and slow-3 bands, we studied effect of psychosis on BOLD signal power disruption. We implemented a new measure as, Amplitude of Frequency Fluctuations, (AFF) to characterize this disruption in BOLD signal power. Earlier studies have reported disruption of AFF in slow-4 frequency bands in psychosis patients, with increased AFF observed in frontal cortex of brain while decreased AFF observed in posterior section of the brain with respect to healthy controls. In the current study, we extend these results to slow-2 and slow-3 frequency bands, and observed similar differences in AFF value across groups, implying that the effect of psychosis has a wide spread effect on BOLD signal power.

In summary, through this dissertation, we show neuronal basis and cognitive importance of high frequency resting state BOLD signal fluctuations in human brain functions.

REFERENCES

1. Biswal B, Zerrin Yetkin F, Haughton VM, Hyde JS. Functional connectivity in the motor cortex of resting human brain using echo-planar mri. Magn Reson Med 1995;34(4):537–41.
2. Kiviniemi V, Kantola J-H, Jauhiainen J, Hyvärinen A, Tervonen O. Independent component analysis of nondeterministic fMRI signal sources. Neuroimage 2003;19(2):253–60.
3. Beckmann CF, Smith SM. Probabilistic Independent Component Analysis for Functional Magnetic Resonance Imaging. IEEE Trans Med Imaging 2004;1(2):1–27.
4. Friston KJ, Frith CD, Liddle PF, Frackowiak RS. Functional connectivity: the principal-component analysis of large (PET) data sets. J Cereb Blood Flow Metab 1993;13:5–14.
5. Greicius MD, Supekar K, Menon V, Dougherty RF. Resting-State Functional Connectivity Reflects Structural Connectivity in the Default Mode Network. Cereb Cortex 2009;19(1):72–8.
6. Musso F, Brinkmeyer J, Mobascher A, Warbrick T, Winterer G. Spontaneous brain activity and EEG microstates. A novel EEG/fMRI analysis approach to explore resting-state networks. Neuroimage 2010;52(4):1149–61.
7. Buzsáki G, Draguhn A. Neuronal oscillations in cortical networks. Science 2004;304(5679):1926–9.
8. Llinas RR. The intrinsic electrophysiological properties of mammalian neurons: insights into central nervous system function. Science 1988;242(4886):1654–64.
9. Penttonen M. Natural logarithmic relationship between brain oscillators. Thalamus Relat Syst 2003;2(2):145–52.
10. Cordes D, Haughton VM, Arfanakis K, et al. Frequencies Contributing to Functional Connectivity in the Cerebral Cortex in "' Resting-state '" Data. 2001;(8):1326–33.
11. Wu CW, Gu H, Lu H, Stein EA, Chen J-H, Yang Y. Frequency specificity of functional connectivity in brain networks. Neuroimage 2008;42(3):1047–55.
12. Ogawa S, Lee TM, Nayak AS, Glynn P. Oxygenation-sensitive contrast in magnetic resonance image of rodent brain at high magnetic fields. Magn Reson Med 1990;14(1):68–78.
13. Ogawa S, Lee T. Brain magnetic resonance imaging with contrast dependent on blood oxygenation. Proc Natl Acad Sci U S A 1990;87(24):9868–72.
14. Bandettini PA, Wong EC, Hinks RS, Tikofsky RS, Hyde JS. Time course EPI of human brain function during task activation. Magn Reson Med 1992;25(2):390–7.

15. Fristen KJ, Frith CD, Fletcher P, Liddle PF, Frackowiak RSJ. Functional topography: Multidimensional scaling and functional connectivity in the brain. Cereb Cortex 1996;6(2):156–64.

16. Fox MD, Snyder AZ, Vincent JL, Corbetta M, Van Essen DC, Raichle ME. The human brain is intrinsically organized into dynamic, anticorrelated functional networks. Proc Natl Acad Sci U S A 2005;102(27):9673–8.

17. Hampson M, Peterson BS, Skudlarski P, Gatenby JC, Gore JC. Detection of functional connectivity using temporal correlations in MR images. Hum Brain Mapp 2002;15(4):247–62.

18. Xiong J, Parsons LM, Gao JH, Fox PT. Interregional connectivity to primary motor cortex revealed using MRI resting state images. Hum Brain Mapp 1999;8(2-3):151–6.

19. Shehzad Z, Kelly a MC, Reiss PT, et al. The resting brain: unconstrained yet reliable. Cereb Cortex 2009;19(10):2209–29.

20. Biswal BB, Mennes M, Zuo X-N, et al. Toward discovery science of human brain function. Proc Natl Acad Sci 2010;107(10):4734–9.

21. Birn RM, Diamond JB, Smith M a., Bandettini P a. Separating respiratory-variation-related fluctuations from neuronal-activity-related fluctuations in fMRI. Neuroimage 2006;31(4):1536–48.

22. Feinberg D a., Moeller S, Smith SM, et al. Multiplexed Echo Planar Imaging for Sub-Second Whole Brain FMRI and Fast Diffusion Imaging. PLoS One 2010;5(12):e15710.

23. Feinberg DA, Yacoub E. The rapid development of high speed, resolution and precision in fMRI. Neuroimage 2012;62(2):720–5.

24. Jesmanowicz A, Nencka AS, Li S-J, Hyde JS. Two-Axis Acceleration of Functional Connectivity Magnetic Resonance Imaging by Parallel Excitation of Phase-Tagged Slices and Half k-Space Acceleration. Brain Connect 2011;1(1):81–90.

25. Lee H-L, Zahneisen B, Hugger T, LeVan P, Hennig J. Tracking dynamic resting-state networks at higher frequencies using MR-encephalography. Neuroimage 2013;65:216–22.

26. Boubela RN, Kalcher K, Huf W, Kronnerwetter C, Filzmoser P, Moser E. Beyond Noise: Using Temporal ICA to Extract Meaningful Information from High-Frequency fMRI Signal Fluctuations during Rest. Front Hum Neurosci 2013;7(May):168.

27. Watts DJ, Strogatz SH. Collective dynamics of "small-world" networks. Science1998;393(6):440–2.

28. Iturria-Medina Y, Canales-Rodríguez EJ, Melie-García L, et al. Characterizing brain anatomical connections using diffusion weighted MRI and graph theory. Neuroimage 2007;36(3):645–60.

29. Iturria-Medina Y, Sotero RC, Canales-Rodríguez EJ, Alemán-Gómez Y, Melie-García L. Studying the human brain anatomical network via diffusion-weighted MRI and Graph Theory. Neuroimage 2008;40(3):1064–76.

30. Bullmore E, Sporns O. The economy of brain network organization. Nat Rev Neurosci 2012;13(5):336–49.

31. Bullmore E, Sporns O. Complex brain networks: graph theoretical analysis of structural and functional systems. Nat Rev Neurosci 2009;10(3):186–98.

32. Hagmann P, Cammoun L, Gigandet X, et al. Mapping the structural core of human cerebral cortex. PLoS Biol 2008;6(7):1479–93.

33. Achard S, Bullmore E. Efficiency and cost of economical brain functional networks. PLoS Comput Biol 2007;3(2):e17.

34. Bassett DS, Bullmore E. Small-World Brain Networks. Neurosci 2006;12(6):512–23.

35. He Y, Chen Z, Evans A. Structural insights into aberrant topological patterns of large-scale cortical networks in Alzheimer's disease. J Neurosci 2008;28(18):4756–66.

36. Attwell D, Laughlin SB. An energy budget for signaling in the grey matter of the brain. J Cereb Blood Flow Metab 2001;21(10):1133–45.

37. Laughlin SB, Sejnowski TJ. Communication in Neuronal Networks. Science (80-) 2003;301(5641):1870–4.

38. Latora V, Marchiori M. Efficient behavior of small-world networks. Phys Rev Lett 2001;87(19):198701.

39. Achard S, Salvador R, Whitcher B, Suckling J, Bullmore E. A resilient, low-frequency, small-world human brain functional network with highly connected association cortical hubs. J Neurosci 2006;26(1):63–72.

40. Bernhardt BC, Chen Z, He Y, Evans AC, Bernasconi N. Graph-theoretical analysis reveals disrupted small-world organization of cortical thickness correlation networks in temporal lobe epilepsy. Cereb Cortex 2011;21(9):2147–57.

41. Turken A, Whitfield-Gabrieli S, Bammer R, Baldo J V, Dronkers NF, Gabrieli JDE. Cognitive processing speed and the structure of white matter pathways: convergent evidence from normal variation and lesion studies. Neuroimage 2008;42(2):1032–44.

42. Lo CZ, Su T, Huang C, Hung C, Chen W, Lan T. Randomization and resilience of brain functional networks as systems-level endophenotypes of schizophrenia. 2015;

43. Wang J, Zuo X, He Y. Graph-based network analysis of resting-state functional MRI. Front Syst Neurosci 2010;4(6):1–14.

44. Sasai S, Homae F, Watanabe H, et al. Frequency-specific network topologies in the resting human brain. Front Hum Neurosci 2014;8(12):1–19.

45. Smit DJ a, Stam CJ, Posthuma D, Boomsma DI, De Geus EJC. Heritability of "small-world" networks in the brain: A graph theoretical analysis of resting-state EEG functional connectivity. Hum Brain Mapp 2008;29(12):1368–78.

46. Smit DJ a, de Geus EJC, van de Nieuwenhuijzen ME, et al. Scale-free modulation of resting-state neuronal oscillations reflects prolonged brain maturation in humans. J Neurosci 2011;31(37):13128–36.

47. Harvey PD, Green MF, McGurk SR, Meltzer HY. Changes in cognitive functioning with risperidone and olanzapine treatment: a large-scale, double-blind, randomized study. Psychopharmacology (Berl) 2003;169(3-4):404–11.

48. Harvey PD, Artiola i Fortuny L, Vester-Blockland E, De Smedt G. Cross-national cognitive assessment in schizophrenia clinical trials: a feasibility study. Schizophr Res 2003;59:243–51.

49. Shenton ME, Dickey CC, Frumin M, McCarley RW. A review of MRI findings in schizophrenia. Schizophr Res 2001;49:1–52.

50. Ross C a., Pearlson GD. Schizophrenia, the heteromodal association neocortex and development: Potential for a neurogenetic approach. Trends Neurosci 1996;19(5):171–6.

51. Satterthwaite TD, Baker JT. How can studies of resting-state functional connectivity help us understand psychosis as a disorder of brain development? Curr Opin Neurobiol 2015;30(10):85–91.

52. Liang M, Zhou Y, Jiang T, et al. Widespread functional disconnectivity in schizophrenia with resting-state functional magnetic resonance imaging. Neuroreport 2006;17(2):209–13.

53. Bluhm RL, Miller J, Lanius RA, et al. Spontaneous Low-Frequency Fluctuations in the BOLD Signal in Schizophrenic Patients: Anomalies in the Default Network. Schizophr Bull 2007;33(4):1004–12.

54. Calhoun VD, Maciejewski PK, Pearlson GD, Kent A. Temporal Lobe and "Default" Hemodynamic Brain Modes Discriminate Between Schizophrenia and Bipolar Disorder. 2009;29(11):1265–75.

55. Whitfield-Gabrieli S, Thermenos HW, Milanovic S, et al. Hyperactivity and hyperconnectivity of the default network in schizophrenia and in first-degree relatives of persons with schizophrenia. Proc Natl Acad Sci U S A 2009;106(4):1279–84.

56. Butler PD, Javitt DC. Early-stage visual processing deficits in schizophrenia. Curr Opin Psychiatry 2005;18(2):151–7.

57. Rabinowicz EF, Silipo G, Goldman R, Javitt DC. Auditory Sensory Dysfunction in Schizophrenia. Arch Gen Psychiatry 2000;57:1149–55.

58. Hanslmayr S, Backes H, Straub S, et al. Enhanced resting-state oscillations in schizophrenia are associated with decreased synchronization during inattentional blindness. Hum Brain Mapp 2013;34(9):2266–75.

59. Razavi N, Jann K, Koenig T, et al. Shifted Coupling of EEG Driving Frequencies and fMRI Resting State Networks in Schizophrenia Spectrum Disorders. PLoS One 2013;8(10).

60. Hoptman MJ, Zuo X-N, Butler PD, et al. Amplitude of low-frequency oscillations in schizophrenia: A resting state fMRI study. Schizophr Res 2010;117(1):13–20.

61. Turner J a., Damaraju E, Van Erp TGM, et al. A multi-site resting state fMRI study on the amplitude of low frequency fluctuations in schizophrenia. Front Neurosci 2013;7(8):1–13.

62. Huang X-Q, Lui S, Deng W, et al. Localization of cerebral functional deficits in treatment-naive, first-episode schizophrenia using resting-state fMRI. Neuroimage 2010;49(4):2901–6.

63. Yu R, Chien Y-L, Wang H-LS, et al. Frequency-specific alternations in the amplitude of low-frequency fluctuations in schizophrenia. Hum Brain Mapp 2014;35(2):627–37.

64. Nooner KB, Colcombe SJ, Tobe RH, et al. The NKI-Rockland Sample: A Model for Accelerating the Pace of Discovery Science in Psychiatry. Front Neurosci 2012;6(10):1–11.

65. Cox RW. AFNI: software for analysis and visualization of functional magnetic resonance neuroimages. Comput Biomed Res 1996;29(3):162–73.

66. Jenkinson M, Beckmann CF, Behrens TEJ, Woolrich MW, Smith SM. FSL. Neuroimage 2012;62(2):782–90.

67. Taylor P a., Gohel S, Di X, Walter M, Biswal BB. Functional Covariance Networks: Obtaining Resting-State Networks from Intersubject Variability. Brain Connect 2012;2(4):203–17.

68. Chai X, Castañón an, Öngür D, Whitfield-Gabrieli S. Anticorrelations in resting state networks without global signal regression. Neuroimage 2012;59(2):1420–8.

69. Behzadi Y, Restom K, Liau J, Liu TT. A component based noise correction method (CompCor) for BOLD and perfusion based fMRI. Neuroimage 2007;37(1):90–101.

70. Zuo X-N, Di Martino A, Kelly C, et al. The oscillating brain: Complex and reliable. Neuroimage 2010;49(2):1432–45.

71. Xia M, Wang J, He Y. BrainNet Viewer: A Network Visualization Tool for Human Brain Connectomics. PLoS One 2013;8(7):e68910.

72. Yu-Feng Z, Yong H, Chao-Zhe Z, et al. Altered baseline brain activity in children with ADHD revealed by resting-state functional MRI. Brain Dev 2007;29(2):83–91.

73. Chang C, Glover GH. Time–frequency dynamics of resting-state brain connectivity measured with fMRI. Neuroimage 2010;50(1):81–98.

74. Gohel SR, Biswal BB. Functional Integration Between Brain Regions at Rest Occurs in Multiple-Frequency Bands. Brain Connect 2015;5(1):23–34.

75. Bharath RD, Munivenkatappa A, Gohel S, et al. Recovery of resting brain connectivity ensuing mild traumatic brain injury. Front Hum Neurosci 2015;9(9):1–13.

76. Friston KJ, Williams S, Howard R, Frackowiak RS, Turner R. Movement-related effects in fMRI time-series. Magn Reson Med 1996;35(3):346–55.

77. Yan C-G, Cheung B, Kelly C, et al. A comprehensive assessment of regional variation in the impact of head micromovements on functional connectomics. Neuroimage 2013;76:183–201.

78. Dosenbach NUF, Nardos B, Cohen AL, et al. Prediction of individual brain maturity using fMRI. Science 2010;329(5997):1358–61.

79. Rubinov M, Sporns O. Complex network measures of brain connectivity: uses and interpretations. Neuroimage 2010;52(3):1059–69.

80. Jacomy M, Venturini T, Heymann S, Bastian M. ForceAtlas2, a continuous graph layout algorithm for handy network visualization designed for the Gephi software. PLoS One 2014;9(6):1–12.

81. Bassett DS, Meyer-Lindenberg A, Achard S, Duke T, Bullmore E. Adaptive reconfiguration of fractal small-world human brain functional networks. Proc Natl Acad Sci U S A 2006;103(51):19518–23.

82. Taylor P a., Saad ZS. FATCAT: (An Efficient) Functional And Tractographic Connectivity Analysis Toolbox. Brain Connect 2013;3(5):523–35.

83. Zou Q-H, Zhu C-Z, Yang Y, et al. An improved approach to detection of amplitude of low-frequency fluctuation (ALFF) for resting-state fMRI: fractional ALFF. J Neurosci Methods 2008;172(1):137–41.

84. Power JD, Barnes K a, Snyder AZ, Schlaggar BL, Petersen SE. Spurious but systematic correlations in functional connectivity MRI networks arise from subject motion. Neuroimage 2012;59(3):2142–54.

85. Van Dijk KRA, Hedden T, Venkataraman A, Evans KC, Lazar SW, Buckner RL. Intrinsic functional connectivity as a tool for human connectomics: theory, properties, and optimization. J Neurophysiol 2010;103(1):297–321.

86. Jenkinson M, Bannister P, Brady M, Smith S. Improved optimization for the robust and accurate linear registration and motion correction of brain images. Neuroimage 2002;17(2):825–41.

87. Buzsáki G, Watson BO. Brain rhythms and neural syntax: Implications for efficient coding of cognitive content and neuropsychiatric disease. Dialogues Clin Neurosci 2012;14(4):345–67.

88. Logothetis NK, Pauls J, Augath M, Trinath T, Oeltermann a. Neurophysiological investigation of the basis of the fMRI signal. Nature 2001;412(6843):150–7.

89. Laufs H, Lengler U, Hamandi K, Kleinschmidt A, Krakow K. Linking generalized spike-and-wave discharges and resting state brain activity by using EEG/fMRI in a patient with absence seizures. Epilepsia 2006;47(2):444–8.

90. Mantini D, Perrucci MG, Del Gratta C, Romani GL, Corbetta M, Gratta C Del. Electrophysiological signatures of resting state networks in the human brain. Proc Natl Acad Sci U S A 2007;104(2):13170–5.

91. Helps SK, Broyd SJ, James CJ, Karl A, Sonuga-Barke EJS. The Attenuation of Very Low Frequency Brain Oscillations in Transitions from a Rest State to Active Attention. J Psychophysiol 2009;23(4):191–8.

92. Saad ZS, Gotts SJ, Murphy K, et al. Trouble at Rest: How Correlation Patterns and Group Differences Become Distorted After Global Signal Regression. Brain Connect 2012;2(1):25–32.

93. Glover GH, Li TQ, Ress D. Image-based method for retrospective correction of physiological motion effects in fMRI: RETROICOR. Magn Reson Med 2000;44(1):162–7.

94. Chen JE, Glover GH. BOLD fractional contribution to resting-state functional connectivity above 0.1Hz. Neuroimage 2014;107:207–18.

95. Stam CJ, De Bruin EA. Scale-free dynamics of global functional connectivity in the human brain. Hum Brain Mapp 2004;22(2):97–109.

96. Kitzbichler MG, Henson RNA, Smith ML, Nathan PJ, Bullmore ET. Cognitive effort drives workspace configuration of human brain functional networks. J Neurosci 2011;31(22):8259–70.

97. Ringo JL. Neuronal interconnection as a function of brain size. Brain Behav Evol 1991;38(1):1–6.

98. Chklovskii DB, Mel BW, Svoboda K. Cortical rewiring and information storage. Nature 2004;431(10):782–8.

99. Salvador R, Suckling J, Coleman MR, Pickard JD, Menon D, Bullmore E. Neurophysiological architecture of functional magnetic resonance images of human brain. Cereb Cortex 2005;15(9):1332–2342.

100. Meunier D, Achard S, Morcom A, Bullmore E. Age-related changes in modular organization of human brain functional networks. Neuroimage 2009;44(3):715–23.

101. Lui S, Li T, Deng W, et al. SHort-term effects of antipsychotic treatment on cerebral function in drug-naive first-episode schizophrenia revealed by “resting state” functional magnetic resonance imaging. Arch Gen Psychiatry 2010;67(8):783–92.

102. He Z, Deng W, Li M, et al. Aberrant intrinsic brain activity and cognitive deficit in first-episode treatment-naive patients with schizophrenia. Psychol Med 2013;43(04):769–80.

103. Anticevic a., Hu X, Xiao Y, et al. Early-Course Unmedicated Schizophrenia Patients Exhibit Elevated Prefrontal Connectivity Associated with Longitudinal Change. J Neurosci 2015;35(1):267–86.

104. Zou Q, Yuan B-K, Gu H, et al. Detecting Static and Dynamic Differences between Eyes-Closed and Eyes-Open Resting States Using ASL and BOLD fMRI. PLoS One 2015;10(3):e0121757.

105. Feigenson KA, Keane BP, Roché MW, Silverstein SM. Contour integration impairment in schizophrenia and first episode psychosis: state or trait? Schizophr Res 2014;159(2-3):515–20.

106. Jahshan C, Wynn JK, Mathis KI, Green MF. The neurophysiology of biological motion perception in schizophrenia. Brain Behav 2015;5(1):n/a – n/a.

107. Franco JG, de Pablo J, Gaviria AM, Sepulveda E, Vilella E. Smooth pursuit eye movements and schizophrenia: literature review. Arch Soc Esp Oftalmol 2014;89(9):361–7.

108. Hoptman MJ, Zuo X-N, D'Angelo D, et al. Decreased interhemispheric coordination in schizophrenia: a resting state fMRI study. Schizophr Res 2012;141(1):1–7.

109. Ford JM, Palzes VA, Roach BJ, et al. Visual Hallucinations Are Associated With Hyperconnectivity Between the Amygdala and Visual Cortex in People With a Diagnosis of Schizophrenia. Schizophr Bull 2015;41(1):223–32.

110. Khadka S, Narayanan B, Meda SA, et al. Genetic association of impulsivity in young adults: a multivariate study. Transl Psychiatry 2014;4:e451.

111. Calderone DJ, Hoptman MJ, Martínez A, et al. Contributions of Low and High Spatial Frequency Processing to Impaired Object Recognition Circuitry in Schizophrenia. Cereb Cortex 2013;23 (8):1849–58.

112. Orr JM, Turner JA, Mittal VA. Widespread brain dysconnectivity associated with psychotic-like experiences in the general population. NeuroImage Clin 2014;4:343–51.

113. Winterer G, Weinberger DR. Genes, dopamine and cortical signal-to-noise ratio in schizophrenia. Trends Neurosci 2004 ;27(11):683–90.